Norwegian University
of Life Sciences

Master's Thesis 2022 60 ECTS
Faculty of Chemistry, Biotechnology and Food Science

Characterization of a Lytic Polysaccharide Monooxygenase from *Schizophyllum commune* belonging to Auxiliary Activity Family 9

Karen Hennum
Biotechnology

Characterization of a Lytic Polysaccharide Monooxygenase from *Schizophyllum commune* belonging to Auxiliary Activity Family 9

Master thesis

Karen Hennum

Protein Engineering and Proteomics Group

Department of Chemistry, Biotechnology and Food Science

The Norwegian University of Life Sciences

2022

Acknowledgments

The work for this thesis was carried out at the Faculty of Chemistry, Biotechnology and Food Science at the Norwegian University of Life Sciences, with Professor Vincent Eijsink, Heidi Østby, and Olav Asseth Hegnar as supervisors.

First, I must thank Heidi Østby, who has taught me how everything in the laboratory works. I am beyond grateful for her patience and interest in my work, and how she has always made time for me. This thesis would not have been completed without her help and guidance.

Olav Asseth Hegnar has not only helped me with my experiments, but he has also cheered me up and kept me motivated. With his positive attitude, I have learned to see the learning potential in every step of the laboratory work.

Professor Vincent Eijsink is the reason why I chose a biotechnology master, and I am genuinely grateful for the opportunity of writing for the Protein engineering and Proteomics Group. His engagement and super-brain have thought me to see the beauty in science, and that hard work do pay off.

In addition to my advisors, I must also thank every member of the PEP group, who has always taken their time to answer my questions and showed me tips and tricks, making life at the laboratory much easier. I have learned so much from each member, and their patience and engagement have made the past year both educational and inspiring.

I also owe my family everything. For always supporting and cheering me, besides loving me unconditionally regardless of how I perform at school. Even though they do not understand anything about enzymes and laboratory techniques, they have always made time to listen to me rant about failed experiments, or endlessly describe how amazing LPMOs are and how exciting science is. They have also offered me a shoulder to cry on and welcomed me home for food and rest whenever I needed a break.

Lastly, I must thank Mia, for being my best friend and the sister I never got. Mia was the first person I talked to at NMBU and has been by my side ever since. After spending almost every single day together through the 5 years at NMBU, and being partners in every subject at the bachelor, Mia knows me like no one else. I am grateful to have a friend I can turn to no matter

what. Even though we won't be neighbours anymore, I am sure our friendship will last forever, and I am truly excited for what the future will hold for the both of us.

One more lastly, because I did not expect to find a boyfriend during a pandemic, while being at the laboratory 24/7, but life happens. So, thank you Ådne, for being the most genuine and kind person I have met, and for making me dream about something else than enzymes for a change. I knew you would be patient enough to handle me when our first date ended up at the laboratory because I did not manage to finish my experiment in time. You are the best!

Moss, Mai 8th, 2022

Karen Hennum

Abstract

Biomass is a promising feedstock to reduce our dependence on fossil reserves. By using biomass, such as lignocellulose, products can be produced more climate-friendly and are therefore of large industrial interest. Biomass is also renewable, in contrast to fossil reserves, like oil and coal. However, the downside of biomass is that lignocellulose and other polysaccharides can be a challenge to degrade because of their crystalized and insoluble structure.

Previously, hydrolytic enzymes were thought to be the only enzymes degrading polysaccharides. However, in 2010, a new paradigm was born, when researchers first described a protein that degraded chitin through oxidative cleavage. Subsequently, the enzymes have been characterized as lytic polysaccharide monooxygenases (LPMOs), and they do not only work on chitin, but also on cellulose and other recalcitrant polysaccharides. The discovery of LPMOs was a big step in the direction toward more efficient degradation of recalcitrant polysaccharides. LPMOs act on parts of the substrate that hydrolytic enzymes cannot properly degrade, thus making recalcitrant polysaccharides more available for traditional hydrolases by creating free chain ends.

LPMOs are oxidative mono-copper enzymes that can oxidatively cleave glycosidic bonds in polysaccharides. To complete a catalytic cycle, the active site copper Cu(II) must be reduced to Cu(I), and the LPMOs require a dioxygen co-substrate, either O_2 or H_2O_2.

Since LPMOs show variation in their ability to attack various forms of cellulose, it is important for the industry to have a wide spectrum of LPMOs to use on different substrates. Therefore, *Sc*LPMO9A from *Schizophyllum commune,* which is one of several LPMOs that have not been completely characterized yet, was studied, and compared with *Nc*LPMO9C from *Neurospora crassa* for this thesis.

*Sc*LPMO9A and *Nc*LPMO9C are both exclusively C4 oxidizing LPMOs, acting on soluble substrates. Results from this study show, for example, that *Sc*LPMO9A depolymerises various forms of cellulose and hemicelluloses and that the substrate specificity and product formation differ from *Nc*LPMO9C. For example, *Sc*LPMO9A is active on xyloglucan, glucomannan and soluble cello-oligosaccharides, but not active on more crystalline forms of cellulose, like Avicel, while *Nc*LPMO9C is active on more crystalline forms of cellulose. In addition, they

also show that the reaction rate is increased by adding H_2O_2 to the reactions for both *Sc*LPMO9A and *Nc*LPMO9C. The results from this thesis give important information about the biochemistry of *Sc*LPMO9A, that can be used for further studies.

Sammendrag

Biomasse er en lovende råvare for å redusere bruken av fossile energikilder. Ved å bruke biomasse, som for eksempel lignocellulose, kan produkter bli produsert mer klimavennlig, og derfor er biomasse en stor interesse for industrien. I tillegg til dette er biomasse fornybart, i motsetning til fossile energikilder som olje og kull. Den største ulempen ved å bruke biomasse i industrien at det kan være en utfordring å bryte den ned, da polysakkarider som lignocellulose er krystalliserte og uløselige, men det kommer stadig bedre løsninger for dette.

Før trodde man at hydrolytiske enzymer var de eneste enzymene som brøt ned polysakkarider. I 2010 startet derimot et nytt paradigme i enzymatisk degradering, da forskere fant et enzym som katalyserer nedbrytingen av kitin. Senere er det funnet flere enzymer med samme mekanisme, som i dag er klassifisert som lytisk polysakkarid monooksygenaser (LPMOer). Disse enzymene bryter ikke bare ned kitin, men også cellulose og andre polysakkarider. Funnet av disse enzymene har gjort nedbrytningen av polysakkarider mer effektiv, siden LPMOer kan bryte ned deler av substratet som hydrolytiske enzymer ikke kan bryte ned. Dette fører til at polysakkaridet blir mer tilgjengelige for tradisjonelle hydrolaser ved at det er dannet frie kjedeender.

LPMOer er oksidative mono-kobber enzymer som kan katalysere brytingen av glykosid bindinger i polysakkarider. For å fullføre en katalytisk syklus, må kobberet i det aktive setet Cu(II) bli redusert til Cu(I). I tillegg krever LPMOet et di-oksygen co-substrat, enten fra O_2 eller fra H_2O_2.

Siden LPMOer fungerer på ulike substrater er det viktig for industrien å ha et vidt spekter av LPMOer som kan brukes på ulike substrater. Derfor ble *Sc*LPMO9A fra *Schizophyllum commune,* som er et av flere LPMOer som ikke er komplett karakterisert enda, studert og sammenlignet med *Nc*LPMO9C fra *Neurospora crassa* for denne oppgaven.

*Sc*LPMO9A og *Nc*LPMO9C er begge C4 oksiderende LPMOer som kan bryte ned løselige substrater. Resultater fra dette studiet viser for eksempel at *Sc*LPMO9A bryter ned ulike cellulose- og hemicellulose-substrater og at substratspesifisiteten og produktdannelsen er forskjellig fra *Nc*LPMO9C. For eksempel er *Sc*LPMO9A aktivt på xyloglukan, glukomannan, og løselige cello-oligosakkarider, mens det ikke er aktivt på mer krystalliserte former av cellulose som Avicel. *Nc*LPMO9C er derimot også aktiv på de mer krystalliserte formene av

cellulose. I tillegg vises det at begge enzymene reagerer raskere ved å tilsette hydrogenperoksid. Disse resultatene gir informasjon om biokjemien til *Sc*LPMO9A som kan brukes i videre studier.

Abbreviations

AA	Auxiliary Activity
AscA	Ascorbic Acid
BG	β - glucosidase
CAZyme	Carbohydrate active enzyme
CV	Column Volume
CBH	Cellobiohydrolase
CBM	Carbohydrate-binding module
CBM1	Carbohydrate-binding module family 1
DM	Dry matter
DMP	Dimethoxyphenol
DP	Degree of polymerization
DTT	Dithiothreitol
E. coli	*Escherichia coli*
EDTA	Ethylenediaminetetraacetic Acid
GH	Glycoside hydrolases
HIC	Hydrophobic interaction chromatography
HRP	Horse radish peroxygenase
HPAEC	High-performance anion-exchange Chromatography
HPLC	High-performance Liquid Chromatography

ICS	Ion Chromatography System
IPCC	Intergovernmental panel on climate change
KGM	Konjac glucomannan
LB	Lysogeny Broth
LDS	Lithium dodecyl sulfate
LPMO	Lytic polysaccharide monooxygenase
mL	Milliliter
mg	Milligram
MSA	Multiple sequence alignment
µL	Microliter
µM	Micro Molar
N. crassa	*Neurospora crassa*
nm	Nanometres
MWCO	Molecular weight cut-off
PAD	Pulsed Amperometric Detection
PASC	Phosphoric-acid swollen cellulose
PBP	Penicillin-binding proteins
P. pastoris	*Pichia Pastoris*
S. commune	*Schizophyllum commune*
SDS	Sodium dodecyl sulfate

SDS-PAGE	Sodium Dodecyl Sulfate PolyAcrylamide Gel Electrophoresis
SEC	Size Exclusion Chromatography
TXG	Tamarind xyloglucan
XO	Xyloglucan oligosaccharides
YPD	Yeast extract- Peptone-Dextrose

Table of contents

1. Introduction

1.1 The future is green

One of the major challenges facing the world today, is to provide sufficient energy and food, as well as maintain the current lifestyle. In August 2021, the Intergovernmental Panel on climate change (IPCC), published an article about climate change and how it will influence the near future. Some of the aspects in this report were that for the last four decades, the weather has been the hottest on record since 1850, the sea level is continuously rising, and extreme weather is more intense and happens more frequently (IPCC, 2021). Without decreasing the emission of CO_2, the world will come to a point of no return. Therefore, the emissions must be decreased, and this must happen now.

To decrease CO_2 emissions, renewable energy sources like solar-, wind- and wave energy has been more commonly used. With an increased interest in renewable energy sources, we have come a long way towards solving some of the climate challenges, but renewable energy sources alone are not enough to meet today's energy needs (Lund, 2007). To be able to meet today's energy needs without having major consequences for the environment, we must proceed from a fossil economy to a bioeconomy. In short, the fossil economy is not sustainable because the oil reservoirs are used faster than new oil is produced. Moreover, the oil industry is one of the biggest sources of CO_2 emissions. In contrast, the bioeconomy is based on renewable sources and raw materials and is, therefore, more climate-friendly than the fossil economy (Vivien et al., 2019).

The fact that raw material is renewable means that you do not use oil, coal, and gas, but rather use biomass, which is organic material derived from plants or animals. Since plant biomass is produced by photosynthesis, the CO_2 in the atmosphere is converted to the biomass, which leads to a positive effect on global climate change. In the theory, biomass has a net zero CO_2 emission, while fossil recourses transfer quantities of CO_2 into the atmosphere which gets trapped and makes the CO_2 in the atmosphere rapidly rising.

Examples of biomass are wood, plants, and agricultural products. Because of the large variety of biomass characteristics, many different products can be formed from biomass in an environmentally friendly manner. Biomass can for example be used to produce biofuels without releasing large quantitates of CO_2, which is what happens when a fossil resource is used to produce fuel (Villares et al., 2017). Furthermore, biomass can also be used to produce bio-based plastic, which again reduces the emission of CO_2 and creates a more circular economy (Brodin et al., 2017). Some other products that can be produced from biomass are food packaging, cosmetics, and bandages. In addition, biomass can also be used as bioenergy (Horn et al., 2012). Examples of biomass used as bioenergy are starch, sugar, and lignocellulose. Both starch and sugar are also important food sources, therefore, lignocellulose and other non-food biomass are the leading biomass for the future.

Since lignocellulose is the most abundant biomass resources on earth it has a big potential for the industry (Barikani et al., 2014). However, because of the crystalized structure, it has been a big challenge to degrade the polysaccharides into monosaccharides. The crystallized structure is not only highly insoluble, but it also exists in a co-polymeric heterogeneous structure, which is highly resistant to enzymatic depolymerization (Van Dyk & Pletschke, 2012). As a result of this, pretreatment is essential before enzymes can depolymerize the polysaccharides, and this is often time-consuming, inefficient, and expensive (Mankar et al., 2021). Therefore, scientists are trying to find new methods that can utilize biomass in a cost-effective and climate friendly manner.

1.2 Carbohydrates

The most abundant organic compound in nature are carbohydrates, and the main sources of carbohydrates are found in plants, animals, and microorganisms. Carbohydrates play a key role in many biological processes, such as being an energy resource, a backbone element in DNA and RNA, and structural elements in plants and insects (Cocinero & Çarçabal, 2015). Carbohydrates consist of three or more carbons and include at least one alcohol- or carbonyl-group. They can therefore be classified as polyhydroxy aldehydes or ketones, as shown in Figure 1.2.1.

The basic unit of carbohydrates are monosaccharides. Monosaccharides consist of three to seven carbon atoms, and by connecting these monosaccharides by glycosidic bonds, disaccharides, oligosaccharides, or polysaccharides are made (Cocinero & Çarçabal, 2015). Figure 1.2.1 shows glucose and fructose, which are both examples of monosaccharides.

Disaccharides consists of two monosaccharides linked together, while oligosaccharides consist of three to ten monosaccharides linked together. Lastly, polysaccharides consist of more than ten monosaccharides linked together, forming a long chain that is either linear or branched. Examples of disaccharides are sucrose and lactose, while raffinose and maltotriose are examples of oligosaccharides. Cellulose and chitin are both polysaccharides and function as structural elements, while starch is an example of a polysaccharide that serves as energy storage.

The formation of glycosidic bonds are catalysed by a group of enzymes called glycosyltransferases (Forsberg, 2014). The bond is formed between the hemiacetal group on one monosaccharide and the hydroxyl group on the other monosaccharide. Both oligosaccharides and polysaccharides are further synthesized into linear or branched structures, all with different chemical and physical properties. Because of the different bonds between the monosaccharides, for example β - 1,4, α - 1,4 and α - 1,2 bonds, and different branches, carbohydrates consist of many different conformations. In addition to different conformations of carbohydrates, the carbohydrates can also be modified and have different glycosidic linkages, making the diversity even bigger.

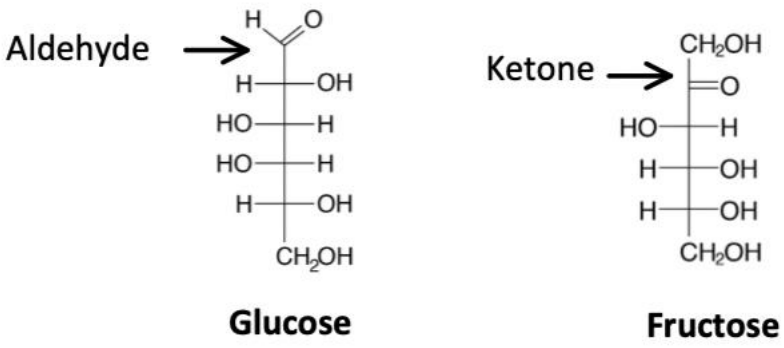

Figure 1.2.1. Open ring representation of glucose and fructose. The picture was taken from Oregon State University and modified for the purpose of this thesis (Oregon-State)

1.3 Lignocellulose

Lignocellulose is the most abundant organic component on earth and is what makes up the cell wall of lignified plants. The major components are the cellulose, hemicelluloses, and lignin, with cellulose and hemicelluloses being polysaccharides and lignin an aromatic polymer (Zoghlami & Paës, 2019). In addition to these polymers, lignocellulose also consists of proteins, lipids, pectin, soluble sugars, and minerals (Horn et al., 2012).

The polymers in lignocellulose are packed in a hetero-matrix, with cellulose and hemicelluloses bound together by hydrogen bonds and lignin covalently linked to hemicelluloses (Zoghlami & Paës, 2019). The hydrogen bonds between cellulose and hemicelluloses together with the lignin-carbohydrate bond reduce the area of cellulose that is accessible for enzymes, making hydrolysis a challenge (Zoghlami & Paës, 2019). Therefore, to be able to degrade lignocellulose, many enzymes must work synergically. Some of these enzymes are hemicellulose-active enzymes, lignin-active enzymes, LPMOs, and cellulases.

In this thesis, cellulose and hemicelluloses are further discussed, since several LPMOs and other enzymes work on these substrates. Yet, there is no known simple way to depolymerize lignin enzymatically.

1.3.1 Cellulose

Cellulose is the most abundant polysaccharide in lignocellulose biomass, representing 40-60% of the mass of lignocellulose (Horn et al., 2012). It consists of hundreds to over ten thousand β -1,4 linked glucose units, making cellulose a linear and non-branched polymer, as illustrated in Figure 1.3.1.

The glucose units are rotated 180 degrees related to each other, which makes cellobiose the repeating unit. Inter- and intramolecular hydrogen bonding and van der Waals interactions ensure that the cellulose chains aggregate into highly ordered structures, called microfibrils (Horn et al., 2012). The inner core of the microfibrils is highly organized, in contrast to the fibril surface, which is less organized because of fewer intramolecular bonds. These amorphous areas are usually the areas exposed to enzymatic degradation.

Due to the abundance of cellulose and its homogenous composition, cellulose is of big industrial and scientific interest. Glucose from cellulose is of special interest for the industry because it can be used to produce fuels, for example, bioethanol and other useful products. However, because of the crystalline form of the microfibrils, together with the non-soluble structure of cellulose, enzymatic decomposition is challenging (Horn et al., 2012).

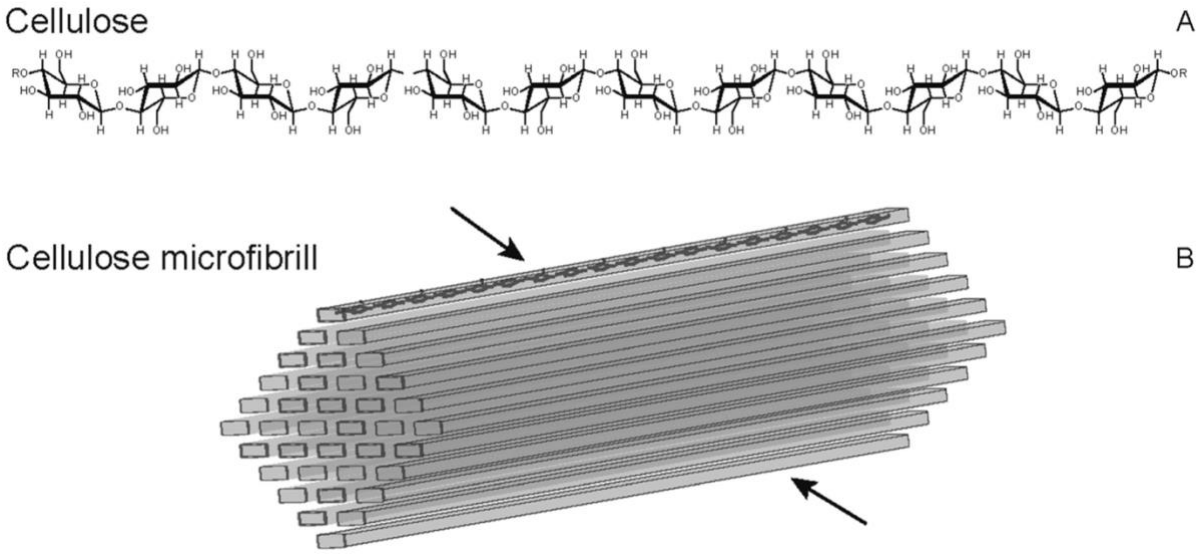

Figure 1.3.1. A structural overview of a cellulose chain (A) and a cellulose microfibril (B). Both arrows show hydrophobic faces of the microfibril. This figure is taken from Horn et al. (2012).

1.3.2 Hemicelluloses

Hemicelluloses show, in contrast to cellulose, large variations, both between plant species, but also in the same plant. Most hemicelluloses have a β - 1,4 linked backbone and are generally less recalcitrant than cellulose (Zoghlami & Paës, 2019). Although certain hemicelluloses like xylans and glucomannans are often branched and acylated, making them recalcitrant and hard to degrade (Forsberg, 2014).

Xyloglucans, xylans, mannans, glucomannans, and mixed β -1,3(4)-linked glucans are all hemicelluloses with different compositions (Forsberg, 2014). These hemicelluloses are found

in the plant cell walls in all terrestrial plants, except β -1,3(4)-linked glucans, which are only found in Poales and a few other select groups (Scheller & Ulvskov, 2010). The relative abundance and occurrence of these hemicelluloses can vary between plant tissues, cell wall layers and species. Xylans are the most abundant hemicelluloses found in hardwoods (angiosperms), while glucomannans are the other most abundant hemicellulose found in softwoods (gymnosperms). Xyloglucans, mannans and mixed β -1,3(4)-linked glucans are also important hemicelluloses in the plant cell walls.

Since xylan and glucomannan are the most common hemicelluloses, xylan-specific and glucomannan-specific enzymes are among the most studied enzymes that act on hemicellulose (Østby et al., 2020). However, recent studies on LPMOs show that some of these enzymes act on hemicelluloses as well as other recalcitrant polysaccharides. These LPMOs, mainly in family AA14 and AA9, cleave the polysaccharide backbones, which help to liberate the cellulose from hemicellulose. Some of these LPMOs are active on isolated hemicellulose, while others are only active on hemicellulose bound with cellulose (Østby et al., 2020).

With efficient enzymes that can break down hemicelluloses, hemicelluloses can also be used in the industry, together with cellulose. However, the disadvantage of hemicelluloses is that degradation yields a mixture of sugars and these contain pentoses that are difficult to ferment (Horn et al., 2012). Regardless, the industry needs efficient and cost-effective ways to degrade hemicelluloses to release the cellulose chains for further degradation. Therefore, LPMOs working on both hemicelluloses alone and hemicelluloses bound with cellulose can be a gamechanger in industrial degradation.

1.4 Enzymes

Enzymatic degradation of carbohydrates is the most efficient method to convert biomass into monomer sugars (Van Dyk & Pletschke, 2012). The advantage of converting biomass with the use of enzymes is that it preserves the original carbohydrate structure, compared to a thermochemical conversion that destructs the carbohydrate structure (Horn et al., 2012).

To degrade carbohydrates, multiple enzymes are used. These enzymes act together on the substrate in content, making the degradation more efficient that what is achievable with single

enzymes (Van Dyk & Pletschke, 2012). Several microorganisms have evolved enzymatic machineries to degrade recalcitrant polysaccharides in nature, with fungi being the primary lignocellulose degraders (Sanchez, 2009). By studying microbial enzyme systems, industrial enzyme cocktails can be designed for biomass saccharification.

In industry, an enzyme cocktail with several enzymes working in synergy is commonly used. However, the main problem with the enzymatic degradation of polysaccharides is that the polysaccharides are challenging to degrade because of their crystallized structure. Different pretreatment methods can therefore be used to make the enzymatic degradation more efficient.

Some of the most used pretreatment methods are wet oxidation, hydrothermal pretreatment, steam explosion, dilute acid treatment, ammonia fibre expansion, and sulfite pulping (Østby et al., 2020). These methods make the polysaccharide more assessable for the enzymes. On the other hand, the need for pretreatment makes the progress less efficient and more expensive, and it is therefore desirable to find enzyme cocktails that require as little pretreatment as possible.

1.4.1 Carbohydrate active enzymes

Carbohydrate-Active enzymes (CAZymes) are enzymes that act on carbohydrate substrates. These enzymes are involved in the synthesis, degradation, and modification of all carbohydrates, making them extremely important (Si-Quiang Ye, 2020). To break down the carbohydrates, the enzymes must have high specificity, but because of the minor variation between some of the carbohydrates, this can be a challenge when the enzymes are used in industry (Cantarel et al., 2009).

According to CAZy database classification (Lombard et al., 2014). CAZymes are currently divided into five classes: Glycoside hydrolases (GHs) which hydrolytically cleave glycosidic bonds, glycosyltransferases (GTs) which are involved in the synthesis of glycosidic bonds from phospho-activated sugar donors (Forsberg, 2014), carbohydrate esterases (CEs) which remove ester-based modifications, and polysaccharide lyases (PLs) that non-hydrolytically cleave glycosidic bonds (Forsberg, 2014). Finally, auxiliary activities (AAs), which include

LPMOs (see later), are a redox enzymes that act in concert with other CAZymes (Si-Quiang Ye, 2020). In addition, carbohydrate-binding modules (CBMs), are also categorized in the CAZy database, which are non-catalytic binding modules which bind various carbohydrates (Forsberg, 2014).

Even though the CAZy database consists of a big number of enzymes, the number of CAZymes families are still growing, and the database will most likely continue to expand. The families are grouped based on a common fold, catalytic machinery, and the same mechanism (Cantarel et al., 2009). Therefore, enzymes that act on different substrates can be grouped in the same family, and enzymes that act on the same substrate can be found in several families.

1.4.2 Enzymatic degradation of cellulose

In industrial applications, the first step in utilizing lignocellulosic biomass is often a pre-treatment to open the plant cell wall to make the polysaccharides more accessible to enzymatic digestion. Different approaches can be taken, including physical, chemical, thermal or enzymatic in order to remove lignin and/or hemicelluloses (Chandra et al., 2016). After pre-treatment, an enzyme cocktail is typically used to depolymerize cellulose and/or hemicelluloses.

The classical scheme for cellulose degradation consists of three classes of enzymes that act in synergy. First, the endo-acting enzymes (Endo- 1,4- β-glucanases) cleave internal bonds in the cellulose chain, generating new reducing and non-reducing chain ends for the exo-acting enzymes (Exo-1,4- β-glucanases). Then, the exo-acting enzymes release cellobiose by attacking the reducing or non-reducing cellulose ends. Finally, β-glucosidases convert the cellobiose to glucose (Horn et al., 2012).

This traditional approach to enzymatic degradation has some challenges. For example, that the conversion yields are typically far below 100%, and the need for pre-treatments adds a significant energy cost. Therefore, there is great interest in industry to increase efficiency and reduce energy costs in enzymatic degradation of lignocellulose.

1.5 Lytic Polysaccharide Monooxygenases

In 2005, enzymes degrading chitin with the help form a CBP21 protein were discovered from the gram-negative bacterium *Serratia marcescens* (Vaaje-Kolstad et al., 2005). This enzyme (CBP21) was classified as a family 33 carbohydrate-binding module (CBM33) in the CAZy database, and genes coding this family is common in bacteria and some viruses. An enzyme family (GH61) commonly found in fungi, which was previously known to display similar boosting effects with cellulases, was in 2008 shown to have a similar fold to the CBP21 enzyme (Karkehabadi et al., 2008).

Enzymes in both CBM33 and GH61 families were shown to have flat substrate-binding surfaces, and in 2010, researchers discovered that they cleave polysaccharide chains in an oxidative manner. This mechanism is dependent on a divalent metal ion and an electron donor (Horn et al., 2012). When the glycosidic bonds in chitin are cleaved, a non-reducing chain end and a chain end with a C1 oxidized sugar are generated, making it more assessable to other enzymes (Horn et al., 2012).

Following the discovery of CBP21 as an oxidative enzyme, a bacterial enzyme (CelS2) that potentiated hydrolysis by cellulase in the same manner as CBP21 degraded chitin was described (Horn et al., 2012), and was shown to oxidize cellulose at the C1 position. Several studies on these enzymes concluded that they were copper-dependent, and were collectively named “lytic polysaccharide monooxygenases” (LPMOs)(Horn et al., 2012) (Chylenski et al., 2019).

After the discovery of the catalytic function of these enzymes, they were reclassified as auxiliary activities, and CBP21 and CelS2 were placed in family 10 (AA10) and GH61 in family 9 (AA9) (Chylenski et al., 2019). Until recently, the CAZy database consisted of 7 LPMO families, AA9, AA10, AA11, AA13, AA14, AA15, and AA16. Where AA9 is produced in fungi and works on cellulose and hemicellulose, AA10 is produced in bacteria, plants, and viruses and cleaves cellulose and chitin. AA11, AA13, and AA14 are produced in fungi and break down chitin, starch, and xylan respectively. AA15 is primarily found in insects, oomycetes and a variety of alae and cleave cellulose, while AA16 cleave cellulose and is found primarily in fungus and oomycotes.

These LPMO families have great variations in how they attack recalcitrant polysaccharides, but all the LPMO enzyme families act on the cell wall and degrade cell wall components. However, in addition to the seven families mentioned, a new LPMO family was identified in 2021, as the AA17 family produced in oomycote. These LPMOs does not cleave traditionally LPMO substrates, most likely because of the lack of a flat binding surface. Instead, AA17 works on pectin (Sabbadin et al., 2021).

Since the discovery of LPMOs, the interest in these enzymes has continued to increase because of their promising results and putative applications. Today, several LPMOs have yet not been characterized, therefore, it is important to continuously characterize these enzymes. Characterization studies provide important information on how LPMOs work, moreover, it gives the biorefining industry new LPMO candidates for more efficient and specific degradation.

In addition to biomass degradation, it is also suggested that LPMOs have different roles in nature, for example, to serve as a viral virulence and bacterial pathogenicity. Furthermore, it has also been suggested that the AA15 can play a role in the development and food digestion (Forsberg et al., 2019). These findings are still being studied, but it is likely that several LPMOs have numerous biological roles.

1.5.1 LPMO9 structure

The flat LPMO structure is very different from the GHs, that have a binding site described as groove, cleft, or tunnel (Hamre et al., 2017). Although most LPMO9s consist of a flat substrate-binding site, the surface can vary in both size and shape (Chylenski et al., 2019). Because of this, LPMO9s also have varying substrate specificities, as well as varying oxidative regioselectivity (Chylenski et al., 2019). Therefore, some exclusively oxidize either the C1 or the C4 carbon in the glycoside bond, while others can oxidize both C1 and C4 carbons (Chylenski et al., 2019).

The histidine brace with the copper ion has also high variations. However, the overall fold in LPMO9s is conserved. The substrate-binding surface includes two conserved histidines that

coordinate a single copper atom in a histidine brace, one of them being an N-terminal histidine (Vaaje-Kolstad et al., 2017) This N-terminal histidine carries a methylation that most likely aid to protect the LPMOs from oxidative damage (Quinlan et al., 2011). In addition to the histidine brace, there is a second coordination sphere, that accommodates the coordination of the co-substrate and helps in shaping the active site. In all LPMO9s, both the histidine brace and the tyrosine in the protein-facing axial position are highly conserved (Borisova et al., 2015).

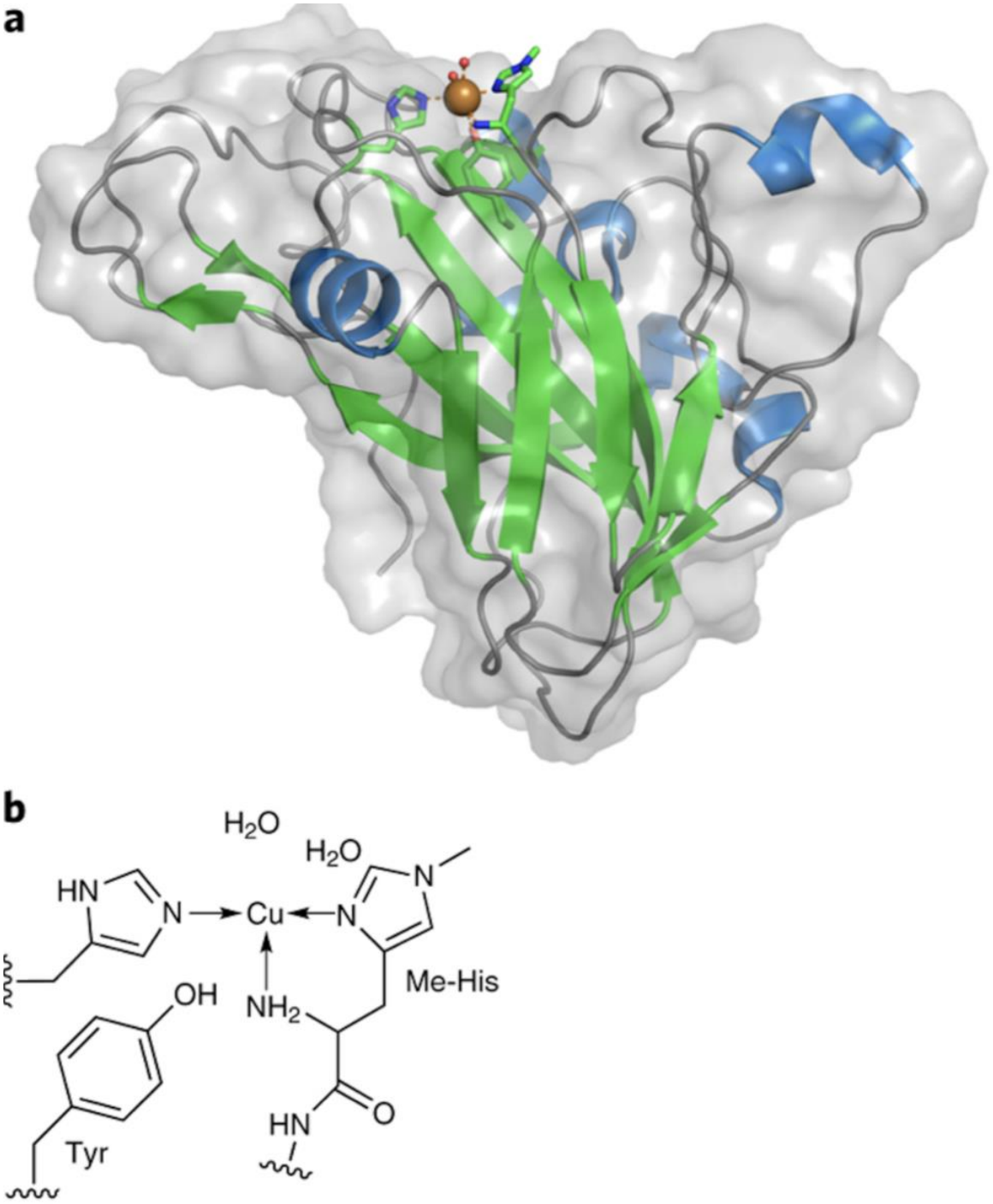

Figure 1.5.1. Structure of a typical LPMO9 together with a representation of the active site. (a) Overall structure of AA9 LPMO from *Thermoascus aurantiacus*. The secondary structure elements are shown in green (β-sheets), blue (α-helixes) and grey (loops). The active site copper is shown as a sphere and the active site residues are shown as sticks. **(b)** Schematic representation of the copper active site observed in LPMO9s. (Hemsworth et al., 2014).

The core in the LPMO9s consists of a β-sandwiches, which are made up of β-sheets that again consist of β-strands. Loops and short helices connect the antiparallel strands. The loops have different numbers of α-helix insertions, and because of variation between the loops, the substrate-recognizing surface is different between different LPMO9s (Forsberg, 2014). For

example, the long “L2” region shows large variation, making this region important in determining substrate specificity (Vaaje-Kolstad et al., 2017). Other region that shows large variations are the LS, and LC loops. Additionally, LPMO9s that only oxidize the C4 carbon also contain an insertion, the L3 loop (Borisova et al., 2015). This loop may affect the substrate-binding surface. As a result of these variations, LPMO9s have different substrate specificities even though they are in the same family.

In addition to a catalytic domain, some LPMO9s consist of one or more carbohydrate-binding modules (CBMs) that are often connected by a flexible linker (Tuveng et al., 2020). CBMs bind to the polysaccharide and bring the catalytic domains closer to the target substrates (Forsberg, 2014). Some LPMO9s contain one, or occasionally more than one CBM, and other LPMO9s do not contain any CBMs at all. The presence of CBMs in the catalytic domain of the enzymes can change the affinity for different substrates, making differences in substrate specificity among the LPMOs. Different LPMOs also show differences between redox stability, and CBMs can play a role in these differences (Østby et al., 2020).

1.5.2 LPMO catalytic mechanism

In short, the LPMO catalytic mechanism is induced when the flat surface of the LPMO is connected to the flat surface of the crystallized polysaccharide. A big advantage of LPMOs is that they can act on the surface of insoluble substrates which improves the accessibility for hydrolases. Without LPMOs, the degradation in the recalcitrant parts of the substrate would happen much slower, or not happen at all (Chylenski et al., 2019). The reduction of the copper co-factor is also necessary for the reaction.

Initially, it was believed that LPMOs were monooxygenases that used molecular oxygen (O_2) as co-substrate, requiring two electrons and two protons to complete a catalytic cycle. However, in 2016, Bissaro et al. (2017) showed that H_2O_2 can be used as a co-substrate instead of O_2, which leads to an increased reaction rate. The advantage of the peroxygenase reaction over the monooxygenase reaction is that H_2O_2 requires less amount of reductant to reduce the LPMO to the Cu(I) state, which is the active state (Østby et al., 2020). In the O_2 driven mechanism, a reduction of Cu(II) is required for each catalytic circle, while in the

H_2O_2 mechanism, the copper stays reduced for several cycles after the catalysis, as shown in Figure 1.5.2.

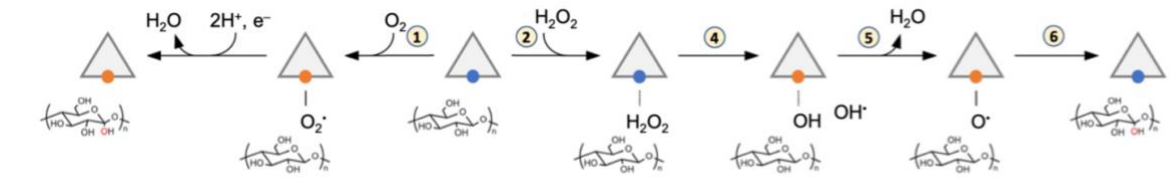

Figure 1.5.2. The figure shows both O_2 driven catalysis (left) and H_2O_2 driven catalysis (right) after initial reduction. The triangles represent LPMOs, while the orange dots represent Cu(II) and the blue dots represent Cu(I). When using oxygen as a co-substrate, the reduced LPMO reacts with the substrate forming a superoxide. Then, one hydrogen atom from C1 or C4 is abstracted, and one hydroxyl group is added to the substrate. This proses requires electrons and protons together with oxygen, and water is released in the final step. On the other hand, the H_2O_2 driven catalysis does not require protons and electrons, besides the copper stays in the reduced state after the reaction, allowing it to start a new circle without a reducing power (Østby et al., 2020). In step 4, the O-O bound in the H_2O_2 is broken and in step 5 an oxyl intermediate is formed. Then, one hydrogen atom can be abstracted before a hydroxyl group is added to the substrate radical and the binding is broken because of unstable structure. Note that both the reactions schemes are only possible reaction schemes as the mechanism is not fully understood yet.

The monooxygenase reaction can be described as $R\text{-}H + O_2 + 2e^- + 2H^+ \rightarrow R\text{-}OH + H_2O$, where R-H is the carbohydrate substrate (Bissaro, Streit, et al., 2020). This reaction occurs when the LPMOs act on a carbohydrate substrate with a reductant. Only one oxygen from O_2 is used in the final product, hence the name "monooxygenase". In this reaction, the LPMO also requires two electrons and two protons to catalyse the reaction. The disadvantage of this is, when the LPMOs are bound to a polysaccharide substrate, the access of reductants to the active site is limited. This disadvantage is reduced when using H_2O_2 as a co-substrate, making the reaction $R\text{-}H + H_2O_2 \rightarrow R\text{-}OH + H_2O_2$ (Bissaro, Streit, et al., 2020). When H_2O_2 is used instead of O_2, it provides oxygen, electrons, and protons to the reaction, making the need for a second electron and proton unnecessary (Bissaro, Streit, et al., 2020).

As previously mentioned, LPMOs can either oxidize the C1 or the C4 carbon, while some LPMOs show mixed C1/C4 oxidation. When the C1 carbon is oxidized, the result is the formation of 1,5-δ-lactones that are hydrated spontaneously to a more stable aldonic acid

form. On the other hand, oxidation of the C4 carbon results in 4-ketoaldoses that again are hydrated to their corresponding gemdiol form, as shown in Figure 1.5.3 (Tuveng et al., 2020).

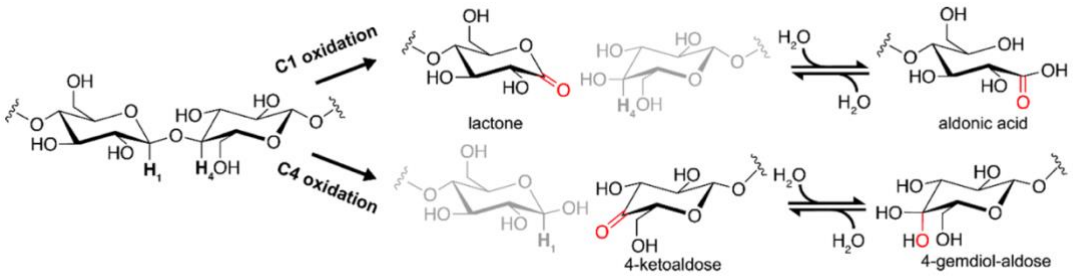

Figure 1.5.3. Aldonic acid and 4-gemidol-aldose are produced when LPMOs degraded cellulose. Aldonic acid is produced when C1 is oxidized, while 4-gemidol-aldose is produced when C4 is oxidized. This figure is taken from Chylenski et al. (2019).

LPMOs that oxidize C1 generate optimal ends for CBH2 which is cellobiohydrolases that attack the non-reducing cellulose chain end, while LPMOs that oxidize C4 generate optimal ends for CBH1which is cellobiohydrolases attacking the reducing end on the cellulose chain (Horn et al., 2012).

1.5.3 H_2O_2 or O_2 driven reaction of LPMOs

There is still a debate whether LPMOs are monooxygenases or peroxygenases. Some claim that the peroxygenase reaction is less specific than the monooxygenase reaction, thus indicating that LPMOs are monooxygenases (Rieder et al., 2021). In addition to this, it is also claimed that high concentrations of H_2O_2 lead to more enzymatic damage, compared to a high concentration of O_2 (Rieder et al., 2021).

However, Chen et al. (2021) state that LPMO9s are less exposed to oxidative damage in the H_2O_2 driven reaction. It is also known that LPMOs can produce H_2O_2 from molecular oxygen *in situ* when they are not bound to a substrate, as shown in Figure 1.5.4. Moreover, when the LPMOs are bound to a substrate, the production of H_2O_2 is reduced, indicating that the H_2O_2 is used in the reaction where the copper reacts with H_2O_2 or O_2, generating an oxygen species.

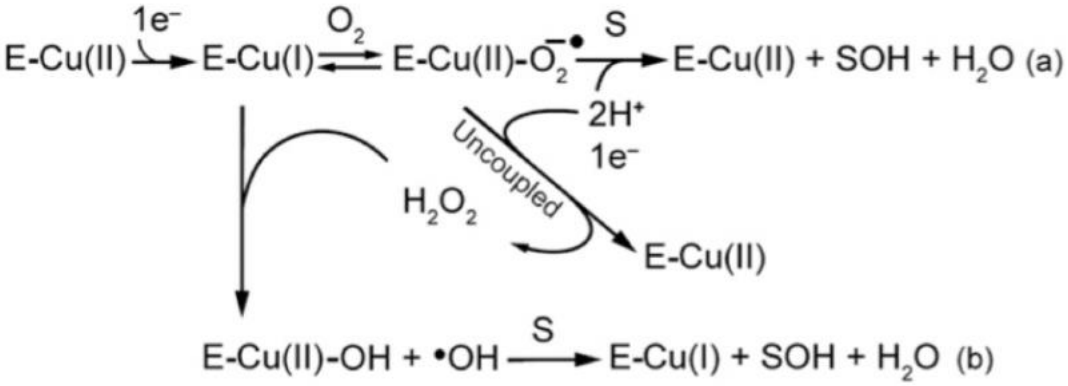

Figure 1.5.4. Reaction scheme for LPMO reactions. The LPMOs are described as E and the polysaccharide substrate as S. O_2 binds to the reduced Cu(I) in the active site. This leads to substrate hydroxylation in the presence of a polysaccharide substrate (pathway **a**), or production of H_2O_2 in the absence of a polysaccharide substrate. This *in situ* produced H_2O_2 can react with the reduced Cu(I) active site and oxidize the substrate when a polysaccharide substrate is bound (pathway **b**) (Hangasky et al., 2018).

In addition to Rieder and Chen et al findings, Bissaro et al. (2020) have shown that the reoxidation of LPMO-Cu(I) to LPMO-Cu(II) is 2,000-fold faster with H_2O_2 than with O_2. These studies show that LPMOs can use H_2O_2 as a co-substrate, but until further notice, it is still not proven that H_2O_2 is the preferred or only co-substrate, or that all LPMOs prefer the same co-substrate.

In closing, even though LPMOs require oxygen, either from O_2 or from H_2O_2 to catalyse the reaction, large quantities of oxygen inactivate the LPMOs in both O_2 and H_2O_2 driven reactions. This happens because oxygen generates oxygen species that damage the residues near the catalytic copper ion (Chen et al., 2021).

1.5.4 *Nc*LPMO9C

*Nc*LPMO9C from *Neurospora crassa* is a well characterized LPMO9, with a known crystal structure, that acts on both cellulose oligomers, and non-cellulose β-glucans (Borisova et al., 2015). The enzyme degrades the substrate by cleaving the β-1,4-glycosidic bonds (Dimarogona & Sandgren, 2016). Since *Nc*LPMO9C is a C4 oxidizing LPMO, it cleaves the substrates leaving the nonreducing end oxidized. A reason why *Nc*LPMO9C is of special interest, is because it can act on soluble substrates, unlike many other LPMOs. Since

*Nc*LPMO9C is one of the most studied LPMOs, it is also commonly used in comparative studies with other LPMOs.

N. crassa is a filamentous fungus, commonly found in nature, that produces several LPMOs and GH enzymes that depolymerize plant cell wall components. The *N. crassa* genome carries 14 LPMO9s, 6 of which have a family 1 carbohydrate-binding module (CBM1), including *Nc*LPMO9C (Petrović et al., 2019).

*Nc*LPMO9C consists of two domains: an N-terminal catalytic LPMO9 domain and a CBM1. The CBM1 is connected to the LPMO domain by a serine- and threonine-rich linker of about 50 amino acid residues (Borisova et al., 2015). The catalytical domain consists of a highly polar substrate-binding surface, like many other LPMOs. *Nc*LPMO9C also has a common LPMO core, with β-sheets forming a β-sandwich fold with loops sticking out. The N-terminal histidine, together with His83, coordinates the copper ion. The hydroxyl group to a tyrosine (Tyr166) occupies the axial coordination positions, which shapes the copper-site that is in the centre of the flat surface (Dimarogona & Sandgren, 2016).

The catalytic domain (Figure 1.5.5) consists of 227 amino acids and has a predicted molecular weight of 23.3 kDa, whereas the full-length protein (with CBM1) has a predicted mass of 35.8 kDa. In addition to this, the sequence allows both o- and n-glycosylations, so the observed molecular weight is often higher than this.

Studies on *Nc*LPMO9C conclude that the substrate-binding surface together with the CBM1 module is the reason why *Nc*LPMO9C works as efficiently as it does (Petrović et al., 2019). Because the substrate-binding surface is extended and highly polar, *Nc*LPMO9C can bind to complex and branched polysaccharides, for example, xyloglucan (Borisova et al., 2015). This makes the *Nc*LPMO9C of special interest to the industry.

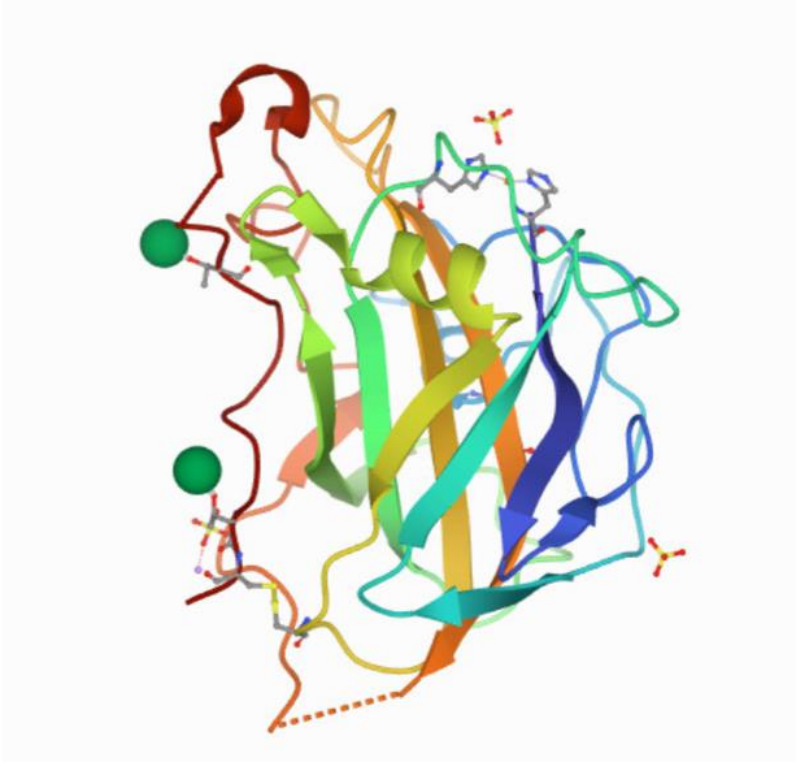

Figure 1.5.5. Crystal structure of the 4D7U catalytic domain of *Nc*LPMO9C, taken from RCSB Protein Data Bank (Borisova et al., 2015). The molecular weight of the catalytic domain is 23.3 kDa and the protein sequence consists of 227 amino acids.

1.5.5 *Sc*LPMO9A

*Sc*LPMO9A is a cellulose-active C4 oxidizing LPMO9 from the grey-rot fungus *Schizophyllum commune.* The catalytic domain consists of 228 amino acids and has molecular weight of 24.5 kDa, without the signal-peptide. The theoretical pI is 4.63 and the molar extinction coefficient is 51005 M^{-1} cm^{-1} as calculated using the ExPASy server (Gasteiger et al., 2003). In contrast to *Nc*PMO9C, *Sc*LPMO9A does not have a CBM domain, even though they both work on soluble substrates. Another difference between *Sc*LPMO9A and *Nc*LPMO9C is that are not found in the same fungi, indicating that they play somehow different roles in nature.

S. commune is a basidiomycete fungus that causes white-rot on woody biomass. The singular does not only secrete LPMO9s, but also other carbohydrate degrading enzymes like cellulose hydrolases, xylanases, and endoglucanases. Over 150 genera of woody plants act as substrates for *S. commune*, in addition to softwood and grass silage (Tovar-Herrera et al., 2018). In addition to this, *S. commune* can degrade all the components of lignocellulosic biomass, with

a genome that contains 240 gene candidates for glycoside hydrolases, revealed in 2010 when the genome sequence was published (Tovar-Herrera et al., 2018). The sequencing also showed presence of 22 genes encoding LPMO9s (Kües et al., 2010). Hence, there is no doubt that *S. commune* is an important biomass degrader in nature, and by adopting the efficient enzyme machinery to *S. commune* in the industry, products like bioethanol can be produced more efficiently and cost friendly.

In contrast to *Nc*LPMO9C, *Sc*LPMO9A has not been well characterized, and only a single study has been done on this enzyme (Frandsen et al., 2021). However, it has been shown that *Sc*LPMO9A also acts on soluble substrates, like *Nc*LPMO9C. Therefore, it is of interest to compare these enzymes.

1.6 The aim of this study

Because of the major industrial and scientific interest in LPMOs, it is important to obtain a better understanding of how these enzymes work and under which conditions they are most efficient. Their ability to increase saccharification yield makes them highly interesting. However, it is still several LPMOs that have not been characterized and studied.

By comparing *Sc*LPMO9A with the more studied *Nc*LPMO9C, similarities and differences between the enzymes can be found, with the differences being of main interest. These insights into how the LPMOs work can become a driving force for developing more efficient enzyme cocktails for biomass hydrolysis. In addition to a reduction in the costs of lignocellulosic ethanol production (Rodrigues et al., 2017).

Since the discovery of LPMOs, there has been a great interest in understanding why there are so many LPMOs in nature and their biological relevance. Since both *Sc*LPMO9A and *Nc*LPMO9C works on soluble substrates, they can be used to study functional differences and to obtain an insight into how these differences affect the biological roles of the enzymes.

During the course of the characterization of *Sc*LPMO9A undertaken by our group, a study comparing several LPMO9s, including *Sc*LPMO9A, was published (Frandsen et al., 2021). The initial substrate screenings on various hemicelluloses had already revealed activity of

*Sc*LPMO9A on xyloglucan and glucomannan, in contrast to what was reported by Frandsen et al. It was therefore considered worthwhile to pursue the functional characterization of this LPMO. Indeed, as part of the present study, activity of *Sc*LPMO9A was also demonstrated on cellotetraose, on which Frandsen et al. did not detect activity.

2 Materials

2.1 Equipment and materials

Table 2.1.1 shows an overview of equipment and materials used throughout the laboratory work.

Table 2.1.1. Overview of equipment and materials, along with the manufacture, used to perform the methods described in Section 3.

Category	Equipment	Manufacture
Appliance	Autoclave (Certoclav sterilizer A-4050)	Certoclav
	Freezer, -20 °C	Bosch
	Freezer, -80 °C	Sanyo
	Incubator	Termaks and Infors
	Laminar Flow Workbench	Azbil Telstar
	MasterFlex L/S Economy drive	Cole-Parmer
	Milli-Q Direct water purification system	Merck Millipore
	Ultrospec 10 Cell Density Meter	Biochrom
	Refrigerator, 4 °C	Bosch
	Sonics Vibra-Cell Ultrasonic Processor	Sonic & Materials, Inc
	ThermoMixer C	Eppendorf
	Vortex	IKA
	Viva Flow 2000	Sartorius

	Vivaspin 20 Sentrifugal concentrator 10.000 MWCO PES membrane	Sartorius
	Weight (Sartorius)	VWR
	Water bath, 100 °C	Stuart
Centrifuges and rotors	Avanti J-26S XP Centrifuge	Beckman Culter
	Cellstar Centrifuge tubes 15 mL, 50 mL and 1 L	Greiner bio-one
	F9-6x1000 LEX rotor to Sorwall centriguge	Thermo Scientific
	F21-8x50y rotor to Sorwall centrifuge	Thermo Scientific
	Galaxy mini star centrifuge	VWR
	JA10 rotor to Avanti centrifuge	Thermo Scientific
	JA 25 rotor to Avanti centrifuge	Thermo Scientific
	Mini centrifuge, MiniStar	Thermo Fisher
	Multifuge X1R Centrifuge	Thermo Scientific
	Spin MS 3 basic centrifuge	IKA
	Sorwall LYNX 6000 Centrifuge	Thermo Scientific
Filtration equipment	Filter Upper Cup 250 mL bottle top filter 0.22 µm PES membrane	VWR
	Filter Upper Cup 250 mL bottle top filter 0.45 µm PES membrane	VWR
	Filtropur S 0.22 µm PES membrane	Sarstedt
	Membrane dry vacuum pump/compressor	VWR
	Syringe 2 mL	BD emerald
	Syringe Filtration Unit, Filtropur S 0.45 µm PES Membrane	BD emerald

Gel equipment	Benchtop UV Transilluminator	UVP
	Electrophoresis Cell, Mini-PROTEAN Tetra Vertical Electrophoresis System	Bio-Rad
	Electrophoresis System, Mini-Sub Cell GT Horizontal	Bio-Rad
	Gel Casting Tray	Bio-Rad
	Gel Imaging System, Gel Doc EZ	Bio-Rad
	Power Supply, PowerPac 300	Bio-Rad
	Precast SDS Gels, Mini-PROTEAN TGX Stain- Free	Bio-Rad
	Stain-Free Sample Tray	Bio-Rad
Instruments and columns	AKTAprime plus	BE healthcare Bio-Science AB
	AKTApurifier with Frac-920, box-900, UPC-900, and P-900	BE healthcare Bio-Science AB
	BioPhotometer	Eppendorf
	Eppendorf BioPhotometer	VWR
	HiLoad 16/600 Superdex 75 pg column	Cytiva
	HiTrap DEAF FF column	Thermo Scientific
	HiTrap Phenyl FF column	Thermo Scientific
	Nanophotometer C40	Implen
	PD-10-columns	Cytiva
	pH Meter, 827 pH Lab	Metrohm
	Ultraspec 10 cell density meter	Biochrom
	UV/vis spectrometer	Agilent Technologies
	Varioskan lux	Thermo Scientific
HPLC Equipment	Carbopac PA200 column (3x250) 10 μM particles	Dionex, Thermo Scientific

	Carbopac PA200 guard column (3x50)	Dionex, Thermo Scientific
	Dionex UltiMate 3000 Autosampler	Thermo Scientific
	Dionex Ultimate 3000 RSLC	Thermo Scientific
	Dionex Ultimate 3000 RS Columns compartment	Thermo Scientific
	Dionex UltiMate 3000 Pump	Thermo Scientific
	ICS 5000	Thermo Scientific
	MultiScreen 96-Well Plates	Millipore
	PE-Snapring cap 11 MM	VWR
	Refractive Index Detector Shodex R1-101	Shodex
	Rezex ROA-Organic Acid H+ (8%) (300x7.8 mm)	Phenomenex
	Snap Ring Micro-Vial (0.3 mL PP)	VWR
	3 x 250 mm CarboPac PA200 analytical column	Dionex, Thermo Scientific
Miscellaneous Equipment	Beakers 100 and 250 mL	VWR
	Cultivation flasks 500, 1000 and 2000 mL	Duran Group
	Cuvettes (disposable)	Brand
	Cuvettes (glass)	Eppendorf
	Glassware	Duran Group
	Inoculation loops	Sarstedt
	Magnet, Teflon Stirring Bar	SP scienceware
	Magnetic Stirrer, RCT Basic	IKA
	Measuring cylinders 10, 25, 50, 100, 250 and 500 mL	Duran Group
	Micro test tube rock	Brand
	Parafilm	Bemis
	Pipettes	Thermo Scientific

	Pipettes (plastic)	VWR
	Pipette tips	Sarstedt AG & Co
	Sealing tape	Thermo Scientific
	Serological pipettes	Sarstedt
Tubes, Vials, and Plates	Eppendorf tubes 1.5 mL	Eppendorf
	PCR tubes 0.2 mL	Axygen
	Petri dishes 90 mm	Heger
	Screw cap micro tube (2 mL)	Sarstedt

2.2 Chemicals

Table 2.2.1 shows the chemicals used in this study.

Table 2.2.1. Chemical compounds used to perform the methods described in Section 3, along with the manufacture.

Compound	Manufacture
Acetic acid (glacial) (CH_3COOH)	EMSURE
Acetonitrile (ACN) (C_2H_3N)	Sigma-Aldrich Corporation
Agar powder ($C_{14}H_{24}O_9$)	Sigma-Aldrich Corporation
Ampicillin, Sodium salt ($C_{16}H_{18}N_3NaO_4S$)	Sigma-Aldrich Corporation
Ammonium sulfate ($(NH_4)_2SO_4$)	Supelco
Amplex Red (10-acetyl-3,7-dihydroxyphenoxazine)	Sigma-Aldrich Corporation
Ascorbic acid ($C_6H_8O_6$)	Sigma-Aldrich Corporation
Bacto Yeast extract	BD emerald
Bacto Tryptone	BD emerald
Bis-Tris ($C_8H_{19}NO_5$)	VWR
Copper sulfate ($CuSO_4$)	VWR
Ethanol absolute (C_2H_5OH)	VWR
Ethylenediaminetetraacetic Acid ($C_{10}H_{16}N_2O_8$)	Merck
Glucose ($C_6H_{12}O_6$)	VWR
Glycerol, 85% ($C_3H_8O_3$)	Merck

Hydrochloric acid (HCl)	Merck
Hydrogen peroxide (H_2O_2)	EMSURE
Magnesium Chloride ($MgCl_2$)	Sigma-Aldrich Corporation
m-toluic acid ($C_8H_8O_2$)	Sigma-Aldrich Corporation
N,N,N´,N´- tetramethyl-1,4-phenulenediamine (TMP)	Sigma-Aldrich Corporation
Peptone from casein	VWR
Peroxidase from horseradish	Sigma-Aldrich Corporation
Piperazine-N,N´bis ($C_8H_{18}N_2O_6S_2$)	Sigma-Aldrich Corporation
Sodium acetate (CH_3COONa)	Sigma-Aldrich Corporation
Sodium chloride (NaCl)	AnalaR NormaPUR
Sodium hydroxide (NaOH)	EMSURE
Sodium phosphate (Na_3PO_4)	Sigma-Aldrich Corporation
Sucrose ($C_{12}H_{22}O_{11}$)	Sigma-Aldrich Corporation
Sulfuric acid (H_2SO_4)	Sigma-Aldrich Corporation
Trace select water	Thermo Scientific
Tris Base ($C_4H_{11}NO_3$)	Sigma-Aldrich Corporation
2,5-Dihydroxybezoinc acid (DHB) ($C_7H_6O_4$)	Sigma-Aldrich Corporation

2.3 Substrates and standards

Carbohydrate substrates and standards used in this study are shown in Table 2.3.1.

Table 2.3.1. Substrates and standards used in the laboratory work and manufacture.

Carbohydrate substrates	Manufacture
Avicel	Sigma-Aldrich Corporation
Beta-glucan	Megazyme
Cellobiose	Megazyme
Cellotetraose	Megazyme
Cellotriose	Megazyme
Cellopentaose	Megazyme

Cellohexaose	Megazyme
Konjac glucomannan	Megazyme
PASC	Made from Avicel, described in Section 2.10.1
Sulfite pulped Norway Spruce Batch DP 3319 (VASP)	Norwegian biorefining company, Borregaard AS
Xyloglucan from tamarind seed	Megazyme
Xyloglucan oligos	Megazyme

2.4 Standard solutions

Standards and solutions made by other than me, used during this study are shown in Table 2.4.1

Table 2.4.1. The table shows standard solutions, and solutions made by other than me used in the laboratory work.

Buffers, enzymes, standard solutions, and kits	Use	Manufacture
Amplex Red solution	Amplex Red Hydrogen Peroxide assay	Thermo fisher
Benchmark protein ladder	SDS-PAGE	Invitrogen
C4 oxidizing standard	ICS-5000	Prepared in-house
Glucose and cellobiose standard	Rezex-HPLC	Prepared in-house
Protein Assay Dye reagent concentrate	Bradford protein Assay	Bio-Rad
Reducing agent (10x)	SDS-PAGE	Invitrogen
Sample buffer (x4)	SDS-PAGE	Novex
Sodium phosphate buffer pH 6.0	LPMO reactions	Prepared in-house
1* Tris-Glycine-SDS buffer	SDS-PAGE	Bio Rad

1 M Tris-HCL pH 7.5	Spheroplast buffer	Prepared in-house
2,6-DMP	Breslmayr assay	Prepared in-house
20% ethanol	AKTApurifier and AKTAprime	VWR
500 mM EDTA	Spheroplast buffer	Prepared in-house

2.5 Enzymes

Table 2.5.1 shows the sequences of the enzymes used in this study, and Table 2.5.2 shows the enzymes used for synergy experiment together with *Sc*LPMO9A.

Table 2.5.1. Primary structure of LPMOs used in this work. The signal peptide of *Sc*LPMO9A and *Nc*LPMO9C is shown in green as predicted by SignalP 5.0.

Enzyme
>*Sc*LPMO9A (UniprotID: D8Q364) MVRLASLAVLGSVIATASAHTRVWGVYVNGEYQGDGIGQYVRSPPTNNPV KDLTSAAMKCNVNDAREFEVPKRVSVAGGDELSFEWYHDYRNDDIIASSH HGPIQVYMSGDDGATWTKIASDGYDTGSSTWAVDRLISAGGKHSVIIPDV PAGDYLLRAEIVALHEADVAYDQNPIRGAQNYPSCTQITVTSNGSDALPA DGVKFPGAYTDSTPGIIFNIWPPNAQDPATYQVPGPAVWDKAPGGSV
>*Nc*LPMO9C (UniprotID: Q7SHI8) MKTGSILAALVASASAHTIFQKVSVNGADQGQLKGIRAPANNNPVTDVMSSDIICN AVTMKDSNVLTVPAGAKVGHFWGHEIGGAAGPNDADNPIAASHKGPIMVYLAKV DNAATTGTSGLKWFKVAEAGLSNGKW AVDDLIANNGWSYFDMPTCIAPGQYLMRAELIALHNAGSQAGAQFYIGCAQINVT GGGSASPSNTVSFPGAYSASDPGILINIYGGSGKTDNGGKPYQIPGPALFTCPAGGS GGSSPAPATTASTPKPTSASAPKPVSTTA STPKPTNGSGSGTGAAHSTKCGGSKPAATTKASNPQPTNGGNSAVRAAALYGQCG GKGWTGPTSCASGTCKFSNDWYSQCLP

Table 2.5.2. Enzymes used in synergy experiment together with ScLPMO9A.

Enzyme	Manufacture
Celluclast cocktail	Novozymes AS
β-Glucanase	Novozymes AS

2.6 Buffers

Different buffers were used to maintain pH in all reactions. A general rule is to retain the buffer within 1.0 pH unit of the protein's isoelectric point.

2.6.1 50 mM Tris-HCl buffer pH 7.5

50 mM Tris-HCl buffer pH 7.5 was used for the anion exchange chromatography purification as buffer A when purifying *Sc*LPMO9A. The buffer was also used to concentrate the *Sc*LPMO9A sample after purification and as a buffer in desalting after copper saturation of *Sc*LPMO9A. Moreover, 50 mM Tris-HCl pH 7.5 was used as a storage buffer for *Sc*LPMO9A.

Materials:

- 6.057 g Tris Base
- MilliQ water
- 37 % HCl solution

Method:

6.057 g Tris Base was dissolved in 700 mL MilliQ water in a 1 L measuring flask with a magnet and a magnetic stirrer. Using 37% HCl solution and a pH meter, the pH was adjusted to 7.5 before MilliQ water was added to a final volume of 1 L, with a final concentration of 50 mM Tris Base. A Membrane dry vacuum pump with an 0.22 μm filter was used to filter the

solution into a 1 L blue cap bottle before the solution was stored at room temperature.

2.6.2 50 mM Tris-HCl, 1 M NaCl buffer pH 7.5

50 mM Tris-HCl, 1 M NaCl pH 7.5 was used for anion exchange chromatography purification to elute *Sc*LPMO9A. The elution happens because of the high concentration of salt in the buffer.

Materials:

- 6.057 g Tris Base
- 58.44 g NaCl
- MilliQ water
- 37% HCl solution

Method:

6.057 g Tris Base and 58.440 g NaCl were dissolved in 700 mL MilliQ water in a 1 L measuring flask using a magnet and a magnetic stirrer. Using 37% HCl solution and a pH meter, the pH was adjusted to 7.5 before MilliQ water was added to a final volume of 1 L, with a final concentration of 50 mM Tris Base and 1 M NaCl. A Membrane dry vacuum pump with an 0.22 μm filter was used to filter the solution before the solution was stored at room temperature.

2.6.3 500 mM Sodium acetate buffer pH 5.0

Sodium acetate buffer pH 5.0 buffer was used in LPMO reactions when analysing on high-performance liquid chromatography (HPLC) and high-performance anion-exchange chromatography system (HPAEC) coupled with pulsed amperometric detection (PAD).

Materials:

- 41 g sodium acetate
- MilliQ water
- Acetic acid

Method:

41 g sodium acetate was added to a 1 L measuring flask before MilliQ water was added to 1 L. Then, 700 mL was transferred to a beaker and the pH was adjusted to 7.5 with acetic acid and a pH meter. A Membrane dry vacuum pump with an 0.22 µm filter was used to filter the solution into a 1 L blue cap bottle before the solution was stored at room temperature.

2.6.4 50 mM and 250 mM Bis-Tris-HCl Buffer pH 6.5

Bis-Tris-HCl buffer pH 6.5 was used in Breslmayr and Amplex Red Hydrogen Peroxide assay. The buffer was also used for hydrophobic interaction chromatography (HIC) to elute *Nc*LPMO9C. In addition, 50 mM Bis-Tris-HCl buffer pH 6.5 was used to concentrate *Nc*LPMO9C after size exclusion chromatography (SEC), copper saturation of *Nc*LPMO9C and to store *Nc*LPMO9C.

Materials:

- 10.46/52.31 g Bis-Tris
- MilliQ water
- 37% HCl solution

Method:

To prepare 50 mM Bis-Tris, 10.46 g Bis-Tris was dissolved in 700 mL MilliQ water in a 1 L measuring flask with a magnetic stirrer. The pH was adjusted to 6.5 using 37% HCl solution and a pH meter. After that, MilliQ water was added to a final volume of 1 L, with a final concentration of 50 mM Bis-Tris. The solution was filtered with an 0.22 µm filter and a membrane dry vacuum pump and stored at room temperature.

In the reactions that required a final concentration of 50 mM Bis-Tris-HCl buffer pH 6.5, a 250 mM buffer was used instead of a 50 mM buffer. The method to prepare this was similar, but for 250 mM it was used 52.31 g Bis-Tris instead of 10.46 g.

2.6.5 50 mM Bis-Tris-HCl buffer pH 6.5, 50% ammonium sulfate

50 mM Bis-Tris-HCl buffer pH 6.5 with 50% ammonium sulfate was used for hydrophobic interaction chromatography to load *Nc*LPMO9C. Because of the high concentration of ammonium sulfate, the hydrophobic regions on the surface of the proteins are exposed, and therefore, the proteins can bind to the hydrophobic column.

Materials:

- 9.42 g Bis-Tris
- 285.90 g Ammonium sulfate
- 37% HCl solution
- MilliQ water

Method:

9.42 g Bis-Tris was added to a 1 L beaker before MilliQ water was added to 750 mL, then the solution was mixed with a magnetic stirrer. When the Bis-Tris was fully dissolved, the pH was adjusted to 6.5 with a pH meter and 37% HCl solution. Next, MilliQ water was added to 900 mL to a final concentration of 50 mM Bis-Tris, before 285.90 g ammonium sulfate was added to the solution to a final concentration of 50%. The solution was again mixed with a magnetic stirrer before it was filtered with an 0.22 µm filter and a membrane dry vacuum pump into a 1 L blue cap bottle. The buffer was stored at room temperature.

2.6.6 50 mM Bis-Tris-HCl, 150 mM NaCl buffer pH 6.5

50 mM Bis-Tris-HCl, 150 mM NaCl pH 6.5 was used for SEC for both *Sc*LPMO9A and *Nc*LPMO9C.

Materials:

- 10.46 g Bis-Tris
- 8.76 g sodium chloride
- 37% HCl solution
- MilliQ water

Method:

10.46 g Bis-Tris and 8.76 g NaCl were added to a 1 L flask before 750 mL MilliQ water was added. The solution was mixed with a magnet on a magnet stirrer. To adjust the pH to 6.5, a pH meter was used together with 37% HCl solution. After the pH was adjusted, water was added to a final volume of 1 L and the solution was filtered using an 0.22 μm filter and a membrane dry vacuum pump. The buffer was stored at room temperature.

2.6.7 20% ethanol, 0.2 M sodium acetate

20 % ethanol with 0.2 M sodium acetate was used for washing the SEC system.

Materials:

- Ethanol absolute
- MilliQ water
- 16.41 g Sodium acetate

Method:

To prepare this buffer, 16.41 g sodium acetate was weighed and added to a 1 L flask, to a final concentration of 0.2 M sodium acetate. Then, MilliQ water was added to a volume of

800 mL, before 200 mL ethanol absolute was added, to a 20 % ethanol solution. The solution was mixed using a magnet stirrer before it was filter sterilized using a 0.22 μm filter and a membrane dry vacuum pump. The buffer was stored at room temperature.

2.6.8 200 mM PIPES buffer pH 6.0

200 mM PIPES buffer pH 6.0 was used when measuring the redox potential of *Sc*LPMO9A.

Materials:

- 6.05 g PIPES
- MilliQ water
- 10 M NaOH solution

Method:

6.05 g PIPES was added to a beaker before 75 mL MilliQ water was added. The pH was adjusted to 6.0 with 10 M NaOH solution before MilliQ water was added to 100 mL. Then, the buffer was filter sterilized with a membrane dry vacuum pump and a 0.22 μm filter. The buffer was stored at 4 °C.

2.6.9 Spheroplast buffer pH 7.5

A spheroplast buffer was used for harvesting of *Sc*LPMO9A, making the *Escherichia coli* cells shrink because of the high sugar content.

Materials:

- 85.6 g Sucrose
- 50 mL 1 M Tris-HCl
- 500 μL 500 mM EDTA
- MilliQ water

Method:

85.6 g sucrose, 50 mL 1 M Tris-HCl pH 7.5 and 50 µL 500 mM EDTA was dissolved in 400 mL MilliQ water using a magnet stirrer, to a final concentration of 50 mM sucrose, 100 mM Tris-HCl pH 7.5 and 500 µM EDTA. After the solution was dissolved, MilliQ water was added to a final volume of 500 mL before the solution was filtered with a membrane dry vacuum pump. The buffer was stored at 4 °C.

2.6.10 SDS buffer

When proteins are analysed with SDS-PAGE, all proteins must be linear and have an equal charge, and this is done with the assist of an SDS buffer.

Materials:

- 750 µL 4* sample buffer
- 300 µL 10* reducing agent
- 450 µL MilliQ water

Method:

750 µL 4* sample buffer, 300 µL 10* reducing agent, and 450 µL MilliQ water were added to a 2 mL Eppendorf tube and mixed carefully. The buffer was stored at 4 °C.

2.6.11 500 mM and 200 mM sodium hydroxide

500 mM NaOH solution was used for cleaning the Viva Flow system. 200 mM was used to stop LPMO reactions with soluble substrates.

Materials:

- 50 % Sodium hydroxide
- MilliQ water

Method:

20 mL sodium hydroxide was mixed in 480 mL MilliQ water to a final concentration of 500 mM sodium hydroxide. Then, the solution was filter sterilized using a 0.22 µm filter and a membrane dry vacuum pump. To prepare the 200 mM concentration, 200 mL of the 500 mM solution was mixed with 300 mL MilliQ water and filter sterilized. Both solutions were stored at room temperature.

2.7 Eluents for ISC-5000

Eluents used in Ion Chromatography System (ICS)-5000 were made following the protocol for the ICS system.

Eluent A

- 10.40 mL 50% (w/v) NaOH
- MilliQ water

2 L MilliQ water was transformed from a volumetric flask to an ICS eluent bottle. The eluent bottle was degassed in a Sonics Vibra-Cell Ultrasonic Processor for 20 minutes to ensure that no CO_2 was left in the bottle. Then, the bottle was connected to channel A in the HPLC, and the nitrogen flow was started. Next, the lid was opened and closed 3 times to exchange the air in the headspace before the bottle was removed. 10.40 mL 50% (w/v) NaOH were added and mixed carefully before the flask was attached to the HPLC and the air was exchanged again.

Eluent B

- 82.03 g CH_3COONa
- 5.20 mL 50 (w/v) NaOH

- MilliQ water

82.03 g sodium acetate was added to a 1 L volumetric flask before MilliQ water was added to about 700 mL. The sodium acetate was dissolved in the water by using a magnetic stirrer before water was added to 1 L. Then, the solution was filtered into an ICS eluent bottle with a 0.22 µm PES membrane vacuum filtration system. The eluent bottle was degassed in a Sonics Vibra-Cell Ultrasonic Processor for 20 minutes to ensure that no CO_2 was left in the bottle. Then, the bottle was connected to channel B in the HPLC, and the nitrogen flow was started. The lid was opened and closed 3 times to exchange the air in the headspace before the bottle was removed. Then, 5.20 mL 50% (w/v) NaOH were added and mixed carefully before the flask was attached to the HPLC and the lid was opened and closed 3 times.

Eluent C

- MilliQ water

2 L MilliQ water was added directly to the ICS eluent bottle before the bottle was degassed in a Sonics Vibra-Cell Ultrasonic Processor for 20 minutes to ensure that no CO_2 was left in the bottle. Lastly, the bottle was connected to channel C in the HPLC, the nitrogen flow was started, and the lid was opened and closed 3 times to exchange the air in the headspace.

2.8 Eluents for Rezex HPLC

5 mM sulfuric acid was used as the mobile phase in HPLC with the Rezex column.

Materials:

- 556 µL sulfuric acid
- MilliQ water

Method:

Almost 2 L MilliQ water was added to a 2 L measuring flask before 556 µL sulfuric acid was added to the water. Finally, MilliQ water was added to 2 L and the solution was poured into a 2 L blue cap bottle and attached to the HPLC.

In addition to 5 mM sulfuric acid, 20 % methanol was used as syringe wash.

2.9 Standards for ICS-5000

To convert peak area from chromatograms to concentrations, standard curves were made with the different concentrations, using oligosaccharides of different degrees of polymerization (DP). Stock solutions (1 mM) of cellobiose, cellotriose, cellotetraose, cellopentaose, and cellohexaose were prepared and diluted to appropriate concentrations for analysis.

Materials:

- 3.4 mg cellobiose
- 5.0 mg cellotriose
- 6.7 mg cellotetraose
- 8.3 mg cellopentaose
- 9.9 mg cellohexaose
- MilliQ water

Method:

All standards were made following the same protocol, but with different weights of substrate to obtain 1 mM concentration. To prepare a standard, the substrate was added to a volumetric flask before MilliQ water was added to 10 mL and mixed gently to a concentration of 1 mM substrate. 1 mL aliquots were made from the sample and stored in the freezer at -20 °C. When preparing the standards for the ICS-5000 and ISC-6000, DP2-6 were combined, in addition to different concentrations of DP2 + DP3 and DP4 for standard curves.

2.10 Substrates

2.10.1 Phosphoric acid-swollen cellulose (PASC)

PASC is an amorphous form of cellulose and can be produced by swelling microcrystalline cellulose in concentrated phosphoric acid (Stalbrand et al., 1998). Since PASC is insoluble, reactions with PASC can be stopped by filtering.

The PASC solution used in this study had a concentration of 0.9% and was prepared in-house from Avicel, as described previously (Wood, 1988), prior to this work.

2.10.2 Sulfite pulped Norway Spruce (*Picea abies*)

Norway spruce is a softwood substrate and the Sulfite pulped Norway Spruce used in this study consists of approximately 35% TS, 87% glucan, 3% xylan, 5% mannan and 3% acid insoluble lignin. Sulfite pulped Norway spruce, batch number DP 3319, was supplied by the Norwegian biorefining company, Borregaard AS, and grinded 2 x 5 seconds at 4000 rpm.

2.10.3 Cello-oligosaccharides

In this study, cellotetraose, cellopentaose, and cellohexaose were used in both single time point experiments and time course experiments. These substrates are all soluble cello-oligosaccharides, that are short-chain, linear polymers of glucose.

Materials:

- 6.7 mg cellotetraose
- 8.3 mg cellopentaose
- 9.9 mg cellohexaose
- MilliQ water

Method:

Preparation of cello-oligosaccharides are described in Section 2.9.

2.11 Cultivation Media and Agar

2.11.1 Lysogeny Broth (LB)

To cultivate bacterial strains of *E. coli*, a lysogeny broth medium was used. This medium was both used in liquid form with overnight cultures of *E. coli*, and on agar plates. Together with LB medium, 2* LB medium was also used in liquid form, to optimize the cultivation.

LB medium is a nutrient-rich complex microbial broth that contains peptides, amino acids, and carbohydrates. The medium was used for the cultivation of *E. coli* because of the tryptone and yeast nutrition that optimize the growth of *E. coli.* In addition to this, the medium also contained NaCl that contributes to osmotic balance.

Liquid LB medium

Materials:

- 10 g/L Bacto Tryptone
- 10 g/L NaCl
- 5 g/L Bacto Yeast extract
- MilliQ water

Method:

The components were mixed in 900 mL MilliQ water with a magnetic stirrer, before adding MilliQ water to a final volume of 1 L. Then, the medium was autoclaved at 121 °C for 15 minutes before it was stored at room temperature. Before the medium was used, ampicillin was added to a final antibiotic concentration of 50 μg/mL.

Agar plates

Materials:

- 5 g/L Bacto Tryptone
- 10 g/L NaCl
- 2 g/L Bacto Yeast extract
- 7.50 g/L Agar powder
- MilliQ water

Method:

The components were mixed in 900 mL MilliQ water with a magnetic stirrer, before adding MilliQ water to a final volume of 1 L. Then, the medium was autoclaved at 121 °C for 15 minutes before it was cooled down to about 50 °C. Ampicillin was added to the plates in a laminar flow workbench, to a final concentration of 50 μg/mL. Finally, the medium was poured into petri dishes and the plates were stored at 4 °C.

Liquid 2* LB medium

Materials:

- 20 g/L Bacto Tryptone
- 5 g/L NaCl
- 10 g/L Bacto Yeast extract
- MilliQ water

Method:

The components were mixed in 900 mL MilliQ water with a magnetic stirrer, before adding MilliQ water to a final volume of 1 L. Then, the medium was autoclaved at 121 °C for 15 minutes before it was stored at room temperature. Before the medium was used, ampicillin

was added to a final antibiotic concentration of 50 μg/mL.

2.11.2 Yeast extract- Peptone-Dextrose (YPD) media

To cultivate *Pichia pastoris*, a Yeast Extract-Peptone-Dextrose (YPD) medium was used. The YPD medium was both used in liquid form and on agar plates. In contrast to the LB medium that is optimized for *E. coli*, YPD is optimized for the cultivation of yeast. The yeast extract contains amino acids that are essential for the growth of *P. pastoris* and other yeasts. In addition to this, the YPD medium also consists of peptone that acts as a source of nitrogen, vitamins, and minerals. Lastly, glucose is used as a carbon source.

Liquid YPD medium

Materials:

- 10 g/L Bacto Yeast extract
- 20 g/L Peptone from casein
- 20 g/L Glucose

Method:

5 g yeast extract and 10 g peptone were added to a 500 mL blue cap bottle. Then, 350 mL water was added before the solution was mixed on a magnet stirrer. Next, water was added to a final volume of 450 mL and the blue cap bottle was autoclaved at 121 °C for 15 minutes. In addition to this solution, a glucose solution was made by mixing 200 g glucose in 1 L water on a magnetic stirrer. The glucose solution was filtered with a 0.22 μm PES membrane vacuum filtration system. Finally, 50 mL of the 20% glycerol solution was added to the autoclaved Yeast-Peptone solution in a laminar flow workbench to keep everything sterile. The solution was stored at room temperature.

Agar YPD medium

Materials:

- 10 g/L Bacto yeast extract
- 20 g/L Peptone
- 20 g/L Glucose
- 15 g/L Agar
- 100 mg/mL Zeocin

Method:

The YPD medium was prepared like the liquid medium, but only 250 mL was made, and 3.75 g agar was added before autoclaving. After autoclaving, the solution was incubated at 50 °C for approximately 1 hour. This is because zeocin gets destroyed in higher temperatures.

After the solution had reached a temperature of 50 °C, 250 µL 100 mg/mL of zeocin was added to the plates in a laminar flow workbench, to a final concentration of 100 µg/mL. Finally, the medium was poured into petri dishes and the plates were stored at 4 °C.

2.12 Antibiotics

2.12.1 Ampicillin

Ampicillin is a β-lactam inhibitor and works on a wide spectrum of gram-positive, gram-negative, and anaerobic bacteria (Rafailidis et al., 2007). Ampicillin works by inhibiting bacterial cell wall synthesis when it binds to penicillin-binding proteins (PBPs). By acylating the transpeptidase enzyme, the formation of peptidoglycan is not possible, hence the cell wall formation is inhibited (Rafailidis et al., 2007).

In this study, ampicillin was used to select *E. coli* containing *Sc*LPMO9A. The plasmid with the genes encoding *Sc*LPMO9A also consists of a gene coding for ampicillin resistance. Therefore, by using ampicillin in the cultivated medium, *E. coli* without the plasmid coding for *Sc*LPMO9A is eliminated.

Materials:

- 0.50 g ampicillin sodium salt
- MilliQ water

Method:

An ampicillin stock solution was made by mixing 0.50 g ampicillin sodium salt with MilliQ water in a magnetic stirrer, to a 10 mL solution and a concentration of 50 mg/mL ampicillin. 1 mL aliquots were made of this solution, and stored at -20 °C.

2.12.2 Zeocin

Zeocin is a phleomycin derivate that works on most bacteria, yeast, plants, and mammalian cells (Benko & Zhao, 2011). It is isolated from *Streptomyces verticillus* and is a copper-chelated glycopeptide. When zeocin enters the cell, the copper is reduced and removed, which activates the antibiotic, making zeocin bind and cleave the DNA, causing cell death.

Zeocin was used in the cultivation of *P. Pastoris* with *Nc*LPMO9C. All plasmids inserted in *P. pastoris* are zeocin resistant, therefore zeocin can be used as a selection marker.

Materials:

- 100 mg/mL zeocin

Method:

A zeocin concentration of 100 μg/mL was added to the YPD medium at 50 °C. Since zeocin works on eukaryotes, gloves were always used, and the adding of zeocin was done in a laminar flow workbench.

2.13 Other solutions

2.13.1 100 mM Ascorbic acid reductant (AscA)

LPMO reactions require a reductant for catalysis, and the most common reductant in laboratory experiments is AscA. AscA reduces the copper cofactor by acting as an electron donor and transferring a single electron to the copper ion.

Materials:

- 176.12 g ascorbate salt
- Trace select water

Method:

AscA solution was produced by mixing 176.12 g ascorbate salt with trace select water to a concentration of 100 mM AscA. The solution was proportionated to 100 µL fractions in PCR tubes and stored at -20 °C. Throughout the treatment, the solution was protected against light and thawed AscA solution was discarded instead of being re-frozen.

2.13.2 Inducer

An inducer is used to activate the transcription of a gene. This happens because the inducer inhibits the repressor of the operon so that the repressor cannot inhibit the transcription. In this study, *m*-toluic acid is used as an inducer for *Sc*LPMO9A. *m*-toluic acid is a benzoic acid derivate that induces the gene expression of *Sc*LPMO9A and some other LPMOs.

Materials:

- 1.36 g *m*-toluic acid
- 100 mL ethanol

Method:

1.36 g 0.1 M *m*-toluic acid was dissolved in 100 mL ethanol using a magnetic stirrer, to a final concentration of 10 M *m*-toluic acid. A membrane dry vacuum pump with a 0.22 μm filter was used to filter the inducer before the bottle was stored at 4 °C.

2.13.3 Copper solution

To ensure that all the LPMOs contain a copper atom in the histidine brace, the LPMOs must be copper saturated. This was done by adding 3 times as much copper as LPMO concentration.

Materials:

- 24 mg $CuSO_4$
- Trace select water

Method:

To prepare the solution, 24 mg $CuSO_4$ was dissolved in 10 mL trace select water to a final concentration of 10 mM copper. The amount of copper solution added to the LPMOs was measured independently for every LPMO batch, as the concentrations differs.

2.13.4 Magnesium chloride solution

To ensure that the *Sc*LPMO9A proteins remain stable during harvesting, a magnesium chloride solution was added before the last round of centrifugation when harvesting *Sc*LPMO9A.

Materials:

- 95 mg $MgCl_2$

- MilliQ water

Method:

The magnesium chloride solution was made by dissolving 95 mg $MgCl_2$ in 50 mL water to a final concentration of 20 mM $MgCl_2$. The solution was filtered using a membrane dry vacuum pump and a 0.22 μm filter and stored at room temperature.

2.13.5 H_2O_2 co-substrate

H_2O_2 co-substrate was used in some reactions with *Sc*LPMO9A and *Nc*LPMO9C as a co-substrate and in the Amplex Red Hydrogen Peroxide assay and Breslmayr assay.

Materials:

- 8.92 M H_2O_2 stock solution
- Trace select water

Method:

A 1.8 mM stock was produced from 8.92 M commercial liquid H_2O_2 by diluting the 8.92 M stock 5000x in trace select water. The solution was protected against the light with aluminium foil and kept in the fridge or on ice throughout the entire experiment. Diluted H_2O_2 solutions were only used once, and the 8.92 M stock was kept in the refrigerator at 4 °C and protected against light.

2.13.6 Peroxidase from horseradish

Peroxidase from horseradish (HRP) was used in the Amplex Red Hydrogen Peroxide assay to study the H_2O_2 production of *Sc*LPMO9A and *Nc*LPMO9C.

Materials:

- 0.50 mg peroxidase from horseradish
- MilliQ water

Method:

0.50 mg 199 U/mg HRP was mixed with MilliQ water to a final volume of 1 mL and a final concentration of 100 U/mg.

3 Methods

3.1 Pre-preparation of *Sc*LPMO9A

The ScLPMO9A gene (NCBI: SCHCODRAFT_54466) was codon-optimized for expression in E. coli (ER2566) at the Norwegian University of Science and Technology (NTNU), Trondheim. The first steps in the cultivation had therefore already taken place before the laboratory work for this thesis started.

3.2 Production of *Sc*LPMO9A

To analyse protein functions or structure, the protein must first be produced and purified. Often large amounts of protein in needed for different analyses, and cloning is a commonly used method to induce the number of proteins.

The method for protein cultivation consists of several steps, but in short, it starts with transforming the gene of interest from a cloning vector to an expression vector. This is done with the assist of restriction enzymes and ligases. The restriction enzymes cut out the gene of interest and ligase ligate the gene into the expression vector. The expression vector consists of a promotor and a site for antibiotic resistance that are used as a selection marker. Next, the plasmid with the gene that codes for the protein is transformed to a production host to amplify

the plasmid. Lastly, the plasmid is transformed to an expression host, for example, *E. coli*, that are optimized for protein expression (V. G. H Eijsink; personal communication). An inducer is also commonly used to assist the expression host produce more of the protein of interest.

To cultivate and study *Sc*LPMO9A, *E. coli* was used as an expression host. *E. coli* is commonly used in biotechnology, molecular biology, biochemistry, and genetics, and this makes it one of the most studied model prokaryotic organisms. There are several reasons why *E. coli* is usually used as an expression host. Firstly, the metabolic processes are well understood. Besides, *E. coli* has a rapid growth rate, a simple transformation procedure, and the ability to grow with or without oxygen (Mohammed et al., 2015). It consists of different strains, and many of them are used *in vitro* to express and produce different heterologous proteins.

By inserting the *Sc*LPMO9A gene into a plasmid designed specifically to express this gene, the plasmid can be inserted into an *E. coli* expression host before *E. coli* is cultivated and induced to promote the expression of the desired protein. Since NTNU had already inserted the plasmid into the *E. coli* ER2566 strain, cultivation of *E. coli* in this study started at the pre-cultivation, as described below.

3.2.1 Pre-cultivation of *E. coli* containing *Sc*LPMO9A

To cultivate the *E. coli* ER2566 production strain carrying a pJB_pelB_Sc plasmid encoding *Sc*LPMO9A (residues 20-247), both liquid and agar LB medium was used together with 2*LB medium. In the first cultivation step, agar plates were used to ensure that colonies were obtained from the premade glycerol stock.

Materials:

- LB agar plates with 50 µg/mL ampicillin
- Glycerol stock with *Sc*LPMO9A

- LB medium with 50 µg/mL ampicillin

Method:

First, *E. coli* strain carrying the pJB_pelB_Sc plasmid encoding the *Sc*LPMO9A gene were plated on LB agar plates from a premade glycerol stock. Ampicillin had been added to the agar plates beforehand, with a final concentration of 50 µg/mL, as described in Section 2.11.1. The *E. coli* pJB_pelB_Sc glycerol stock was stored on ice in a laminar flow workbench, while an inoculation loop was used to streak some of the glycerol stock into the agar plates. The agar plates were then cultivated overnight at 30 °C.

After incubating the agar plates overnight, single colonies from the agar plates were selected and cultivated in flasks containing 15 mL LB medium and 30 µL ampicillin to a final concentration of 50 µg/mL ampicillin. This was done in a laminar flow workbench to keep everything sterile. Then, the liquid LB medium with the *E. coli* colonies was cultivated at 30 °C and 220 rpm for 16 hours.

3.2.2 Glycerol stock

The preculture was used for both further cultivation and to prepare a glycerol stock. A glycerol stock was made from the preculture to prevent the cells with the pJB_pelB_Sc plasmid encoding the *Sc*LPMO9A gene from being killed during storing. The stock can be stored in the freezer for a long period, because the glycerol stabilizes the cells and prevents the cell membrane from being destroyed, therefore, the *Sc*LPMO9A can be used for later studies.

Materials:

- 85% (v/v) glycerol
- Pre-cultivated LB medium

Method:

To prepare the glycerol stock, 500 µL sterile 85% (v/v) glycerol was added to a 2 mL screw cap microtube with 1000 µL of the cultivated medium, to a final glycerol concentration of 28% (v/v). This stock was then stored at -80 °C for later use.

When the glycerol stock was used to inoculate new overnight cultures, it was used a sterile inoculation loop to touch the surface of the frozen glycerol stock. This was done in a laminar flow workbench to keep everything sterile. Then, the inoculation loop was inserted into tubes or agar plates containing medium and ampicillin. Lastly, the culture tubes or agar plates were left at 30 °C and 220 rpm overnight.

3.2.3 Main production of *Sc*LPMO9A

Main cultures can be made from the preculture culture by using either the same medium or another medium that is more optimized for growth. In this case, 2*LB was used to prepare the main cultures. In addition to a medium, it is also commonly used an inducer which is a molecule that regulates gene expression. The expression system that produces *Sc*LPMO9A is based on the XylS/*Pm* regulator/promotor system that uses benzoic acid like *m*-toluic acid as an inducer. When the inducer binds to the transcriptional regulator (XylS) the regulator gets activated and binds to the *Pm* regulator. This process stimulates transcription of *Sc*LPMO9A gene (Courtade et al., 2017).

Materials:

- Preculture
- 2* LB medium
- Ampicillin
- *m*-toluic acid

Method:

After approximately 16 hours of incubation, the culture was transformed to a laminar flow workbench and 15 mL of the preculture was transferred to a cultivation flask containing 500 mL 2*LB medium with 100 μg/mL ampicillin. Two 500 mL cultivation flasks were prepared, so in total 1 L culture. The flasks were incubated at 30 °C and 220 rpm until the OD_{600} had reached 0.6-0.8, after approximately 3 hours. The OD_{600} was measured with 2*LB medium as a blank and with 1 mL sample of the culture in an Ultrospec 10 Cell density meter. The flasks were then incubated on ice for 5 minutes and then induced with 500 μL *m*-toluic acid to a final concentration of 0.1 mM. Lastly, the flasks were incubated at 16 °C and 220 rpm overnight.

3.3 Purification of *Sc*LPMO9A

After cultivation, several methods can be used to purify the protein from *E. coli.* However, the protein needs to be harvested before purification. Then, methods like ion-exchange chromatography, reverse phase chromatography, gel filtering, and hydrophobic interaction chromatography can be used, which are some of the most used purification methods.

3.3.1 Harvesting of *Sc*LPMO9A

How the harvesting method is done depends on the host organism. *E. coli* is a gram-negative bacterium and is one of the most used host organisms for protein expression. Because of the gram-negative structure, the proteins of interest can accumulate between the first and the second cell membrane, known as the periplasmic space. Consequently, the proteins can be released by cell lysis, by using osmotic shock with a spheroplast buffer (V. G. H Eijsink; personal communication).

The spheroplast buffer has a high content of sugar, making water in the *E. coli* cells shrink to equalize the osmotic pressure. In addition to this, the spheroplast buffer also consists of EDTA that stabilizes the plasmid. A protease inhibitor makes sure *Sc*LPMO9A is not broken down by proteases. By adding water to the cells after the spheroplast buffer, the cells will absorb the water because there is no sugar gradient to equalize. This makes the cell expand and the outer membrane crack. *Sc*LPMO9A is therefore secreted into the periplasmatic space.

By using centrifugation, the proteins and cells are separated, leaving the proteins of interest in the supernatant for further purification (V. G. H Eijsink; personal communication).

Materials:

- Main culture
- Spheroplast buffer
- Protease inhibitor tablet
- Cold MilliQ water
- 20 mM $MgCl_2$

Method:

After incubating the main culture at 16 °C and 220 rpm overnight, the culture was transferred to a 1 L centrifuge tube and centrifugated at 5000 rpm, 4 °C for 5 minutes in a Sorwall LYNX 6000 Centrifuge with an F9-6x1000 LEX rotor. After 5 minutes, the supernatant was discarded before the pellet was resuspended by pipetting up and down on ice with 60 mL spheroplast buffer with 1 protease inhibitor tablet.

Next, the resuspended cells were incubated on ice for 5 minutes. After incubation, the resuspended cells were centrifugated at 6250 rpm, 4 °C for 10 minutes, in the same centrifuge, but with an F21-8x50y rotor. Then, the supernatant was discarded, and the pellet was incubated at room temperature for 10 minutes. Afterwards, the pellet was resuspended in 50 mL cold MilliQ water and 1 protease inhibitor tablet by pipetting up and down. 3 mL 20mM $MgCl_2$ was now added to the cells to stabilize the proteins. The resuspended cells were then centrifugated at 23000 rpm, 4 °C for 30 minutes.

Both supernatant and pellet was analysed using SDS-PAGE, to ensure that the protein was in the supernatant. When it was confirmed that the protein was in the supernatant, the supernatant with the protein was filtered through a 0.22 μm PES membrane filter and kept at 4 °C until purification with anion exchange chromatography.

3.3.2 Sodium Dodecyl Sulfate-Polyacrylamide Gel Electrophoresis (SDS-PAGE)

SDS-PAGE separates proteins based on their molecular weight and can be used as a checkpoint to ensure that the protein of interest has been fully purified. This is done when proteins travel through a gel with an electric current, towards a positive anode.

Proteins have different compositions of amino acids, hence different charges. Therefore, sodium dodecyl sulfate (SDS) or lithium dodecyl sulfate (LDS) is added to the proteins to make the charge equal. This is done by first disturbing the non-covalent bonds, hence disrupting the tertiary structure. Then, the SDS or LDS, which has a negative charge, binds to the linear protein. Big proteins attract more SDS or LDS than smaller proteins, making all proteins have a net equal charge. In addition to SDS or LDS, dithiothreitol (DTT) is also added to the protein sample to break the intramolecular disulfide bonds, making sure the proteins do not return to their tertiary structure (Kielkopf et al., 2021). The SDS buffer also contains a loading dye, that allows visualization of the protein bands when the proteins migrate through the gel.

Materials:

- Protein samples
- SDS buffer
- 1x Tris-Glycine-SDS buffer
- BenchMark Protein Ladder
- Mini-PROTEAN Tetra Cell
- Mini-PROTEAN TGX Stain-Free gel
- Stain-Free Sample Tray
- Gel Doc EZ

Method:

To prepare protein samples for the SDS-PAGE, 10 µL protein-sample was mixed with 10 µL SDS buffer (Section 2.6.10) in Eppendorf tubes. A pipette tip was used when preparing the

pellet samples, by sticking it into the pellet and adding it to an Eppendorf tube with 10 µL MilliQ water and 10 µL SDS buffer. The tubes were kept on a water bath at 100 °C for 5 minutes before being centrifuged for a few seconds. Then, the samples were applied to a pre-cast SDS-PAGE.

To prepare the electrophoresis chamber, the Mini-PROTEAN TGX Stain-Free gel was placed in a cassette before the cassette was placed into the Mini-PROTEAN Tetra Cell. 1X Tris-Glycine-SDS buffer was added to both the inner and outer chamber. This buffer makes sure that the proteins remain denatured and negatively charged. Then, 4 µL of the Benchmark Protein ladder was loaded into the first well before 10 µL samples were loaded to the remaining wells. The Benchmark Protein Ladder consists of proteins with known molecular weight in kDa. Therefore, the proteins with unknown molecular weight can be compared to the ladder, making it clear if the protein of desire is in the sample or not.

When all samples were loaded to the gel, the system was set at 270V for 17 minutes. When the run was completed, a Stain-Free Sample Tray and a Gel Doc EZ image were used to visualize the proteins and compare them to the ladder. After confirming if the protein of interest was in any of the samples, the samples with the protein were used further.

3.3.3 Anion exchange chromatography

After confirming the presence of *Sc*LPMO9A in the supernatant, the supernatant was purified using anion exchange chromatography. Anion exchange chromatography separates molecules based on their net surface charge. This is done with the help of a positively charged ion exchange resin, that has an affinity for negatively charged molecules.

All proteins have an isoelectric point, that is determined by the protein's amino acid sequence. When the pH is equal to the isoelectric point, the protein has no charge, but if the pH is above the protein isoelectric point, the protein gets a negative charge and opposite when the pH is below the isoelectric point (Cleaves, 2011). Therefore, the buffers must have a pH designed specifically for the protein that is being purified.

Since all proteins have different isoelectric points, they will have different affinities for the positively charged surface groups on the particles in the column. As a result of this, proteins are separated as they have different binding strengths. In addition to pH, a salt gradient is also used to separate the proteins, salt binds to the column and outcompetes the protein-interaction to the column. Proteins with low isoelectric point elutes at high salt concentrations.

Since *Sc*LPMO9A has an isoelectric point at 4.63, it binds to the column when the pH is above this point. Here it is used buffers with a pH of 7.5, therefore *Sc*LPMO9A first binds to the column, before a buffer with NaCl is used to elute the protein.

Materials:

- A HiTrap DEAF FF column
- AKTAprime
- Supernatant containing *Sc*LPMO9A
- 50 mM Tris-HCl buffer pH 7.5 (Buffer A)
- 50 mM Tris-HCl 1 M NaCl pH 7.5 (Buffer B)

Method:

Before purification, the system was washed in 20% ethanol. This was done by a system wash method that bypasses the column. When the system was completely washed, the flow was set to 0.5 mL/min so the column could be inserted. Each purification requires specific columns, but to separate *Sc*LPMO9A, a HiTrap DEAF FF column was used. After the column was inserted, the flow was passed through for a couple more minutes, making sure the column was clean and in 20 % ethanol.

After washing with ethanol, all 3 tubes were placed in MilliQ water. A system wash method made sure all tubes were full of MilliQ water before a manual run was used to ensure that the column also consisted of only MilliQ water. After 5 column volumes (CV) of MilliQ water with a flow of 4 mL/min, the run was stopped and tube A and tube 2 was transferred to 50 mM Tris-HCl pH 7.5 and tube B was transferred to 50 mM Tris-HCl, 1 M NaCl pH 7.5.

When all 3 tubes were transferred to the corresponding buffers, a system wash method was performed. This method bypasses the column and makes sure tube B consists of only 50 mM Tris-HCl, 1 M NaCl pH 7.5 buffer. After the system wash, 5 CV were passed through on a flow of 4 mL/min, ensuring that there was only buffer A in the system and equilibrating the HiTrap DEAF FF column.

After equilibration, tube 2 was placed in the supernatant and the valve port was changed to position 2 before the filtered supernatant was injected into the column at 2 mL/min. When almost all the supernatant was loaded, 10 mL of 50 mM Tris-HCl pH 7.5 was added to the flask the supernatant was in, to ensure that all the supernatant reached the column. Next, tube 2 was placed back in the 50 mM Tris-HCl pH 7.5 buffer and the valve port was changed to position 1. The buffer was loaded until the UV had stabilized, washing out unbound proteins. Then, *Sc*LPMO9A was eluted with a 0-50% gradient buffer B over 90 CV. Lastly, the system was washed with MilliQ water before it was washed and stored in 20 % ethanol.

Samples from some of the fractions from the peaks were analysed using SDS-PAGE to find out which fractions to pool and to observe if only *Sc*LPMO9A were in the fractions. If there are other proteins in the samples after anion exchange chromatography, a second purification step must be performed.

3.3.4 Concentration of *Sc*LPMO9A

After purification with anion exchange chromatography, the SDS-PAGE gel showed some other proteins in the sample. Therefore, SEC was used for final purification. However, before the samples can be loaded to AKTAprime used for SEC, the samples must be concentrated down to approximately 1 mL. To do this, fractions with the eluted *Sc*LPMO9A from anion exchange chromatography were pooled and concentrated using a vivaspin 20 centrifugal concentrator with a 10.000 PES membrane. The same method was also used after SEC and after copper saturating the LPMOs.

Since *Sc*LPMO9A is 24.5 kDa, it is important not to use a concentrator with larger pore size than 25.000 kDa, because proteins smaller than the membrane will travel through the filter and end up in the flow through. By using a concentrator, the protein concentration increases

since the buffers and other molecules from the anion exchange chromatography samples are washed out, in addition to proteins smaller than the filter. This happens when the protein sample is loaded to the centrifugal concentrator, before the concentrator is centrifugated, pushing the solution through a semipermeable membrane with a specific molecular weight cut-off (MWCO).

When concentrating the proteins before SEC, 50 mM Bis-Tris-HCl, 150 mM NaCl pH 6.5 was used for buffer exchange. This buffer was also used in SEC; therefore, the proteins should be equilibrated in this buffer. Together with the Vivaspin 20, 10.000 MWCO PES ultrafiltration unit, a Heraeus Multifuge X1R was used at 4500 x g at 4 °C.

When concentrating after SEC and after copper saturation, 50 mM Tris-HCl pH 7.5 buffer was used, because *Sc*LPMO9A can be stored in this buffer. This buffer removes excess salts from the protein solutions when concentrating the samples after SEC.

Materials:

- *Sc*LPMO9A fractions from anion exchange chromatography
- *Sc*LPMO9A fractions after SEC
- *Sc*LPMO9A after copper saturation
- 50 mM Tris-HCl buffer, pH 7.5
- 50 mM Bis-Tris-HCl, 150 mM NaCl pH 6.5
- Vivaspin 20, 10.000 MWCO PES membrane
- MilliQ water

Method:

Before loading the protein sample to the concentrator, the vivaspin filtration unit was rinsed with MilliQ water. 10 mL MilliQ water was applied to the concentrator before the concentrator was centrifugated at 4500 x g, 4 °C until the water was washed through. Then, the protein fractions were loaded to the concentrator before it was centrifugated again at 4500 x g 4 °C for 10 minutes. This was repeated until all the protein was fully loaded to the concentrator, with approximately 2 mL protein left in the tube. Next, 20 mL 50 mM Bis-Tris-

HCl, 150 mM NaCl pH 6.5 was loaded and centrifugated at 4500 x g, 4 °C until it was 1 mL protein left in the tube. This was repeated twice. All flow through was transferred to a 50 mL tube, to keep as a backup in case the protein went through the membrane.

3.3.5 Size exclusion chromatography

After concentrating the LPMOs down to 1 mL, the samples were filtered using a syringe together with a 0.22 μm filter unit, before SEC.

SEC is a liquid column chromatography that separates the proteins based on size when the sample flows through a column that is filled with porous packing. The largest proteins are eluted before the smaller ones, because of differential pore permeation. The reason why the bigger proteins elutes first are that the volume of the pore is better for the small proteins than for the large proteins (Kostanski et al., 2004). Here, SEC was used as a purification step, but it can also be used to measure molecular weight.

Materials:

- Purified and concentrated *Sc*LPMO9A
- 50 mM Bis-Tris, 150 mM NaCl pH 6.5
- 20% ethanol
- 20% ethanol + 0.2 M sodium acetate
- MilliQ water

Method:

The AKTApurifier used for SEC should always be in 20% ethanol when not used, therefore a pump wash in MilliQ water was used to ensure that there was no ethanol left in the system. This was done before adding the column. After a pump wash of 1 CV with MilliQ water, the flow was set to 0.4 mL/min and the column was mounted. 50 mM Bis-Tris buffer pH 6.5, 150 mM NaCl was then passed through the system at 1 CV.

After 1 CV with buffer, the flow was ended, and the UV light was turned on. The insertion needle was washed with boiled MilliQ water, to remove any ethanol from the needle. This was done with a 10 mL syringe. After washing the needle, the syringe was filled with 50 mM Bis-Tris, 150 mM NaCl pH 6.5 buffer and the needle was added to the syringe. Then, the needle was put in injection position and the mode was set to load mode before the buffer was slowly injected. After all the buffer was injected, the mode was set to inject mode, and the needle was removed. Next, a 1 mL syringe was filled with the protein sample and the sample was loaded in the same manner. After injecting the sample, the flow was set to 0.2 mL/min and increased gradually to 1 mL/min. The fractionation was started after approximately 40 minutes. To fractionate, the "source of fraction" was set to AD_{900}, and "fractionation 900" was set to 2 mL fractions. After the proteins were eluted, the fractionation was stopped.

After the fractionation was stopped, MilliQ water was passed through the column at 1 CV, before 20 % ethanol with 0.2 M Sodium acetate was passed through the column at 1 CV. Then, the column was removed, and a pump wash with 20 % ethanol was performed. Lastly, the sample loop was washed with 20 % ethanol.

After the samples were purified with SEC, the fractions where the proteins had eluted were analysed using SDS-PAGE gel, before the fractions containing *Sc*LPMO9A were pooled and concentrated, this time with 50 mM Tris-HCl pH 7.5 buffer, and the concentration was measured using Bradford protein assay.

3.3.6 Measuring concentration with Bradford protein assay

To measure protein concentration with Bradford protein assay, a Coomassie dye is used to bind to the proteins under acidic conditions. When the acidic solution of Coomassie blue binds to proteins, the absorbance shifts from 465 nm to 595 nm. This gives a colour change, from brown to blue, and by measuring the presence of the basic amino acids; arginine, lysine and histidine, the concentration can be determined using a BioPhotometer (Ernst & Zor, 2010).

Materials:

- Disposable Eppendorf cuvettes 1 mL
- Spectrophotometer
- Protein samples
- Coomassie blue
- MilliQ water

Method:

To measure protein concentration with Bradford protein assay, the protein concentration must lay between 1.25 µL/mL and 10 µL/mL. Therefore, dilutions in MilliQ water of the concentrated protein sample were made to obtain the desired protein concentration. MilliQ water was also used in the blank sample together with Coomassie blue. The dilutions were made in 1.5 mL Eppendorf tubes before 800 µL of the protein samples were mixed with 200 µL Coomassie blue from each dilution. The blank was made by mixing 800 µL MilliQ water with 200 µL Coomassie blue. Then, the samples were incubated at room temperature for 5 minutes.

After 5 minutes, the blank was measured by pipetting 1 mL of the samples in a 1 mL cuvette. The protein samples were measured in the same manner. The samples were measured until the concentration was between 1.25 µL/mL and 10 µL/mL. 3 dilutions were measured, and an average of this concentration was calculated. The concentration was determined with bovine serum albumin as a standard.

The Bradford protein assay gives the protein concentration in mg/mL, this concentration was therefore divided by the mass of the proteins, to get the concentration in mM before the concentration was multiplied with 1000 to get µM. The dilution was also multiplied, to obtain the correct concentration.

3.3.7 Copper saturation

LPMOs need copper in the active site before they can catalyse reactions. Therefore, it is important to copper saturate all LPMOs before reactions can take place. When copper saturating for this thesis, the amount of copper was 3 times as much as the concentration of

the protein. This was to ensure that all LPMOs were copper saturated. However, too much copper in the sample can interact with oxygen, LPMOs, or H_2O_2, making reactive oxygen species, therefore the copper saturated sample was purified using a PD-10-column and a storing buffer to remove excessive copper. After desalting, the protein was again concentrated as described in Section 3.3.4 before the final concentration was be measured.

Materials:

- 50 mM Tris-HCl pH 7.5
- Purified and concentrated protein samples of *Sc*LPMO9A
- 100 mM $CuSO_4$
- DP-10-column
- Vivaspin 20, 10.000 MWCO membrane

Method:

500 µL LPMO was added to an Eppendorf tube before $CuSO_4$ was added in a 3x molar ratio to the LPMO concentration. Then, the sample was incubated at room temperature for 30 minutes to ensure that all LPMO molecules was fully saturated.

After incubating, the sample was desalted using a DP-10-column and storage buffer. First, 25 mL 50 mM Tris-HCl pH 7.5 was added to the column. Then, the protein sample was added, before the buffer was added to a final volume of 2.5 mL. The protein was eluted by adding 3.5 mL buffer. The copper saturated protein was concentrated down to 750 µL using a vivaspin filtration unit as described in Section 3.3.4. Lastly, the protein absorbance was measured with Bradford protein assay and the protein concentration was calculated as described in Section 3.3.6.

3.3.8 PASC screening to check for endoglucanase activity

The last step before further analysis was to check if there was any endoglucanase in the sample. This can be done by performing a reaction with the purified LPMO and a substrate, both with and without a reductant. The sample without any reductant can be used as a control

because LPMOs do not work without reductants, and it should therefore not be any activity in this reaction. Endoglucanases do not need reductants, and it is therefore expected to observe depolymerization activity if endoglucanase is in the sample. A control with only substrate and reductant was also used to check how the substrate interacts with the reductant without LPMO and other enzymes.

Materials:

- Copper saturated *Sc*LPMO9A
- 0.9% PASC
- 100 mM AscA
- MilliQ water
- 500 mM sodium acetate buffer pH 5.0

Method:

The samples were analysed on HPAEC-PAD using a 50-minute gradient, as described in Section 3.11 (Method – Endoglucanase activity screening).

3.4 Pre-preparation of *Nc*LPMO9C

*Nc*LPMO9C from *N. crassa* was produced with *P. pastoris* strain as an expression host. To cultivate *Nc*LPMO9C, the gene coding for *Nc*LPMO9C (UniProtKB: Q7SH18) was codon-optimized for expression in *P. pastoris* and transferred into the pBSYP$_{GCW14}$Z plasmid. This pBSYP$_{GCW14}$Z-LPMO plasmid was inserted into component cells. These steps had already taken place before the laboratory work for this thesis had started and is described in more detail by Rieder et al. (2021).

3.5 Production of *Nc*LPMO9C

P. pastoris containing the pBSYO$_{GCW14}$ plasmid encoding *Nc*LPMO9C were used as an expression host and were cultivated in a YPD medium before purifying.

P. pastoris is commonly used for protein production and is a yeast that can use methanol as a carbon and energy source. Some of the advantages of using *P. pastoris* as an expression host is that *P. pastoris* has a short generation time and fast regeneration time. In addition to this, the proteins that are produced in *P. pastoris* are folded in the endoplasmic reticulum and secreted to the external environment of the cell, making it easy to harvest. Another advantage is that the yeast can grow with high cell density in the cultures, which gives the cultivation a high yield (Gasser et al., 2013).

3.5.1 Cultivation of *Nc*LPMO9C

Both liquid YPD medium and agar YPD medium was used to cultivate *Nc*LPMO9C. Because *P. pastoris* has a slower growth rate than *E. coli*, the incubation time for the agar plates was doubled. After incubation of the agar plates, the agar plates should consist of colonies of *Nc*LPMO9C, and these colonies can be further cultivated in a liquid YPD medium.

Materials:

- YPD agar plates with 100 µg/mL zeocin
- Glycerol stock with *Nc*LPMO9C
- Liquid YPD medium

Method:

After making YPD agar plates as described in Section 2.11.2. *P. pastoris* containing NcLPMO9C from a premade glycerol stock were plated on the agar plates with the use of an inoculation loop. This was done in a laminar flow workbench to keep everything sterile. The agar plates were then cultivated for approximately 48 hours at 30 °C.

After 48 hours of incubation, colonies from the agar plate were transferred to 500 mL of the liquid YPD medium in a cultivation flask. This was done with a sterile inoculation loop in a laminar flow workbench. The medium was incubated at 28 °C, 180 rpm for approximately 60

hours. After approximately 24 hours, a sterile inoculation loop was used to make holes in the aluminium foil on top of the cultivation flask, to ensure proper oxygenation for *P. pastoris*.

3.6 Purification of *Nc*LPMO9C

To purify *Nc*LPMO9C after cultivation of *P. pastoris*, several purification steps can be used. However, before purification, the cultivated medium needs to be harvested. When the *Nc*LPMO9C is fully harvested, hydrophobic interaction chromatography (HIC) is typically used as the first purification step, followed by SEC for final purification.

3.6.1 Harvesting *Nc*LPMO9C

After cultivation, a harvesting step is used to separate the cells from the medium. Since *P. pastoris* is a yeast, the harvesting method differs from the harvesting method used on *E. coli*, which is a gram-negative bacterium. In *P. pastoris* there is no need to use osmotic shock because *P. pastoris* secrete the protein into the media, so the harvesting step is finished after one round of centrifugation.

Materials:

- Cultivated YPD medium
- MilliQ water

Method:

The culture was transferred to a 1 L centrifuge tube, with MilliQ water to a final volume of 900 mL. The culture was then centrifuged at 10 000 x g for 15 minutes in a Sorwall LYNX 6000 Centrifuge with an F9-6x1000 LEX rotor. After centrifugation, an SDS-PAGE gel was performed on both supernatant and pellet to ensure that that the *Nc*LPMO9C was in the supernatant. After confirming the presence of *Nc*LPMO9C, the supernatant was filtered using a 0.45 μm filter before the supernatant was concentrated using a Viva Flow system.

3.6.2 Concentration with Viva Flow

Before further purification of the protein, the supernatant must be concentrated using a Viva Flow system. This concentration system is, among other things, suited to the application of cell culture supernatants. In addition to increasing the protein concentration, Viva Flow can also be used to buffer exchange. Another advantage of using the Viva Flow concentration is that it is more suited for a concentration of big samples than the vivaspin 20 concentration unit (H. Østby; personal communication).

Materials:

- Viva Flow
- Supernatant containing *Nc*LPMO9C
- 20% ethanol
- MilliQ water
- 500 mM NaOH

Method:

20 % ethanol was first passed through the system to ensure all 3 tubes were filled with ethanol. After a few minutes, the ethanol in the collection chamber was replaced with MilliQ water. MilliQ water was passed through the system for 5 minutes, twice, to rinse the cassette. Then, all MilliQ water was pumped out and the MilliQ water in the chamber was discarded. Before loading the protein into the chamber, the filtrate collection tube was detached from the chamber and placed in a 1 L bottle to collect waste. Then, the chamber was placed on ice, and the supernatant was loaded into the chamber. The pump was set at 4.5 to give a pressure below 2 bar. The protein was concentrated to about 100 mL before it was stored at 4 °C.

After the protein was concentrated, the Viva Flow system was washed in 500 mM NaOH for 5 minutes 2 times, before it was washed with MilliQ water for 5 minutes 2 times. Lastly, the system was stored in 20% ethanol.

3.6.3 Hydrophobic interaction chromatography

Hydrophobic interaction chromatography was used in the first purification step on the concentrated supernatant containing *Nc*LPMO9C to separate the proteins based on their hydrophobicity. Since proteins have different hydrophobicity, different buffers can be used to elute different proteins. The main steps in HIC are equilibration, binding, washing and elution.

Hydrophobic interaction chromatography consists of a column with a hydrophobic bead, coated with hydrophobic ligands that interact with the hydrophobic surface of the proteins. Since proteins have different degrees of hydrophobic surfaces, they will have different binding strengths to the column. In the absence of salt, water molecules coat both the proteins and the ligand in the column, shielding the hydrophobic patches. Therefore, the protein and buffer A often consist of a high salt concentration that favours protein binding to the column because the water is dissembled hence to the salt (V. G. H Eijsink; personal communication).

When the column is loaded with protein samples, a buffer without salt is used to wash out different proteins based on decreasing salt levels. Proteins with strong binding to the column need a lower concentration of salt to elute, and therefore, when the characteristic of a protein is known, it is also known when the protein will elute (V. G. H Eijsink; personal communication).

The reason why different proteins require different buffers is because they have different properties and hydrophobicity. When selecting buffers, the most important buffer is buffer A, because the binding process is more selective than the eluting process. Therefore, buffer A must consist of both the correct salt and the correct salt concentration so that the protein of interest binds to the column, while the other proteins are washed away. Here, ammonium sulfate was used in buffer A, which promotes ligand-protein interactions to the column. Because of this, the protein solution had to be mixed with 50 % ammonium sulfate before loading.

Materials:

- Phenyl FF columns

- 50 mM Bis-Tris buffer, 50% ammonium sulfate pH 6.5 buffer
- 50 mM Bis-Tris buffer pH 6.5 buffer
- Concentrated supernatant containing *Nc*LPMO9C
- Ammonium sulfate

Method:

2 phenyl FF columns were added with a flow of 0.5 mL/min ethanol before the system was washed in 20% ethanol for a couple of minutes. By using 2 columns, the binding capacity is increased. Next, the system was washed with MilliQ water, and buffer A and B as described in Section 3.3.3.

Before loading the protein solution, 50% ammonium sulfate was added to the protein solution. The amount of ammonium sulfate was calculated using the EnCor AS calculator. When adding the ammonium sulfate, the protein solution was placed on a magnet stirrer before ammonium sulfate was added slowly to avoid any precipitation of proteins.

When the protein solution was ready and the system was equilibrated with buffer A, tube 2 was placed in the protein solution and the valve port was changed to position 2, before the protein solution was injected into the column at 2 mL/min. When almost all the protein solution was loaded, 10 mL of 50 mM Bis-Tris, 50% ammonium sulfate pH 6.5 was added to protein solution to ensure that all the protein reached the column. Next, tube 2 was placed back in the 50 mM Bis-Tris, 50% ammonium sulfate pH 6.5 buffer and the valve port were changed to position 1. The buffer was loaded until the UV had stabilized, washing out unbound proteins. Then, *Nc*LPMO9C was eluted with a 0-100% gradient buffer B over 40 mL with a flow rate of 1.8 mL/min. Lastly, the system was washed with MilliQ water before it was washed and stored in 20% ethanol. Samples from some of the fractions from the peaks were analysed at SDS-PAGE to find which fractions to be pooled.

3.6.4 Concentration, SEC, and copper saturation of *Nc*LPMO9C

The concentration, SEC, and copper saturation of *Nc*LPMO9C was done similar as for *Sc*LPMO9A, but different buffers were used in some of the steps, as described in this Section.

Materials:

- *Nc*LPMO9C fractions after hydrophobic interaction chromatography
- Concentrated protein samples of *Nc*LPMO9C after SEC
- Purified and concentrated *Nc*LPMO9C
- Copper saturated protein samples of *Nc*LPMO9C
- 50 mM Bis-Tris-HCl buffer pH 6.5
- 50 mM Bis-Tris-HCl, 150 mM NaCl pH 6.5
- 500 mM sodium acetate buffer pH 5.0
- 20% ethanol
- MilliQ water
- 0.9% PASC
- 100 mM AscA
- MilliQ water

Method:

Before SEC, *Nc*LPMO9C was first concentrated using a Vivaspin concentration unit, as described in Section 3.3.4. The concentrated protein sample was purified with SEC as described in Section 3.3.5. After the proteins had been purified and pooled, the purified sample was again concentrated using a Vivaspin concentration unit. When concentrating *Nc*LPMO9C, 50 mM Bis-Tris-HCl buffer pH 6.5 was used instead of 50 mM Tris-HCl pH 7.5 for buffer exchange and storing.

After *Nc*LPMO9C was concentrated down to 1 mL, the absorbance was measured with Bradford protein assay, as described in Section 3.3.6. Then the samples were copper saturated as described in Section 3.3.7, with 50 mM Bis-Tris-HCl pH buffer 6.5 as a buffer in the desalting procedure. The concentration was then measured again with Bradford protein assay.

Finally, an overnight reaction with PASC was analysed to check for endoglucanase activity, as described in Section 3.12 (Method – Endoglucanase activity screening). The

chromatograms from the endoglucanase activity reactions were analysed using Chromeleon 7.2.9 to ensure that no endoglucanase was in the *Nc*LPMO9C sample before further use.

3.7 Measuring H_2O_2 concentration

When using H_2O_2 in reactions, it is important to know the correct concentration of H_2O_2. The concentration can change over time; therefore, UV vis 240 nm can be used to confirm that the theoretical concentration is correct before running reactions with H_2O_2. To measure the concentration, dilution series are used to obtain an absorbance between 0.1 and 0.9 A. 3 samples of every dilution are measured to get an average absorbance. The average absorbance from the dilutions that gives absorbance between 0.1 to 0.9 is then used to calculate the concentration.

To calculate the concentration from the UV absorbance, Beer-Lambert law, $A = \varepsilon * b * c$, is used. A is the absorbance of the solution measured by the BioPhotometer. ε is the extinction coefficient that is unique for all solutions, for example, H_2O_2 has an extinction coefficient at 43.6 M. b is the path length where the light travels, the path length was 1 cm in all measurements in this study. Lastly, c is the sample concentration.

By this information, the concentration can be calculated using the formula: $c = A / \varepsilon$. Before calculating the concentration, the average absorbance must be multiplied by the dilution. Then the final concentration can be calculated.

Materials:

- Trace select water
- H_2O_2
- Agilent Technology Cary 8454 UV-vis
- UV Cuvettes

Method:

Dilutions of H_2O_2 were made by mixing H_2O_2 in trace select water in 1.5 mL Eppendorf tubes. To obtain an accurate concentration, the absorbance must lay between 0.1 and 0.9 A, therefore different dilutions were measured until the absorbance was between 0.1 and 0.9. When the desired dilution was found, the average absorption of 3 samples was measured and used to calculate the H_2O_2 concentration.

3.8 Measuring LPMO H_2O_2 production

H_2O_2 is generated as a by-product in LPMO reactions, most likely when copper in the active site gets reduced, followed by reduction of molecular oxygen to H_2O_2 (Kittl et al., 2012). In 2012, Kittl et al. demonstrated an assay (Amplex Red Hydrogen Peroxide Assay) that measured H_2O_2 production from LPMOs. This is done by the oxidization of Amplex Red by the enzyme horseradish peroxidase (HRP), which uses H_2O_2 as a co-substrate and stoichiometrically converts Amplex Red to resorufin. The oxidized product (resorufin) can then be measured spectrophotometrically with an A_{max} of 563 nm.

Since LPMOs are known as H_2O_2 producers, an assay to measure H_2O_2 production can be used to observe if the purified LPMOs are active or not.

Materials:

- Amplex Red
- *Sc*LPMO9A
- *Nc*LPMO9C
- $CuSO_4$
- AscA
- Sodium acetate buffer pH 5.0
- HRP
- H_2O_2
- MilliQ water
- Cellopentaose

Method:

H_2O_2 production of *Sc*LPMO9A and *Nc*LPMO9C was measured by a time-resolved quantification of H_2O_2 formation in 96-well plates, with a total volume of 100 µL, and a varioskan lux plate reader at 30 °C. First, 1 µM *Sc*LPMO9A, *Nc*LPMO9C or $CuSO_4$ was mixed with assay solution consisting of MilliQ water, Bis-Tris-HCl buffer pH 6.5 (50 mM), Amplex Red (100 µM) and HRP (5U). 1 mM AscA was used as a reductant to start the reactions. Controls with cellopentaose were also made, by adding cellopentaose before LPMO and reductant. A standard curve was made with 0, 0.5, 1, 2, 5, 10, 20, 50 and 100 µM H_2O_2 and 1 mM AscA. The oxidation of resorufin was measured spectrophotometrically with a wavelength of 563 every 10 seconds for 2 hours. Lastly, the data was collected with SkanIt RE 6.0.1 and edited in Microsoft Excel 16.54.

3.9 Measuring LPMO H_2O_2 consumption

H_2O_2 consumption of LPMOs can be measured with the use of the Breslmayr Assay, which is also a common assay to verify LPMO activity. The assay is based on the LPMO oxidation of two 2,6-dimethoxyphenol (DMP) to two 2,6-DMP phenoxy radicals that are dimerized to one hydrocoerulignone. The hydrocoerulignone cannot be measured spectrophotometrically. However, the final product in the reaction, coerulignone, can be measured spectrophotometrically at wavelength 469 nm. Since 1-unit LPMO activity is defined as the conversion of 2 µM 2,6-DMP, or in other words, formation of 1 µM coerulignone (ε_{469}=53.200 M^{-1} cm^{-1}). The concentration of coerulignone and the H_2O_2 consumption can be measured (Breslmayr et al., 2018).

Materials:

- *Sc*LPMO9A
- *Nc*LPMO9C
- 50 mM Bis-Tris- HCl buffer pH 6.5
- $CuSO_4$
- DMP
- H_2O_2

- Trace select water

Method:

Enzyme dilutions were prepared in 50 mM Bis-Tris-HCl buffer pH 6.5, while H_2O_2, DMP and $CuSO_4$ dilutions were prepared in Trace select water.

First, the plate reader was heated up to 30 °C. Then 250 mM Bis-Tris-HCl buffer pH 6.5 pH 7.5 buffer was added to all wells to a final concentration of 50 mM, before $CuSO_4$ was added to relevant wells to a final concentration of 3 µM as a control. Next, trace select water was added to all wells before DMP (1 mM) and H_2O_2 (100 µM) was added to relevant wells. Then, the plate was incubated for 5 minutes at 30 °C in the plate reader. After 5 minutes, the plate was ejected, and the enzyme (3 µM) was added to relevant wells. The formation of coerulignone was measured spectrophotometrically with a wavelength of 469 every 10 seconds for 1 hour. The data was collected with SkanIt RE 6.0.1 and edited in Microsoft Excel 16.54.

3.10 Determining redox potential

To obtain a better understanding of why LPMOs have different reaction rates and consume and produce H_2O_2 at different rates, the redox potential can be measured.

A general trend is that LPMOs affect the redox potential of the active site copper, making it more positive (O. A. Hegnar; personal communication). The more positive the copper redox potential in the LPMO, the more readily the copper gets reduced, hence the faster the LPMO reaction on substrates occur. Visa versa, with a less positive redox potential, the LPMO reduce substances faster, as a stronger electron donor than acceptor.

The redox potential can be measured by adding reduced TMP to a copper saturated LPMO and measuring the oxidized TMP formed. The concentration of oxidized TMP can be measured with the absorbance at 610 nm and calculated based on the extinction coefficient of 14 mM^{-1} cm^{-1}, the determination of the equilibrium constant of the electron transfer reaction,

and the cell potential for oxidized TMP/reduced TMP redox couple that is 273 mV (Borisova et al., 2015). The oxidized TMP concentration equals the LPMO-Cu^{1+} concentration. This allows calculations of equilibrium concentration and electron transfer reaction, thus also the equilibrium constant. The measurements in this experiment were done at 300.85K.

Electron transfer reaction:

$$TMP_{red} + LPMO\text{-}Cu^{2+} \rightleftharpoons TMP_{ox} + LPMO\text{-}Cu^{1+}$$

Equilibrium constant:

$$K \frac{(TMP_{ox})(LPMO-Cu^{1+})}{(TMP_{red})(LPMO-Cu^{2+})}$$

Cell potential for the redox couple:

$$\Delta G_r^\circ = RT\ln K = nFE^\circ$$

Where ΔG_r° is the free energy change, *R* is the gas constant, *T* is the temperature in Kelvin, n is the number of electrons transferred in the reaction and F is the Fraday constant (Westereng et al., 2018).

Materials:

- 200 mM PIPES buffer pH 6.0
- Trace select water
- N,N,N´,N´- tetramethyl-1,4-phenulenediamine (TMP)
- Copper saturated *Sc*LPMO9A

Method:

To determine the redox potential, everything must be done anaerobically, because oxygen will interfere with the TMP measurement as the TMP oxidizes in the presence of oxygen.

Therefore, 200 mM PIPES buffer pH 6.0 and trace select water was flushed with nitrogen for 30 minutes in airtight bottles before it was transferred to an anaerobic chamber and left overnight together with weighted TMP powder.

The following day, the protein samples were flushed with nitrogen for 5 minutes and placed in an anaerobic chamber together with all consumables used (pipets, Eppendorf tubes, NanoPhotometer). A 20 mM stock of PIPES buffer was prepared in the anaerobic chamber and used to make a 300 μM stock of TMP. Then, a 100 μL protein stock with 70 μM protein concentration and 20 mM PIPES buffer concentration was prepared. Next, 30 μL protein solution and 30 μL TMP solution was mixed in triplicates together with a blank with only buffer and TMP. After approximately 5 minutes, when the reaction required equilibrium, the redox potential was measured spectrophotometrically a NanoPhotometer C40, at a wavelength of 610 nm.

3.11 Analysing LPMO products with HPAEC-PAD from single time point experiments, and time course experiments with and without added H_2O_2

LPMO product formation can be analysed using a high-performance anion-exchange chromatography system (HPAEC) coupled with pulsed amperometric detection (PAD) on, for example, an Dionex ICS-5000 or ICS-6000 system. This technique is a common technique to detect carbohydrates. ICS-5000 and ICS-6000 can analyse the degree of polymerization and are ion chromatography systems that can be used for ion chromatography (IC) and high-performance liquid chromatography (HPLC). (H. Østby; personal communication)

HPAEC can separate neutral and charged saccharides without derivatization, and the sugars can be separated by charge, size, composition, branching and linkage isomerism. PAD requires minimal sample preparation, and the samples can be diluted 100 to 1000 times (Mechelke et al., 2017).

*Sc*LPMO9A and *Nc*LPMO9C both oxidize the C4 carbon, hence generating C4 oxidized products. However, the disadvantage with C4 oxidized products with HPAEC-PAD is that they are a challenge to analyse because the column can generate derivates, and the reaction on

the column is not yet fully known (Westereng et al., 2016). Because of these disadvantages, mostly native products are discussed in this thesis.

Since carbohydrates are weak acids, they are partially ionized at high pH levels, and can therefore be separated by HPAEC. As described in Section 2.7, buffer A in HPAEC-PAD using a Dionex ICS-5000 system consists of NaOH, while buffer B consists of both NaOH and sodium acetate. As NaOH is a strong base, the pH of the inserted samples will increase and ionize. Sodium acetate increases the ionic strength, and when the concentration of buffer B increases, samples from the column will elute based on their pkA (Corradini et al., 2012). The principles for ICS-6000 are the same, but the eluents consist of KOH and KMSA instead of NaOH and ammonium sulfate.

HPLC systems are designed to separate charged molecules in a sample when the sample travels through a column consisting of polymers. The system consists of a mobile phase and a stationary phase. The mobile phase, in this case, the eluents, are pushed through the system by the pumps. Before the eluents can travel through the columns, it goes through a degassing device to ensure that there is no oxygen in the eluents. Then, an autosampler and an injector inject the sample into the column. When the sample is ready to be injected into the column, the eluent is stopped, and the sample goes through the column before the eluent can continue to flow through the system (H. Østby; personal communication).

When the sample is injected, it first passes through a guard column that removes compounds like heavy metals, before the sample goes through an analytical column. In this column, molecules with high affinity take longer to elute than molecules with low affinity. To elute the molecules from the column, the eluent concentration is increased over time. When the molecules are eluted, they travel through a suppressor that makes sure only nanopure water and separated molecules are sent to the conductivity detector. This detector measures the conductivity as different molecules pass through the column, making peaks. The concentration of molecules is calculated by measuring the area or hight of the peaks, and then applying a standard curve of compounds of known concentrations (H. Østby; personal communication).

For this work, both HPAEC-PAD using a Dionex ICS-5000 system and Dionex ICS-6000 system were used. Therefore, it is specified in the figure text which system that are used.

Materials:

- *Sc*LPMO9A
- *Nc*LPMO9C
- Substrate
- AscA
- Sodium acetate buffer pH 5.0
- H_2O_2
- 200 mM NaOH
- MilliQ water

Method – Endoglucanase activity screening:

All reactions were prepared in 1.5 mL Eppendorf tubes to a final volume of 100 µL. When mixing the component for LPMO reactions, the sequence of added components is important since reduction of the LPMO will initiate the reaction. Therefore, MilliQ water was first added to the Eppendorf tube, before 500 mM sodium acetate buffer pH 5.0 was added to a final concentration of 50 mM. Then, PASC was added to a final concentration of 0.4% substrate. Next, the LPMOs was added to the solution to a final concentration of 1 µM.

When all Eppendorf tubes were prepared, the tubes were incubated at 40 °C, 1000 rpm for 1 minute before AscA was added to a final concentration of 1 mM. Then the reactions were incubated for approximately 24 hours.

After 24 hours, the reactions were stopped by filtering using 0.45 µm Durapore Membrane and a membrane dry vacuum compressor. The reaction stops because PASC is insoluble and will not travel through the filter. The filtered samples were then diluted in two times in MilliQ water before being transferred to 0.30 mL PP Snap Ring Micro Vial. In addition to the reaction samples, 1 Micro Vial containing C4 oxidizing standard and 1 Micro Vial containing native standard DP2-6 was also prepared.

Before the samples could be analysed, a start-up method was performed to ensure that everything from earlier experiments was eluted. The gradient started with 100% eluent A, flow rate 0.5 mL/min, after 30 minutes the flow was at 70% B and 30 % A and after 42 minutes the flow was set to 100% eluent B.

When the start-up method was finished, blank samples with a full native and oxidizing method was performed, before the samples was analysed with the same method. This method also had a flow of 0.5 mL/min but had a slower gradient towards eluent B than the start-up method. After 4.5 minutes the concentration of eluent B was 5.5%, after 13.5 minutes it was at 15 % and after 30 minutes it was 100% before the gradient was switched to 100% A. The total gradient time was 39 minutes.

Lastly, a "good night" method was performed with a flow of 0.5 mL/min and a gradient from 100% eluent A to 100% eluent C over 15 minutes. The data was analysed with Chromeleon 7.2.9 to check for endoglucanase activity.

Method – Single time point experiments:

When setting up experiments, triplicates were made from each reaction and all reactions were prepared in 1.5 mL Eppendorf tubes. MilliQ water was first added to the Eppendorf tube, before 500 mM sodium acetate buffer pH 5.0 was added to a final concentration of 50 mM. Then, the substrate (cellotetraose, cellopentaose or cellohexaose) was added to a final concentration of 1 mM substrate. Next, the LPMOs was added to the solution to a final concentration of 1 µM.

When all the Eppendorf tubes were prepared, the samples were incubated for 1 minute in a thermomixer at 40 °C and 1000 rpm. After incubation, AscA was added to the reactions to a final concentration of 1 mM. To stop the reactions, 50 µL from the reactions were transferred to 50 µL 200 mM NaOH, after approximately 24 hours.

After reactions were stopped, the solutions were filtered using a 0.45 µm Durapore Membrane and a membrane dry vacuum compressor. Then the filtered samples were diluted two times in MilliQ water and transferred to 0.3 mL PP Snap Ring Micro Vials. DP2, DP3 and DP4 (DP4 only for cellohexaose) standards were also transferred to 0.3 mL PP Snap Ring Micro Vials,

with a concentration of 500 µM, 250 µM, 100 µM 10 µM, 5 µM and 1 µM for making a standard curve.

Next, the samples were placed in the autosampler to ICS-5000. A start after eluent change was first performed, as described in Section 3.11 (Method – Endoglucanase activity screening), before a 14-minute gradient was performed with a stepwise gradient with an increasing amount of eluent B. The method started with 0-10 % B over 5 minutes, then 10 – 100 % B over 3 minutes and 30 seconds before the gradient increased from 100 – 0 % B over 6 seconds. After every sample was analysed with this method, a good night method was performed, to shut down the system, also described in Section 3.11 (Method – Endoglucanase activity screening.

Method – Time course experiments without added H_2O_2:

Triplicates were made from each reaction and all reactions were prepared in 1.5 mL Eppendorf tubes. MilliQ water was first added to the Eppendorf tube, before 500 mM sodium acetate buffer pH 5.0 was added to a final concentration of 50 mM. Then, the substrate (cellotetraose, cellopentaose or cellohexaose) was added to a final concentration of 1 mM. Next, the LPMOs was added to the solution to a final concentration of 1 µM.

When all the Eppendorf tubes were prepared, the samples were incubated for 1 minute in a thermomixer at 40 °C and 1000 rpm. After incubation, AscA was added to the reactions to a final concentration of 1 mM. To stop the reactions, 50 µL from the reactions were transferred to 50 µL 200 mM NaOH, after 30 minutes, 1, 2 and 4 hours for 4-hours time course experiments, or after 30 minutes, 1, 2, 4, 6, 8 and 24 hours for 24-hours time course experiments.

When all reactions were stopped for all time points, the solutions were filtered using a 0.45 µm Durapore Membrane and a membrane dry vacuum compressor. The filtered samples were diluted in MilliQ water and transferred to 0.3 mL PP Snap Ring Micro Vials. In addition to the samples from the reactions, DP2, DP3 and DP4 (DP4 only for cellohexaose) standards were transferred to 0.3 mL PP Snap Ring Micro Vials, with a concentration of 500 µM, 250 µM, 100 µM 10 µM, 5 µM and 1 µM for ICS-5000, and 100, 50, 25, 10, 5 and 1 µM for ICS-6000. DP2-6 standards were also used with a final concentration of 50 µM.

When all samples were prepared and transferred to the Micro Vials, the samples were placed in the autosampler to ICS-5000 or ICS-6000. For ICS-5000, a start after eluent change was first performed, as described in Section 3.11 (Method – Endoglucanase activity screening), before a 14-minute method was performed, as described in Section 3.11 (Method – Single time point experiments)

For ICS-6000, the method used to quantify native products was a 24-minutes gradient starting with 100 mM potassium hydroxide (KOH) and 0 mM potassium methanesulfonate (KMSA) from zero to 6 minutes, then 100 mM KOH and 30 mM KMSA from 6 to 10 minutes and 100 mM of both from 10 to 15 minutes. Nest, the KMSA was decreased to 0 mM over 6 seconds.

Method – Time course experiments with added H_2O_2:

Triplicates were made from each reaction and all reactions were prepared in 1.5 mL Eppendorf tubes. MilliQ water was first added to the Eppendorf tube before 500 mM sodium acetate buffer pH 5.0 was added to a final concentration of 50 mM. Then, the substrate (cellopentaose) was added to a final concentration of 1 mM substrate. H_2O_2 was added with different concentrations (25, 50, 100 and 250 µM). Next, the LPMOs was added to the solution to a final concentration of 1 µM.

When all the Eppendorf tubes were prepared, the samples were incubated for 1 minute in a thermomixer at 40 °C and 1000 rpm. After incubation, AscA was added to the reactions, to a final concentration of either 1 mM or 50 µM specified under the figures. To stop the reactions, 50 µL from the reactions were transferred to 50 µL 200 mM NaOH, after 3, 6, 9, 30 and 60 minutes.

When all reactions were stopped, the solutions were filtered using a 0.45 µm Durapore Membrane and a membrane dry vacuum compressor. The filtered samples were diluted in MilliQ water and transferred to 0.3 mL PP Snap Ring Micro Vials. In addition to the samples from the reactions, DP2 and DP3 standards were transferred to 0.3 mL PP Snap Ring Micro Vials, with a concentration of 100, 50, 25, 10, 5 and 1 µM. DP2-6 standards were also used with a final concentration of 50 µM.

When all samples were prepared and transferred to the Micro Vials, the samples were placed in the autosampler of ICS-6000. The method used to quantify native products were a 24-minutes gradient method described in Section 3.11 (Method – Time course experiments without added H_2O_2).

The chromatograms were analysed using Chromeleon 7.2.9 and figures were made with Microsoft Excel 16.54.

3.12 The synergy between a Cellulase-cocktail and *Sc*LPMO9A

Several studies have shown that cellulases working in synergy give a higher saccharification yield than enzymes working individually and that the conversion is boosted even more by adding LPMOs to the substrate (Tokin et al., 2020). Therefore, cocktails with both LPMOs and cellulases are commonly used in the industry to increase the sugar yield.

To understand how ScLPMO9A affected the sugar yield from sulfite pulped Norway spruce, product formation after adding ScLPMO9A to an LPMO-poor cellulase cocktail were analysed using HPLC with a Rezex ROA-Organic Acid H+ (8%) (300x7.8 mm). The reason why this column was used, is because the column is suitable for mono- and disaccharides, and the main product after depolymerization with a cellulose-LPMO-cocktail is glucose.

In contrast to HPAEC-PAD, which separates the oligosaccharides based on anion exchange, HPLC with Rezex column separates mono and short oligosaccharides based on ion-exclusion. Both UV absorption and refractive index (RI) can be used for detection. In this experiment, the main product was glucose and cellobiose, which have low UV, therefore, IR was used for detection.

Today, most commercial cellulase cocktails include both LPMOs and GBs. However, since the goal in this study was to calculate the effect of the LPMOs relative to a cocktail without LPMOs, a cocktail without LPMOs and BGs was used. Therefore, BGs was added to all reactions, whereas *Sc*LPMO9A were only added to some of the reactions.

Materials:

- Celluclast
- β-glucosidase
- *Sc*LPMO9A
- VASP
- AscA
- 500 mM sodium acetate buffer pH 5.0
- 5 mM sulfuric acid (eluent)

Method:

The reactions were prepared in 60 mL rubber sealed glass vessels with 10 mL working volume and 50 mL headspace, aerobic conditions. Duplicates were made with MilliQ water, sodium acetate buffer pH 5.0 (50 mM), 100 g/L VASP, 3.6 mg/g dry matter (DM) celluclast, 0.4 mg/g DM *Sc*LPMO9A, 0.4 mg/g DM β-glucosidase and 1 mM AscA. Controls without LPMO and AscA were also made. The reactions were initiated by incubation at 50 °C and 200 rpm. The reactions were stopped after 4, 6, 8, 24, 48 and 72 hours by transferring 100 µL of the reaction to 200 µL MilliQ water and heat inactivating the enzymes at 100 °C for 15 minutes.

When the reactions had been stopped at all time points, the solutions were filtered using a 0.45 µm Durapore Membrane and a membrane dry vacuum compressor. The filtered samples were transferred to 0.3 mL PP Snap Ring Micro Vials. In addition to the samples from the reactions, glucose and cellobiose standards combined were transferred to 0.3 mL PP Snap Ring Micro Vials, with a concentration of 10 g/L, 5 g/L, 2.5 g/L, 0.5 g/L and 0.1 g/L. The samples were analysed on Dionex Ultimate 3000 RSCL with a long Rezex column with a 22-minute performance time and with 0.6 mL flow rate. The chromatograms were analysed using Chromeleon 7.2.9 and figures were made with Microsoft Excel 16.54.

The same reactions were also quantified on HPAEC-PAD using a Dionex ISC-5000 system. The procedure was similar to the method described in Section 3.11, except the method had a 39-minutes gradient to quantify C4 oxidized products, starting with 100% A over 4.5 minutes,

before 5.5% B from 4.5 to 13.5 minutes, 15% B to 30 minutes and 100% B for 6 seconds before 100% A.

3.13 Bioinformatics

Bioinformatics is a powerful tool when working with enzymes. For example, multiple sequence alignments (MSA) can give useful insights into conserved structural elements and can also be used to predict phylogenetic relationships. In addition to this, when proteins with known structures show a high enough degree of similarity, modelling can be used to predict a three-dimensional structure of the protein of interest, for example by using threading (e.g. PHYRE 2) or homology modelling (e.g. SWISS-MODEL)

3.13.1 Phylogenetic tree

To predict a phylogenetic tree of 47 known LPMO9s, the sequences were downloaded from CAZy (Drula et al., 2022), and signal and CBMs were removed, as predicted by SignalP (Almagro Armenteros et al., 2019) and Pfam (Mistry et al., 2021) respectively. Next, ClustalW (Madeira et al., 2022) was used to make a MSA of all sequences before the alignment was edited in AliView (Larsson, 2014). Then, the resulting MSA was used for phylogenetic analysis using the ProtTest 3.4 (Darriba et al.) software package using the default settings, and a consensus tree was built with all 120 likelihood scores using the Akaike information criterion (AIC). The resulting phylogenetic tree was uploaded and edited using iTOL V6 (Letunic & Bork, 2021). The tree is shown in supplementary as Figure S1.

3.13.2 Multiple sequence alignment of selected LPMO9s

6 LPMO9s from the phylogenetic tree were used to predict a MSA using ClustalW. *Sc*LPMO9A and *Ns*LPMO9C were chosen because they were analysed in this thesis. *Ls*LPMO9A were chosen because *Ls*LPMO9A are the closest homolog to *Sc*LPMO9A. Lastly, *Ps*LPMO9A, *Nc*LPMO9B and *Tr*LPMO9A were used because they are not closely related to *Sc*LPMO9A, hence they show which amino acids that are conserved.

The multiple sequence alignment (MSA) was predicted by T-coffee expresso (Armougom et al., 2006), and edited in AliView and Microsoft OneNote 16.54.

3.13.3 Prediction of the three-dimensional structure of *Sc*LPMO9A

A structure model was predicted by SWISS-MODEL (Waterhouse et al., 2018) and was built based on *Ls*LPMO9A bound to cellohexaose (PDB: 5ACI) as a template and edited in PyMOL (The PyMOL Molecular Graphics System, Version 2.0, Schrödinger, LLC).

4 Results

The results obtained in this thesis were used to get a better understanding if *Sc*LPMO9A is a suitable candidate for industrial degradation of biomass, and to gain a better understanding of why some LPMOs work on soluble substrates in nature. In addition to laboratory experiments, the genome from *Sc*LPMO9A was analysed using bioinformatic tools.

4.1 Bioinformatics and previous work

4.1.1 Multiple sequence alignment

A MSA of *Sc*LPMO9A, *Ls*LPMO9A, *Nc*LPMO9C, *Ps*LPMO9A, *Nc*LPMO9B and *Tr*LPMO9A was made with T-COFFEE EXPRESSO (Armougom et al., 2006), and edited in Microsoft OneNote 16.54 (Figure 4.1.1).

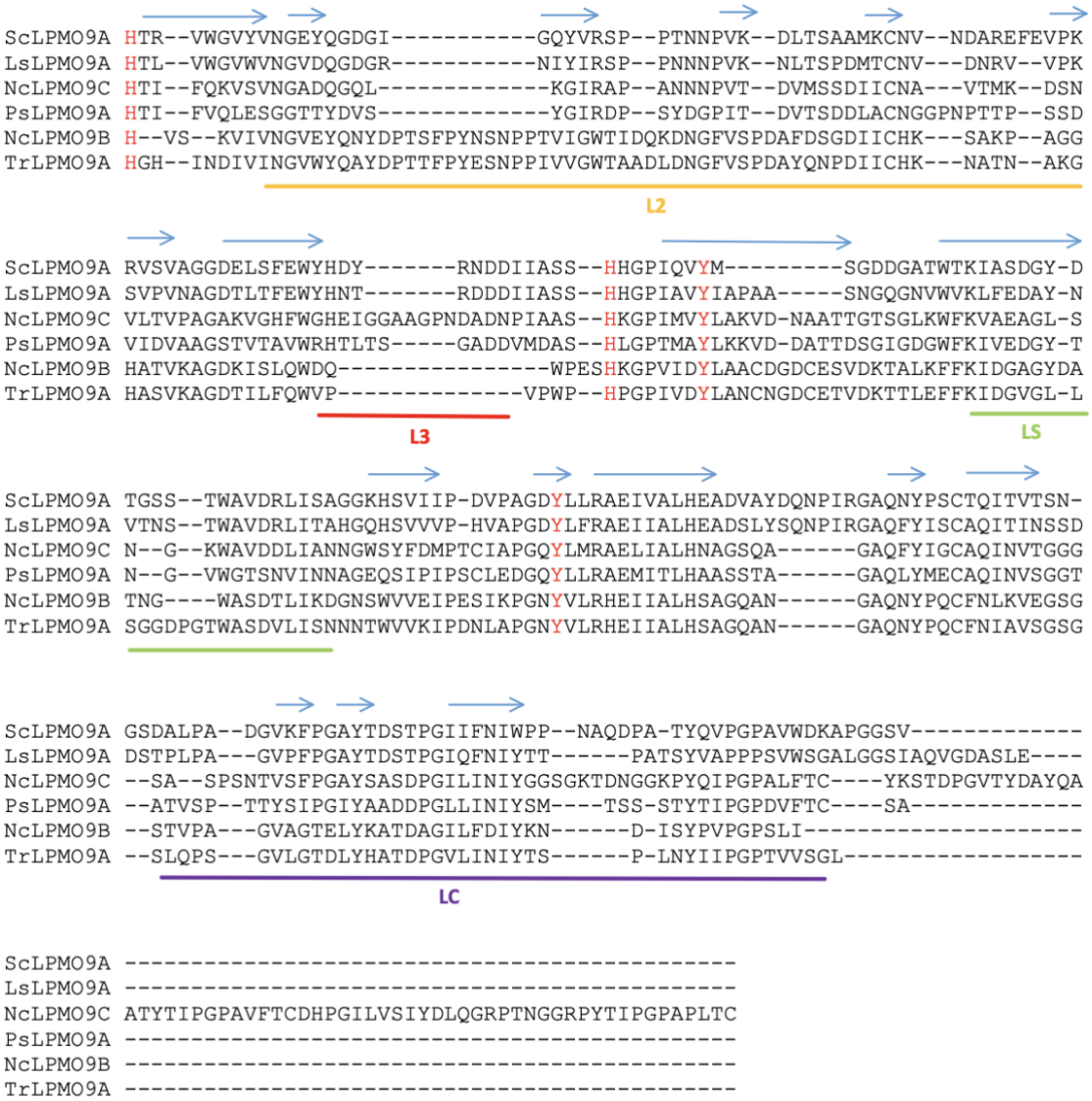

Figure 4.1.1. Multiple sequence alignment of *Sc*LPMO9A, *Ls*LPMO9A, *Nc*LPMO9C, *Ps*LPMO9A, *Nc*LPMO9B and *Tr*LPMO9A. The sequence alignment was made using known sequences of the LPMO9s. The secondary structure is based on *Ls*LPMO9A and is shown above the columns as blue arrows (β -sheet). The lines below the columns show the amino acids of the 4 loop regions and are based on *Nc*LPMO9C, where L2 is coloured orange, L3 red, LS green and LC purple. The active site histidines and the conserved tyrosine are coloured red. All sequences are presented without the signal peptide and CBMs and start from the N-terminal histidine.

The MSA shows that the histidines (His1 and His81) in the histidine brace are conserved in addition to the tyrosine (Tyr163 for *Sc*LPMO9A) supporting the active site. Both close (*Ls*LPMO9A) and distant (*Ps*LPMO9A, *Nc*LPMO9B and *Tr*LPMO9A) related LPMO9s were chosen based on a phylogenetic tree shown in Figure S1.

4.1.2 Prediction of protein structure

SWISS-MODEL was used to predict a protein structure of *Sc*LPMO9A. The results from the SWISS-MODEL showed that *Sc*LPMO9A shares a 61.09% sequence identity with the well-characterized *Ls*LPMO9A (PDB ID: A0A0S2GKZ1), which is the closest homolog with a known structure. Therefore, *Ls*LPMO9A was used as a template to predict a secondary structure of *Sc*LPMO9A. The model was visualised and edited in PyMOL (Figures 4.1.2, 4.1.3 and 4.1.4).

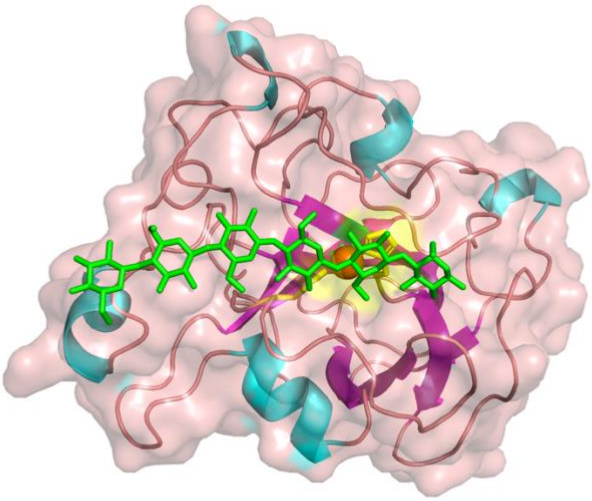

Figure 4.1.2. *Sc*LPMO9A side view made with PyMOL. The secondary structure elements are coloured turquoise (α-helix), magenta (β-sheet) and light pink (loops). The histidines in the histidine brace are coloured yellow and the tyrosine is coloured green. The substrate (cellohexaose) is also shown in green and was superimposed from the *Ls*LPMO9A alignment figure (PDB ID: 5AC1).

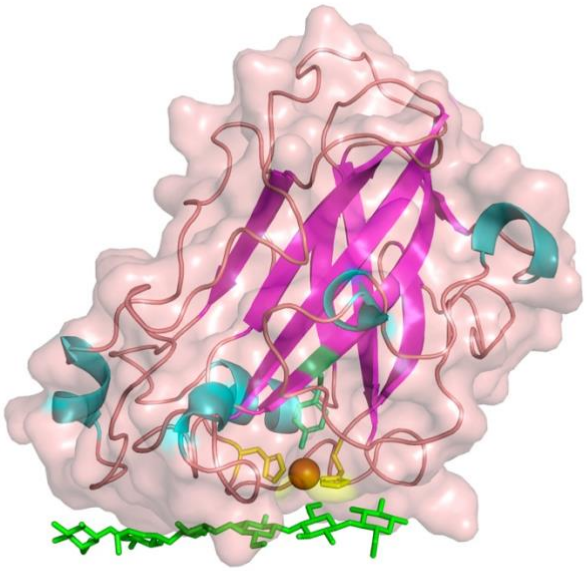

Figure 4.1.3. *Sc*LPMO9A top view made with PyMOL. The secondary structure elements are coloured turquoise (α-helix), magenta (β-sheet) and light pink (loops). The histidines in the histidine brace are coloured yellow and the tyrosine is coloured green. The substrate (cellohexaose) is also shown in green was superimposed from the *Ls*LPMO9A alignment figure (PDB ID: 5AC1).
.

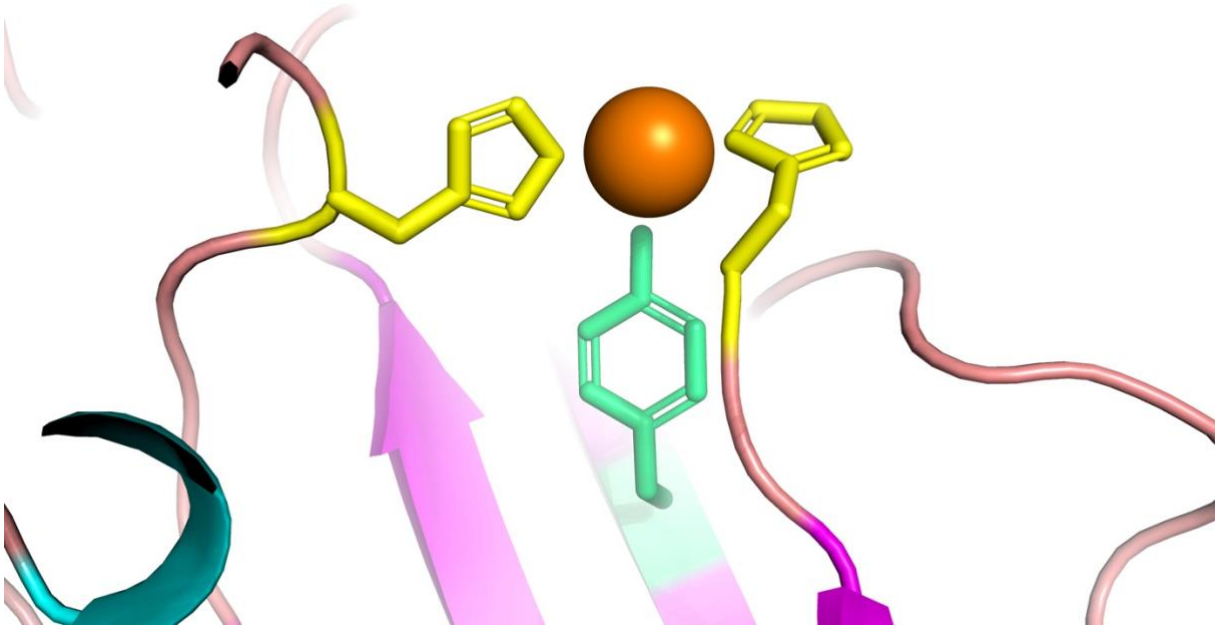

Figure 4.1.4. *Sc*LPMO9A histidine brace with copper. The histidines in the histidine brace are coloured yellow and the tyrosine is coloured green. Copper is coloured orange.

*Sc*LPMO9A consist of a typical AA9 fold with β-sheets, α-helixes, and loops (Figures 4.1.2, 4.1.3 and 4.1.4). The histidine brace supports the copper ion in the active site together with

the tyrosine. The figures also demonstrate that *Sc*LPMO9A consist of a substrate binding site that fits cellohexaose.

4.1.3 Previous work

Prior to the laboratory work for this thesis, substrate screening with HPAEC-PAD was performed by Heidi Østby. Figures 4.1.5-4.1.9 were also produced by Heidi Østby.

The LPMO9s that have been reported to have activity on polysaccharides, are active on celluloses, with some of them also being active on hemicelluloses. Therefore, *Sc*LPMO9A was tested with the following substrates: Avicel, cellopentaose, PASC, sulfite pulped spruce, beta-glucan (BG), xyloglucan oligos (XO), konjac glucomannan (KGM) and xyloglucan from tamarind seed (TXG). In addition, the following substrates were co-incubated in reactions with *Sc*LPMO9A: PASC + BG, PASC + KGM, PASC + TXG and PASC + XO.

Here, C4 oxidized products were analysed, as the chromatogram should only demonstrate if the enzyme was active on the substrate or not, and not be quantified.

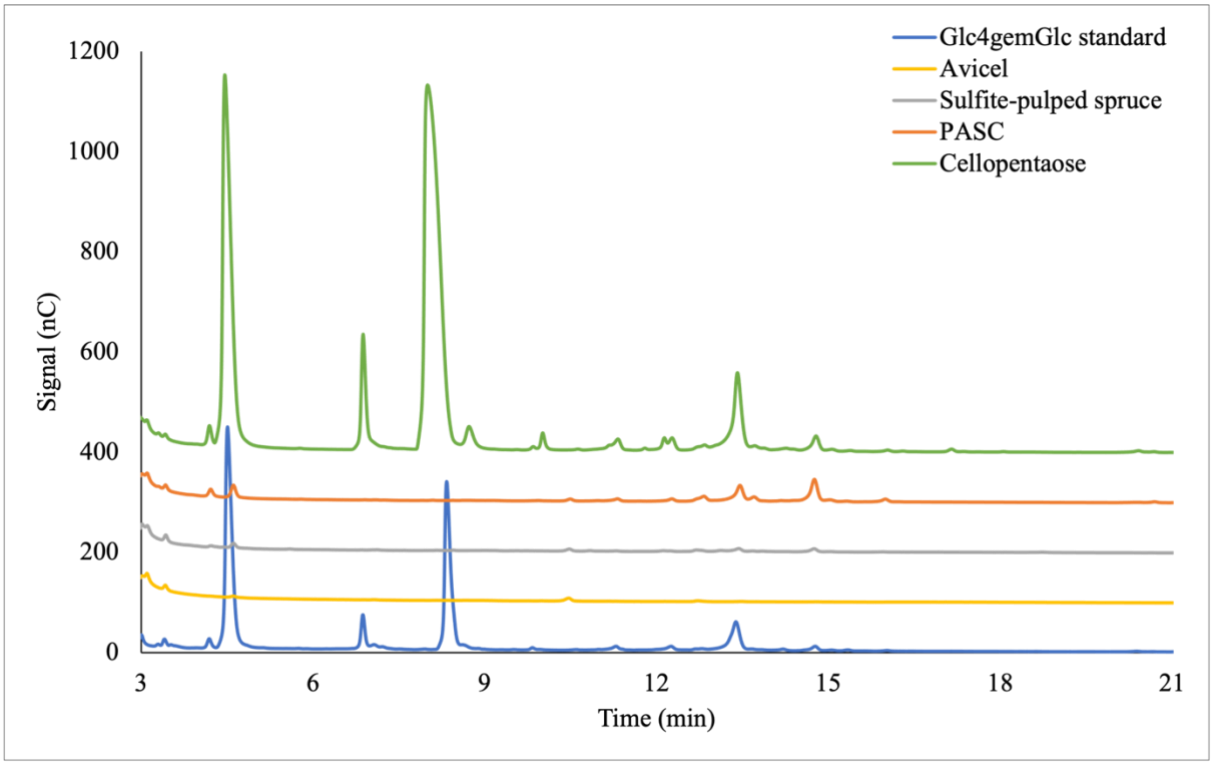

Figure 4.1.5. HPAEC-PAD chromatograms of products generated from reactions of *Sc*LPMO9A with Avicel (yellow), sulfite-pulped spruce (gray), PASC (orange), and cellopentaose (green). The blue chromatogram shows a standard of C4 oxidized cellobiose (Glc4gemGlc) and C4 oxidized cellotriose (Glc4gemGlc$_2$). Cellobiose eluted at approximately 4 minutes, cellotriose at approximately 9 minutes, Glc4gemGlc eluted between 13 and 14 minutes while Glc4gemGlc$_2$ eluted after approximately 15 minutes. All reactions were performed with 1 µM LPMO and 1 mM AscA in 50 mM Bis-Tris-HCl buffer pH 6.5 and incubated at 40°C and 1000 rpm for 16 h. Reactions with Avicel, PASC, and cellopentaose contained 2 g/L substrate; the reaction with sulfite-pulped spruce contained 10 g/L substrate. Control reactions in the absence of AscA did not show any formation of native or C4-oxidized products. The samples were analysed with HPAEC-PAD using a Dionex ICS-5000 system. All reactions were carried out in triplicate and gave identical product profiles.

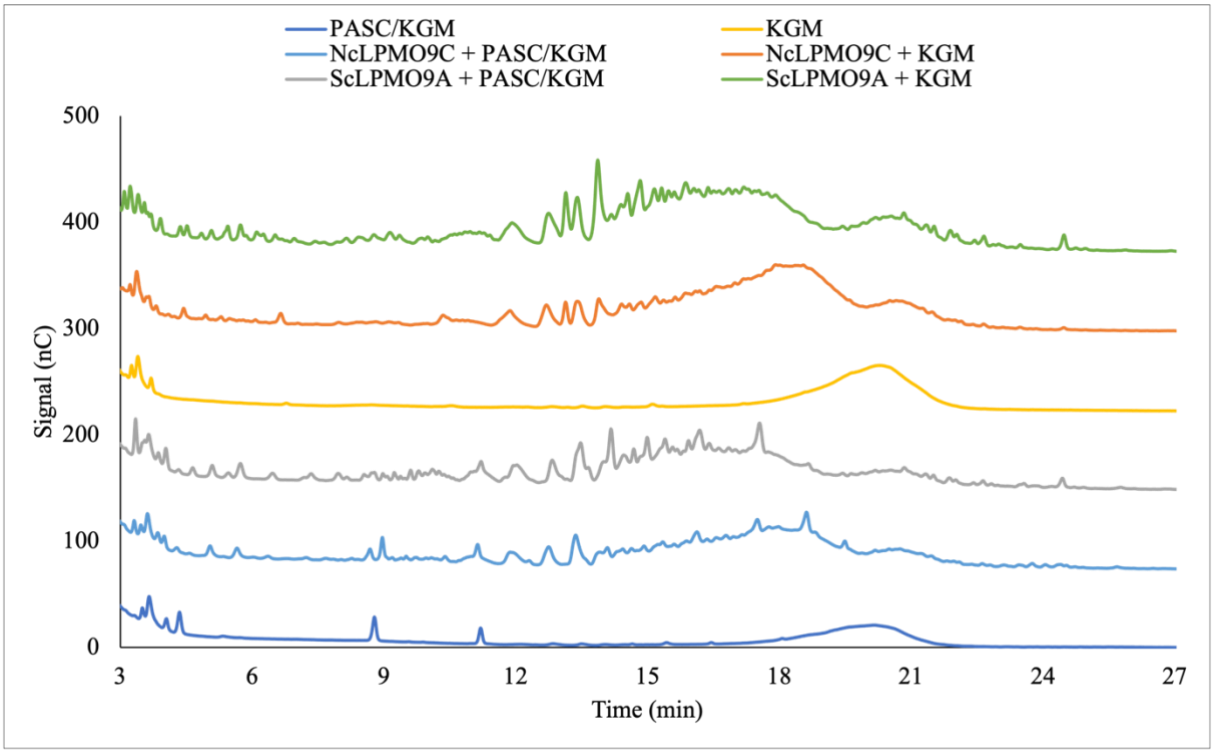

Figure 4.1.6. HPAEC-PAD chromatograms of products generated from reactions of *Sc*LPMO9A or *Nc*LPMO9C with a mixture of PASC and KGM, or with KGM. LPMO reactions were performed with 1 µM LPMO and 1 mM AscA in 50 mM Bis-Tris-HCl buffer pH 6.5 and incubated at 40°C and 1000 rpm for 16 h. Substrate controls without added LPMO were similarly incubated with 1 mM AscA. Reactions with PASC and KGM contained 4 g/L of substrate (2 g/L of each substrate); reactions with KGM contained 2 g/L substrate. Cellobiose products are shown at approximately 4 minutes, cellotriose production at 6 minutes, Glc4gemGlc around 16 minutes and Glc4gemGlc$_2$ around 18 minutes. Control reactions with LPMO in the absence of AscA did not show any product formation. The samples were analysed with HPAEC-PAD using a Dionex ICS-5000 system. All reactions were carried out in triplicate and gave identical product profiles.

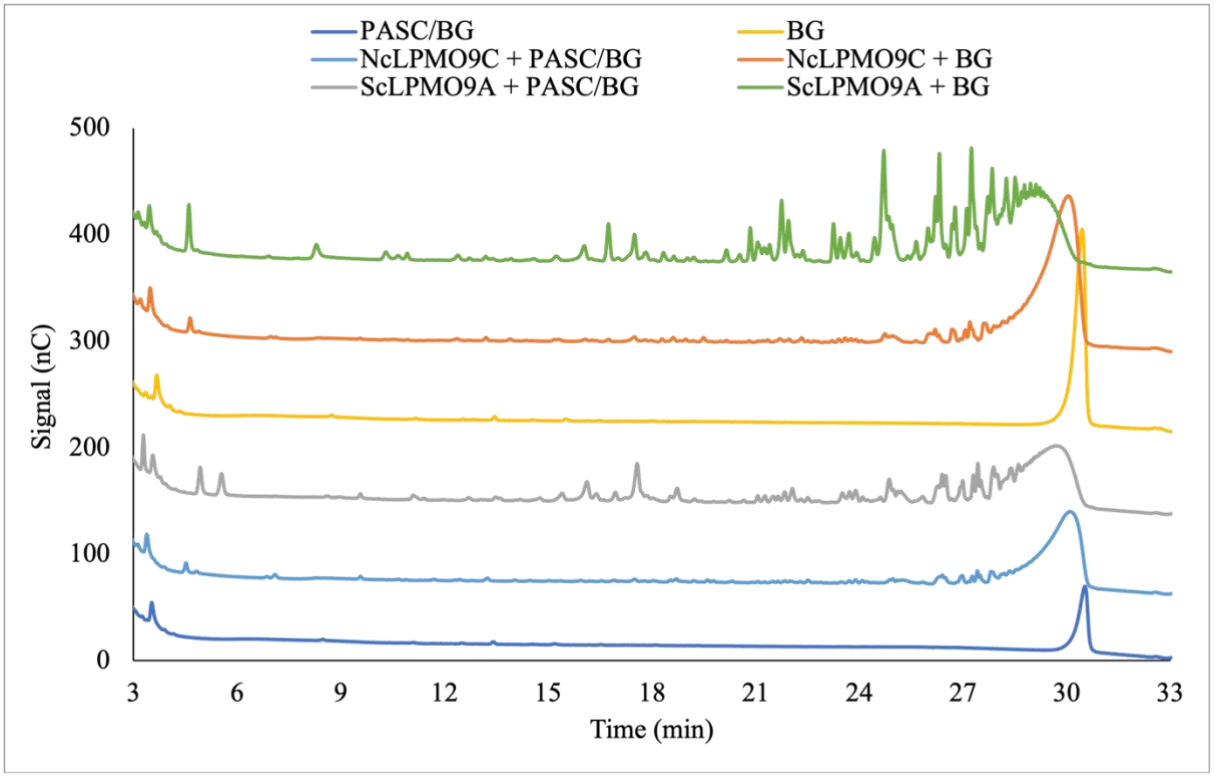

Figure 4.1.7. HPAEC-PAD chromatograms of products generated from reactions of *Sc*LPMO9A or *Nc*LPMO9C with a mixture of PASC and BG, or with BG. LPMO reactions were performed with 1 µM LPMO and 1 mM AscA in 50 mM Bis-Tris-HCl buffer pH 6.5 and incubated at 40°C and 1000 rpm for 16 h. Substrate controls without added LPMO were similarly incubated with 1 mM AscA. Reactions with PASC and BG contained 4 g/L of substrate (2 g/L of each substrate); reactions with BG contained 2 g/L substrate. Cellobiose products are shown at approximately 3 minutes, cellotriose production at 6 minutes, Glc4gemGlc at 16 minutes and Glc4gemGlc$_2$ at 18 minutes. The samples were analysed with HPAEC-PAD using a Dionex ICS-5000 system. All reactions were carried out in triplicate and gave identical product profiles.

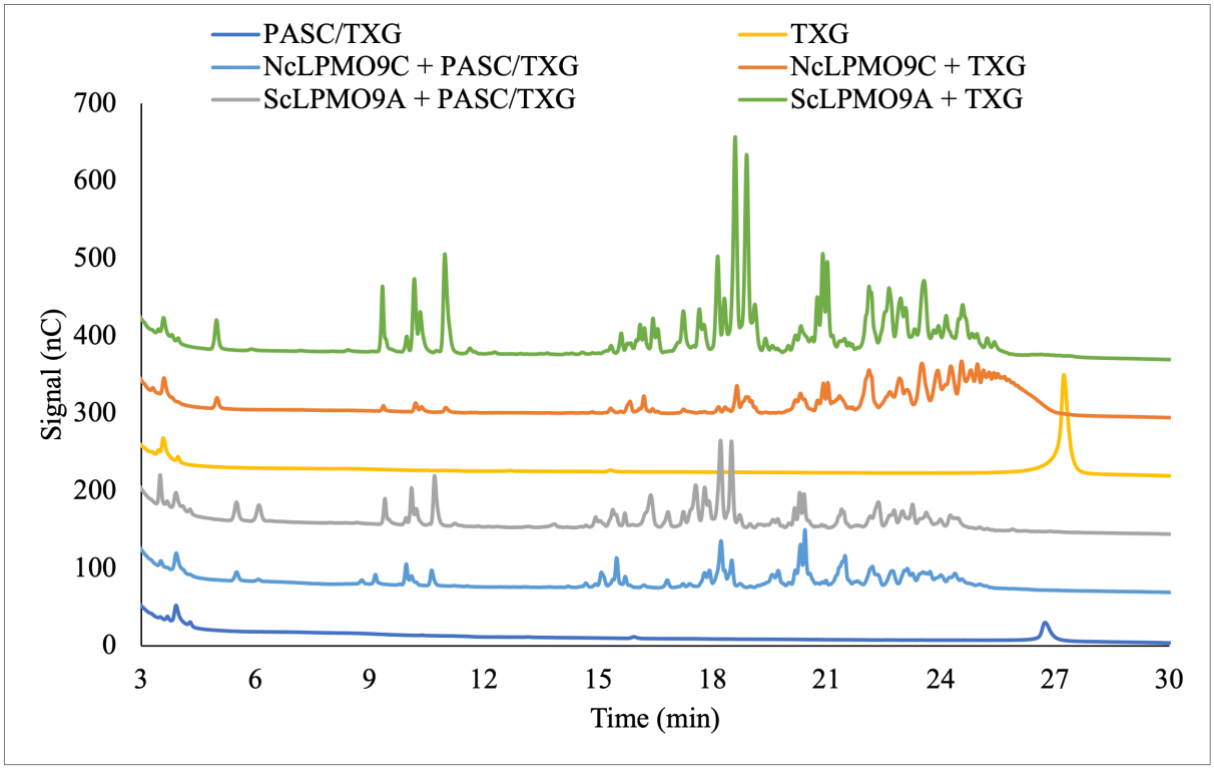

Figure 4.1.8. HPAEC-PAD chromatograms of products generated from reactions of *Sc*LPMO9A or *Nc*LPMO9C with a mixture of PASC and TXM, or with TXM. LPMO reactions were performed with 1 µM LPMO and 1 mM AscA in 50 mM Bis-Tris-HCl buffer pH 6.5 and incubated at 40°C and 1000 rpm for 16 h. Substrate controls without added LPMO were similarly incubated with 1 mM AscA. Reactions with PASC and TXM contained 4 g/L of substrate (2 g/L of each substrate); reactions with TXM contained 2 g/L substrate. Control reactions with LPMO in the absence of AscA did not show any product formation. Cellobiose products are shown at approximately 3 minutes, cellotriose production at 6 minutes, Glc4gemGlc at 16 minutes and Glc4gemGlc$_2$ at 18 minutes. The samples were analysed with HPAEC-PAD using a Dionex ICS-5000 system. All reactions were carried out in triplicate and gave identical product profiles.

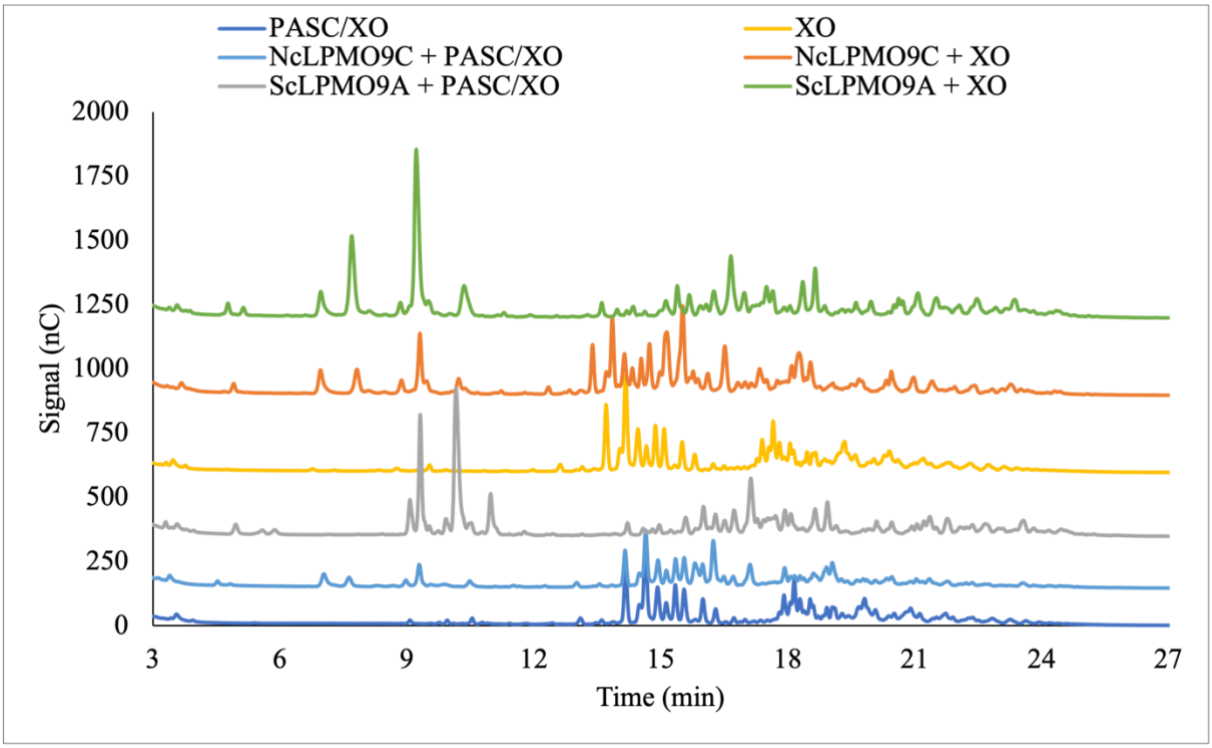

Figure 4.1.9. HPAEC-PAD chromatograms of products generated from reactions of *Sc*LPMO9A or *Nc*LPMO9C with a mixture of PASC and XO, or with XO. LPMO reactions were performed with 1 µM LPMO and 1 mM AscA in 50 mM Bis-Tris-HCl buffer pH 6.5 and incubated at 40°C and 1000 rpm for 16 h. Substrate controls without added LPMO were similarly incubated with 1 mM AscA. Reactions with PASC and XO contained 4 g/L of substrate (2 g/L of each substrate); reactions with XO contained 2 g/L substrate. Control reactions with LPMO in the absence of AscA did not show any product formation. Cellobiose products are shown at approximately 3 minutes, cellotriose production at 5 minutes, Glc4gemGlc at 16 minutes and Glc4gemGlc$_2$ at 18 minutes. The samples were analysed with HPAEC-PAD using a Dionex ICS-5000 system. All reactions were carried out in triplicate and gave identical product profiles.

Initial screening showed that *Sc*LPMO9A generated native and C4 oxidized products in reactions with cellopentaose and PASC (Figure 4.1.5). *Sc*LPMO9A did not show activity on Avicel.

*Sc*LPMO9A and *Nc*LPMO9C were active on KGM, both in the presence and absence of PASC (Figure 4.1.6). Both enzymes were also active on BG, TXG and XO with and without PASC (Figure 4.1.7, 4.1.8 and 4.1.9). There were no C1 oxidized products generated from *Sc*LPMO9A for any of the substrates tested.

4.2 Purification of *Sc*LPMO9A

The first step in the laboratory work for this thesis, after cultivation of *E. coli* carrying the pJB_pelB_*Sc* plasmid encoding the *Sc*LPMO9A gene, was to purify *Sc*LPMO9A. Following the cultivation of *E. coli*, *Sc*LPMO9A was harvested using osmotic shock. After harvesting, samples from both the supernatant and the pellet were analysed using SDS-PAGE. This showed the presence of a large band around 27-28 kDa in the supernatant, corresponding well to the predicted size of *Sc*LPMO9A (24.5 kDa). The increase in mass was probably because of glycosylations.

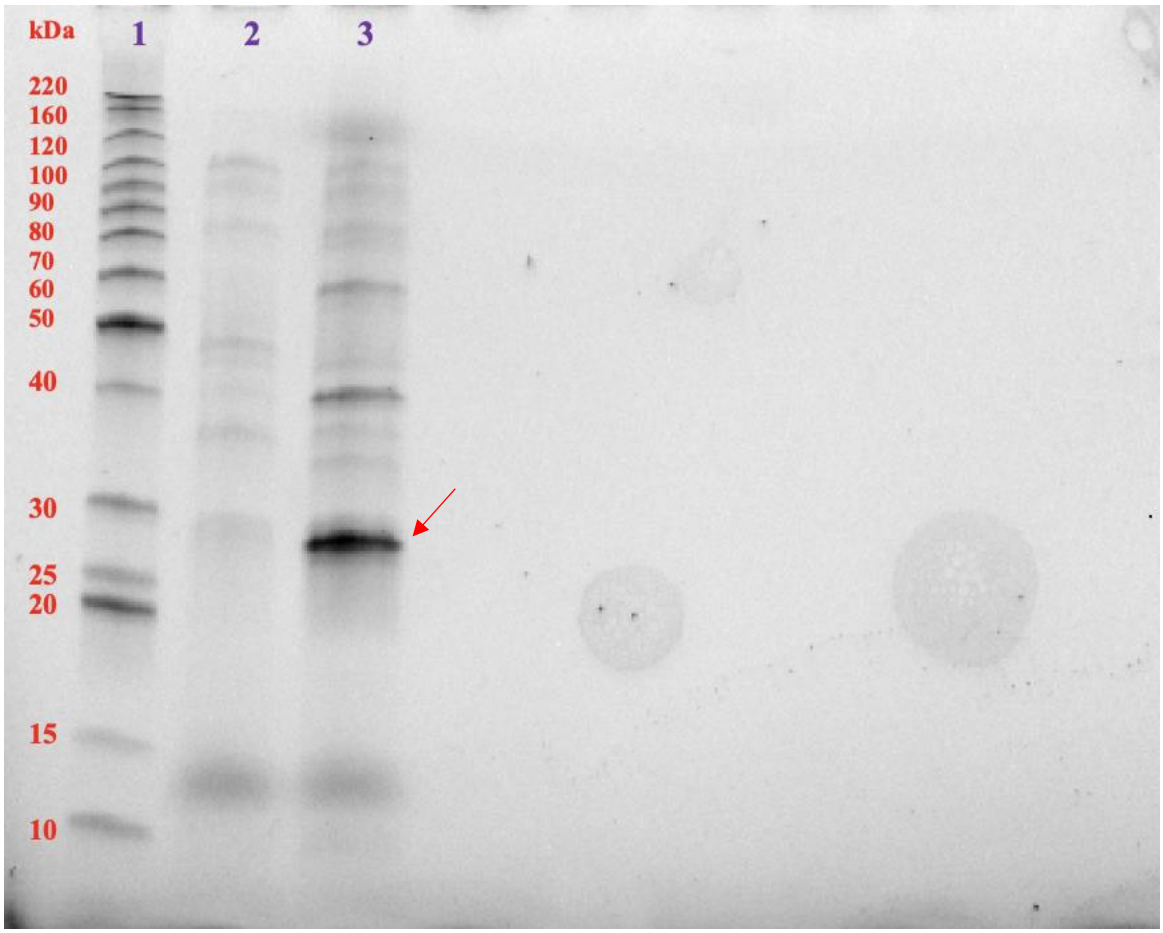

Figure 4.2.1. SDS-PAGE gel after *Sc*LPMO9A had been harvested using osmotic shock. The first well contains the Benchmark protein ladder, the second well contains the pellet and the third well contains the supernatant. *Sc*LPMO9A has a predicted molecular weight of 24.5 kDa. Compared to the Benchmark protein ladder, the marked protein has a molecular weight around that weight in the supernatant, hence the protein was successfully harvested.

Following identification of *Sc*LPMO9A in the supernatant, the protein was purified using anion exchange chromatography.

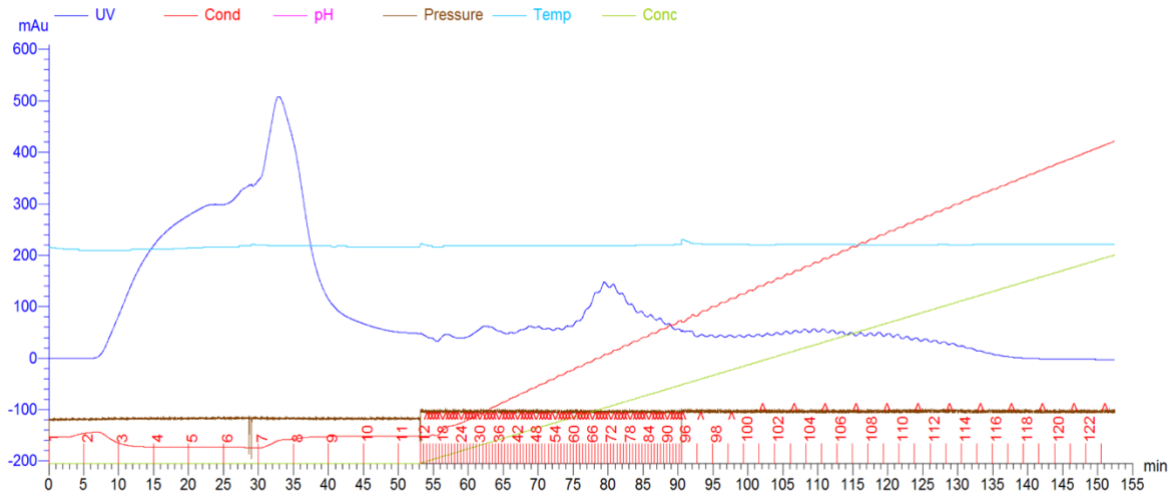

Figure 4.2.2. Anion exchange chromatogram. *Sc*LPMO9A eluted after approximately 75 minutes and with approximately 12% buffer B (buffer B shown as green line).

To ensure that *Sc*LPMO9A had eluted and to find which fractions to be pooled, some fractions from the peaks were analysed at SDS-PAGE.

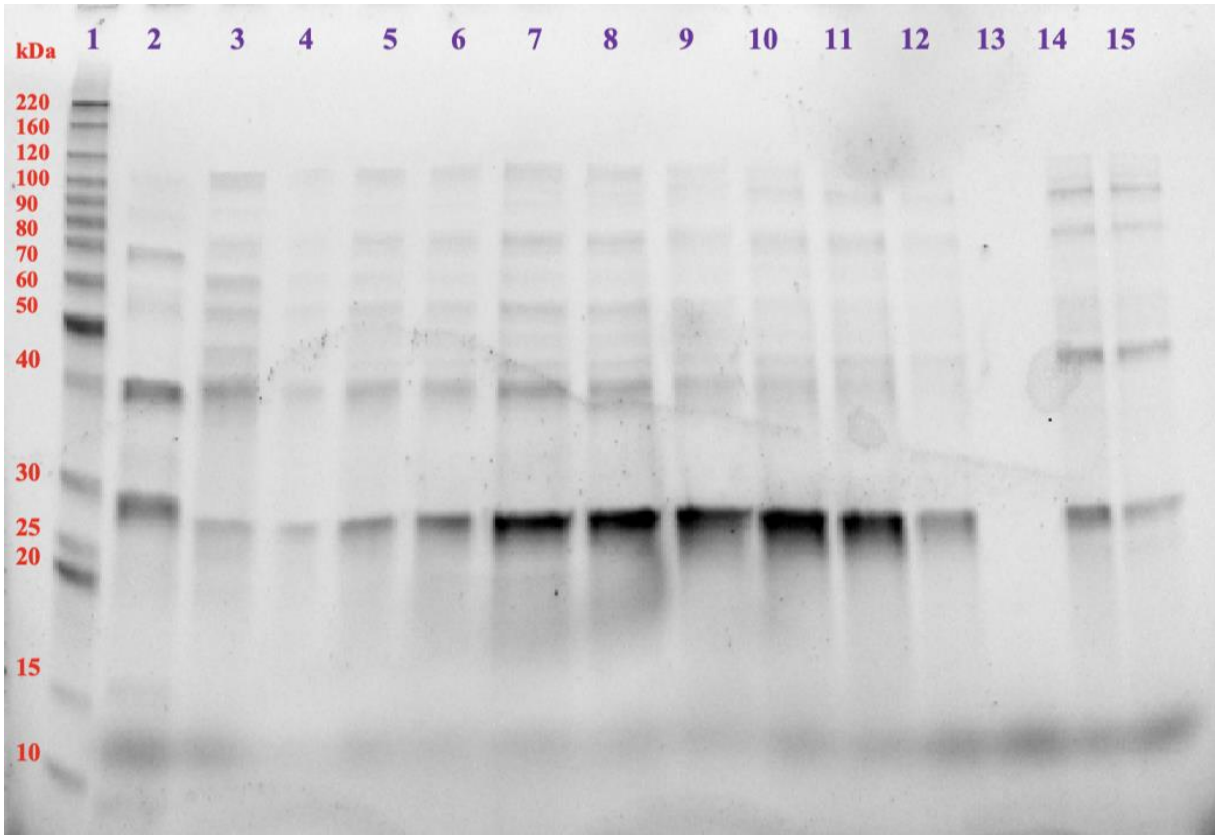

Figure 4.2.3. SDS-PAGE gel of pooled fractions after anion exchange chromatography. The first well contains the Benchmark protein ladder, the second well contains fraction 8 and the rest contains fraction 60, 62, 64, 66, 68, 70, 72, 74, 76, 78, 80, 84 and 86.

The SDS-PAGE gel showed *Sc*LPMO9A in well 7-11 (fractions 68-76). However, the wells also showed other bands, indicating that there were other proteins than *Sc*LPMO9A in the fractions. Therefore, fractions 68 - 76 were pooled and concentrated down to 1 mL before to sample was purified with SEC.

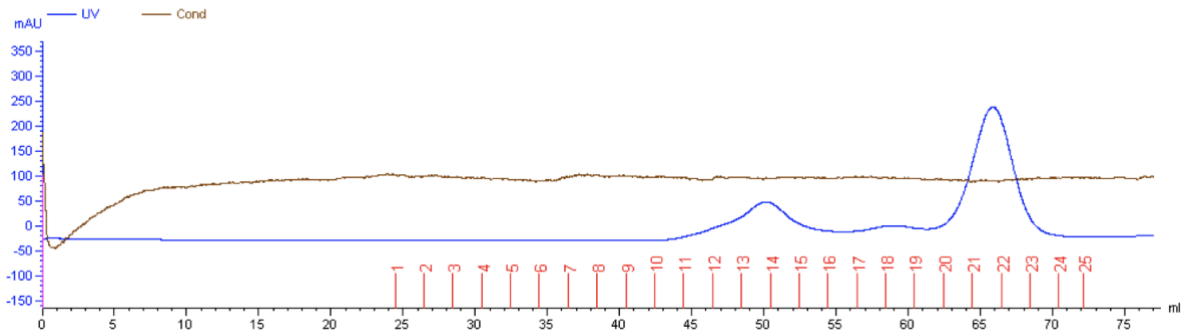

Figure 4.2.4. Size exclusion chromatogram. *Sc*LPMO9A eluted after approximately 63 minutes, as shown in the chromatogram. The flow rate was at 1 mL/min, therefore, mL correlate to minutes.

After SEC, the purified protein was analysed using SDS-PAGE, with fractions from both peaks, to decide which fractions to be pooled.

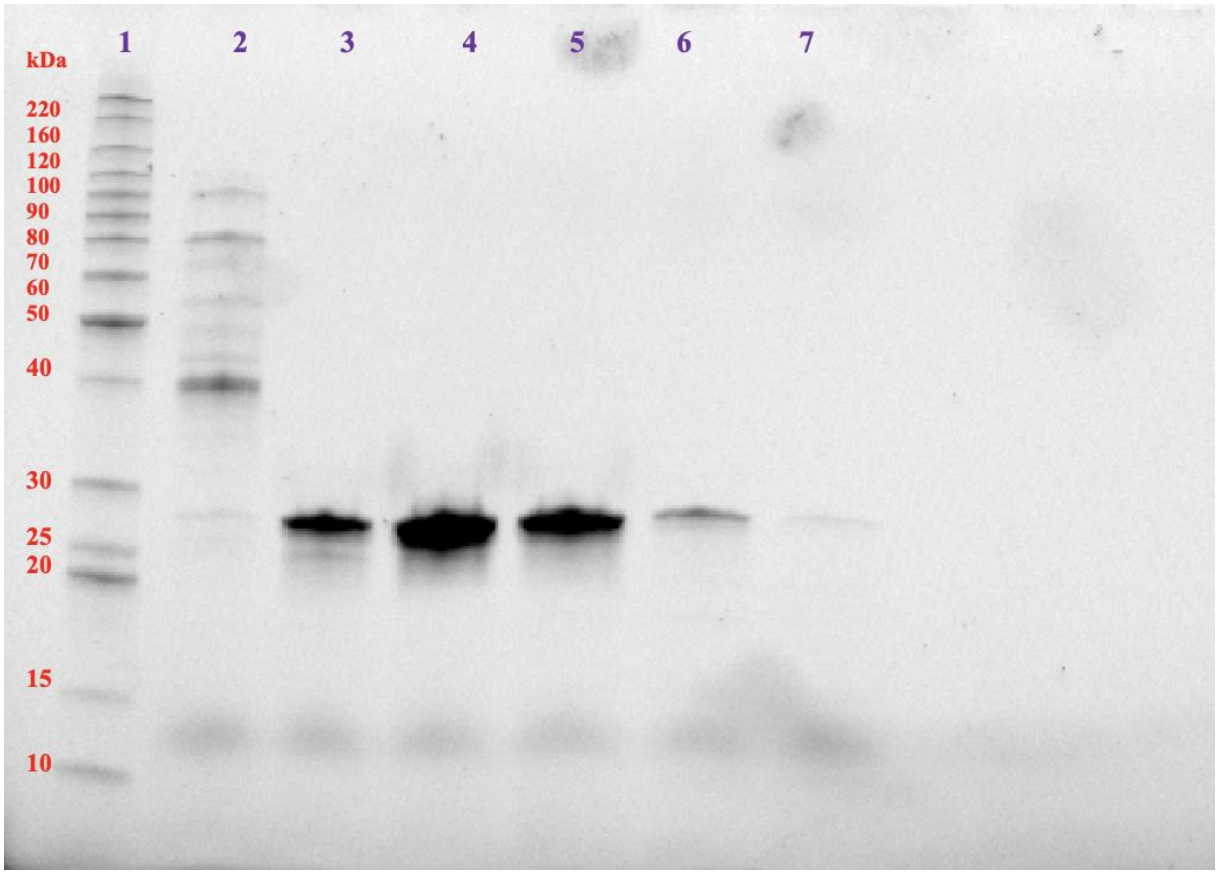

Figure 4.2.5. SDS-PAGE after SEC with fractions from both peaks. The first well contains the Benchmark protein ladder while the second well contains fraction 14. Well 3-7 corresponds to fraction 20-24 from the chromatogram. As the figure shows, well 3-5, corresponding to fractions 20-23, contains *Sc*LPMO9A, therefore these fractions were pooled.

After SEC, fractions 20-23 were pooled and concentrated, and the concentration was measured using Bradford protein assay. Then, the purified proteins were copper saturated to ensure that the LPMOs got a copper in their active site, as LPMOs are copper dependent. After copper saturation, the proteins were concentrated down to 750 µL and the final concentration was measured using Bradford protein assay.

Lastly, a PASC screening was analysed on HPAEC-PAD using a Dionex ISC-5000 system with *Sc*LPMO9A and PASC with and without reductant to check for endoglucanase activity. If the sample without reductant had shown activity, the sample had probably contained endoglucanases, as LPMOs depend on a reductant to catalyse reactions.

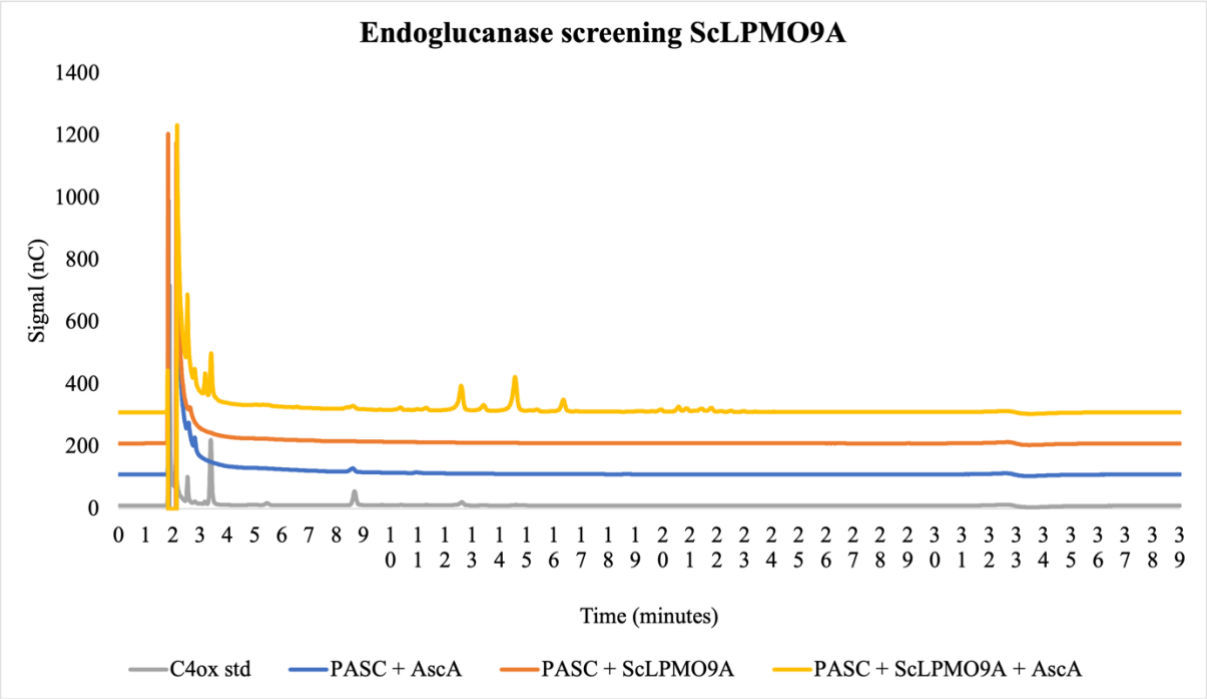

Figure 4.2.6. HPAEC-PAD chromatogram of *Sc*LPMO9A on PASC. The chromatogram has a signal offset at 100 nC between each line. C4 oxidized standard is shown in grey, where C4 oxidized dimer is shown between 12 and 13 minutes, native cellotriose between 8 and 9 minutes and native cellobiose between 3 and 4 minutes. As the chromatography shows, there was no endoglucanase activity in the purified batch, because PASC had no depolymerisation in the reaction without AscA (orange line). The samples were analysed with HPAEC-PAD using a Dionex ICS-5000 system.

The *Sc*LPMO9A batch did not contain any endoglucanases (Figure 4.2.6), therefore the batch was used for further experiments.

The purification yield was measured for all purified batches throughout this study (Table 4.2.1).

Table 4.2.1. *Sc*LPMO9A purification yields. The concentration in mg/mL from µM was measured by multiplying the µM concentration by the molecular weight of *Sc*LPMO9A (24.5 kDa) and dividing by 1000. The yield was measured by multiplying the concentration in mg/mL with 0.750 mL, since this was the volume of the concentrated sample before measuring concentration with Bradford protein assay. The cultivation was done in 1 L medium, except the first cultivation, which was done in 500 mL.

Purification	Concentration (µM)	Concentration (mg/mL)	Yield (mg/L)
1	9.40	0.23	0.08
2	31.37	0.76	0.57
3	211.01	5.16	3.87
4	95.07	2.33	1.74
5	323.02	7.93	5.94

The purification yield varied between each round of purification (Table 4.2.1), However, some *Sc*LPMO9A was purified in each step.

4.3 Purification of *Nc*LPMO9C

P. pastoris containing gene encoding *Nc*LPMO9C, were cultivated in a YPD medium and harvested. After the medium was harvested, both supernatant and pellet were analysed using SDS-PAGE to ensure that *Nc*LPMO9C were secreted into the supernatant.

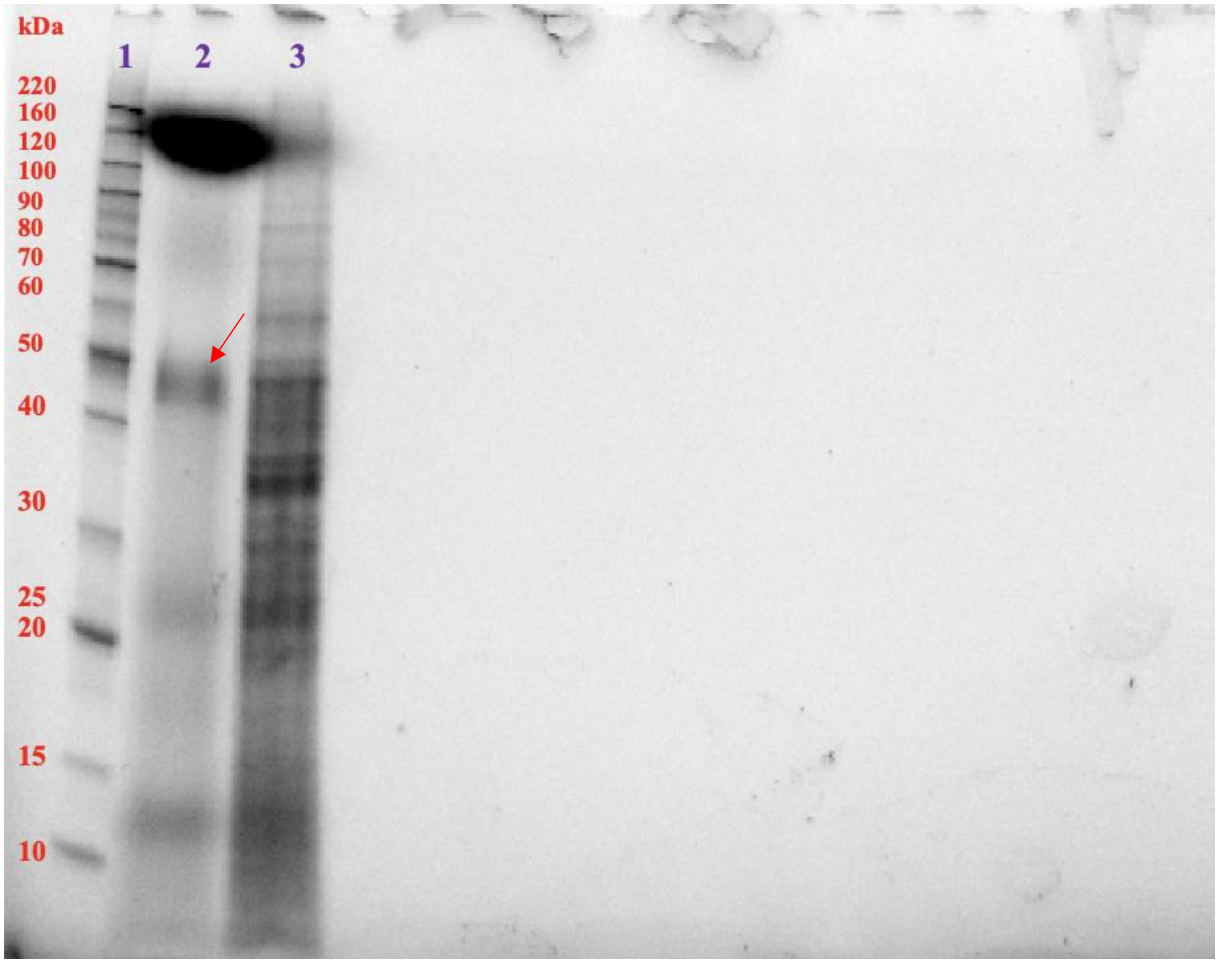

Figure 4.3.1. SDS-PAGE gel after *Nc*LPMO9C had been harvested. The first well contains the Benchmark protein ladder, the second well contains the supernatant and the third well contains the pellet. *Nc*LPMO9C full length has a predicted molecular weight of 35.8 kDa. As shown on the SDS-PAGE gel, the protein with the arrow has a molecular weight higher than this, but because *Nc*LPMO9C usually has n- and o-glycosylations, this protein was expected to be *Nc*LPMO9C.

After confirming that there was *Nc*LPMO9C in the supernatant, the supernatant was purified using HIC (Data not shown). Fractions from the peaks were analysed using SDS-PAGE, to observe if the *Nc*LPMO9C were in some of the fractions and to decide which fractions to be pooled.

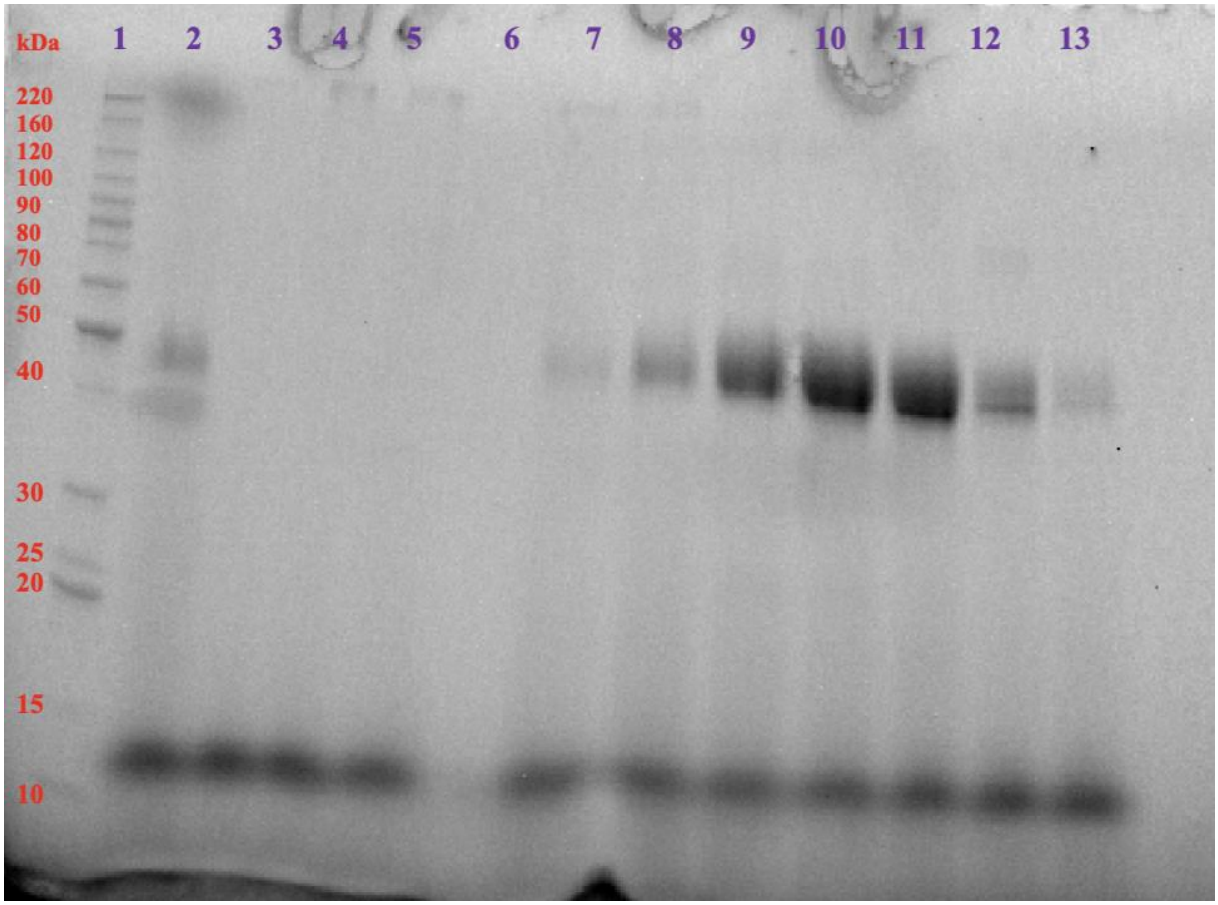

Figure 4.3.2. SDS-PAGE gel with the fractions from HIC, 10x diluted. The first well contains the Benchmark protein ladder. Well 7-12 shows *Nc*LPMO9C and were therefore pooled. Well 2-5 shows fractions from proteins eluted earlier and were not pooled.

The fractions from HIC containing *Nc*LPMO9C were pooled and concentrated (well 7-12), and the sample was further purified using SEC.

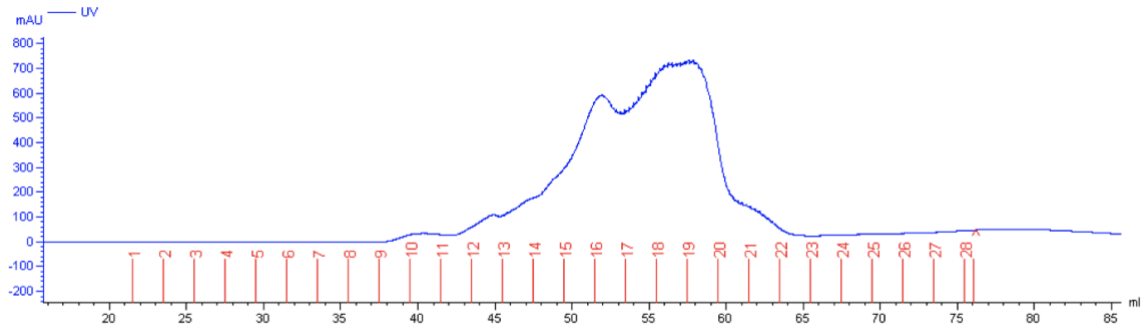

Figure 4.3.3. The chromatogram from SEC. The chromatogram shows that *Nc*LPMO9C eluted between 45 and 65 minutes. The flow rate was at 1 mL/min, therefore, mL correlate to minutes.

Some of the fractions that eluted between 45 and 65 minutes were analysed using SDS-PAGE, to decide which fractions to be pooled.

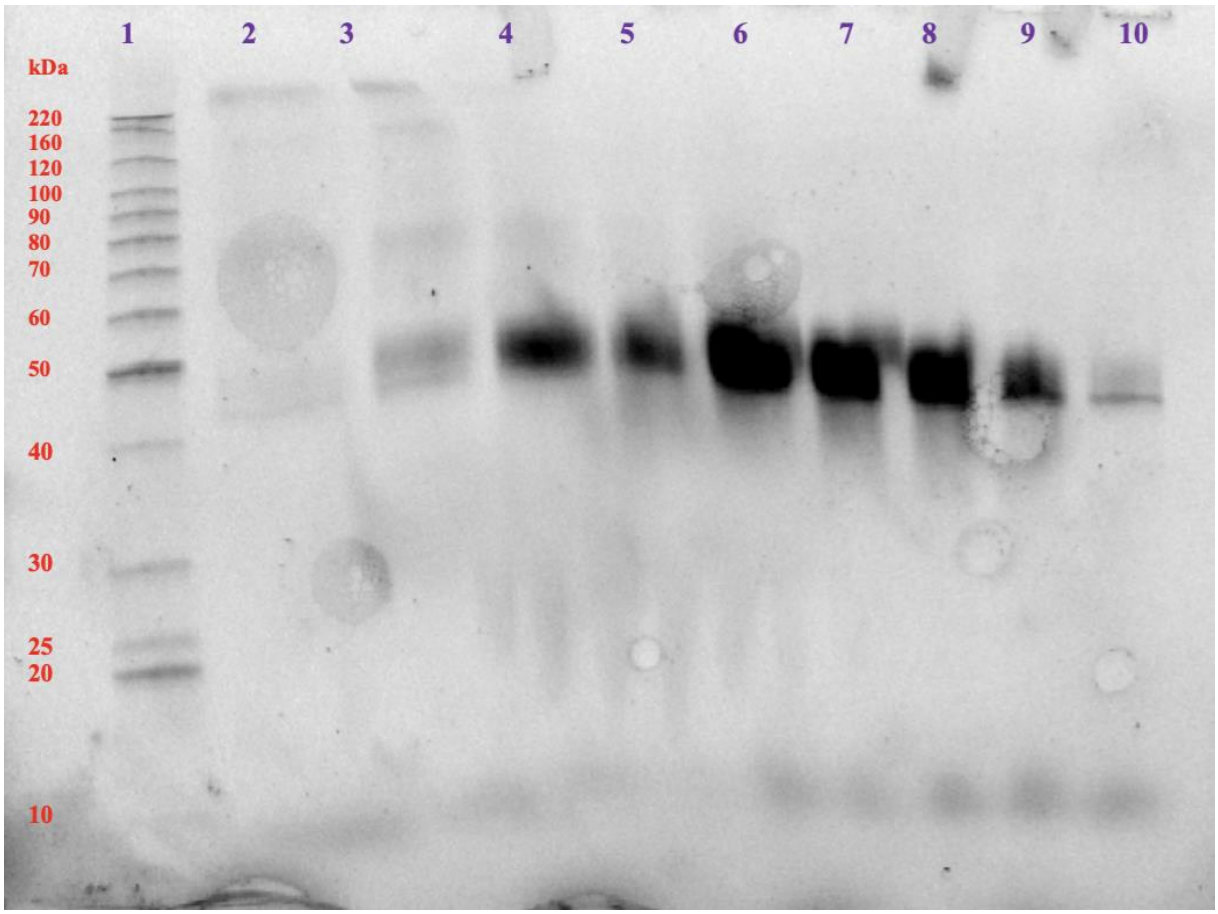

Figure 4.3.4. SDS-PAGE of fractions after SEC, 10x diluted. Well 4-9, corresponding to fraction 15-20, shows *Nc*LPMO9C. Fractions 15-16 and 17-20 were pooled and checked for endoglucanase activity separately.

Fractions 15-16 and 17-20 were pooled separately and both pooled samples were concentrated, copper saturated and screened for endoglucanase activity separately. The separation was to try to exclude endoglucanase from at least one of the batches.

After pooling the fractions, the samples were incubated with PASC, before the samples were analysed using HPAEC-PAD using a Dionex ISC-5000 system to check for endoglucanase activity.

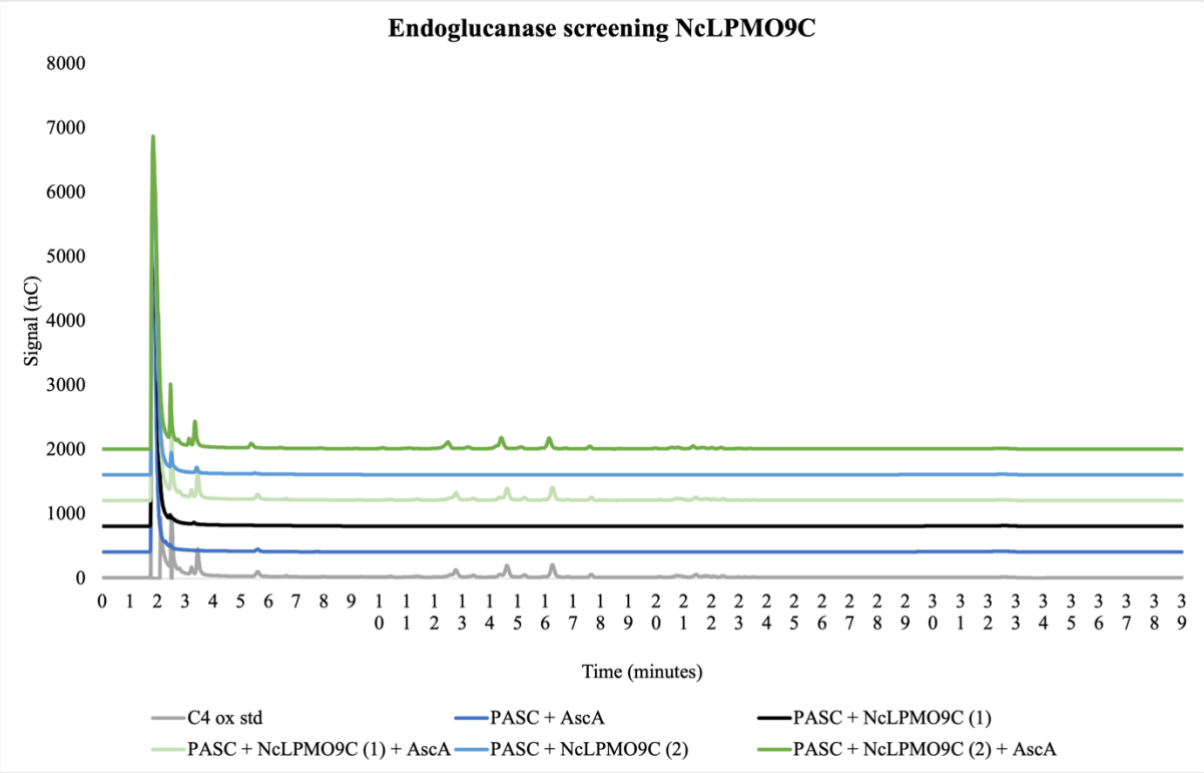

Figure 4.3.5. **HPAEC-PAD chromatogram of reactions with *Nc*LPMO9C on PASC.** The chromatogram has a signal offset at 400 nC between each line. The grey chromatogram shows the C4 oxidized standard, containing both native (1-4 minutes) and oxidized (12-17 minutes) DP2 and DP3. The light and dark green chromatograms show products from reactions with *Nc*LPMO9C + PASC + AscA from both batches. The black and light blue chromatograms show control reactions of *Nc*LPMO9C + PASC in the absence of AscA, for both batches. Finally, the dark blue chromatogram shows an enzyme-free control with PASC + AscA. The samples analysed with HPAEC-PAD using a Dionex ICS-5000 system.

Both batches (1 and 2) of *Nc*LPMO9C consisted of some endoglucanases (Figure 4.3.5). As both the green lines show, there was depolymerization of PASC in the samples with *Nc*LPMO9C + PASC + AscA, as expected. The light blue line (PASC + *Nc*LPMO9C 2) also showed some depolymerization, even though the samples did not contain any reductant. This indicated that there were some endoglucanases in the samples, that can break down PASC without reductant. The black line (PASC + *Nc*LPMO9C 1) did also show some production of native cellobiose, but since the formation was decided to be small enough, the *Nc*LPMO9C (1) stock was used in further studies. Figure 4.3.5 also showed that *Nc*LPMO9C produced C4 oxidized products from PASC and that the reactions without AscA did not result in any C4 oxidized products, as expected.

Purification yield was calculated as with *Sc*LPMO9A (Table 4.3.1).

Table 4.3.1. Purification yield of *Nc*LPMO9C. The concentration in mg/mL from µM was measured by multiplying the µM concentration by the molecular weight of *Nc*LPMO9C (35.8 kDa) and dividing by 1000. The yield was measured by multiplying the concentration in mg/mL with 0.750 mL, since this was the volume of the concentrated sample before measuring concentration, before dividing by 2 to get mg/L since only 500 mL was cultivated.

Purification	Concentration (µM)	Concentration (mg/mL)	Yield (mg/L)
1	85.00	3.04	1.14

As shown in Table 4.3.1, the purification yield of *Nc*LPMO9C was 1.14 mg/L.

4.4 H_2O_2 production

To identify how much H_2O_2 *Sc*LPMO9A and *Nc*LPMO9C produced, and to verify LPMO activity, a Amplex Red Hydrogen Peroxide assay with *Sc*LPMO9A, *Nc*LPMO9C and $CuSO_4$ were analysed, in addition to the same samples together with cellopentaose.

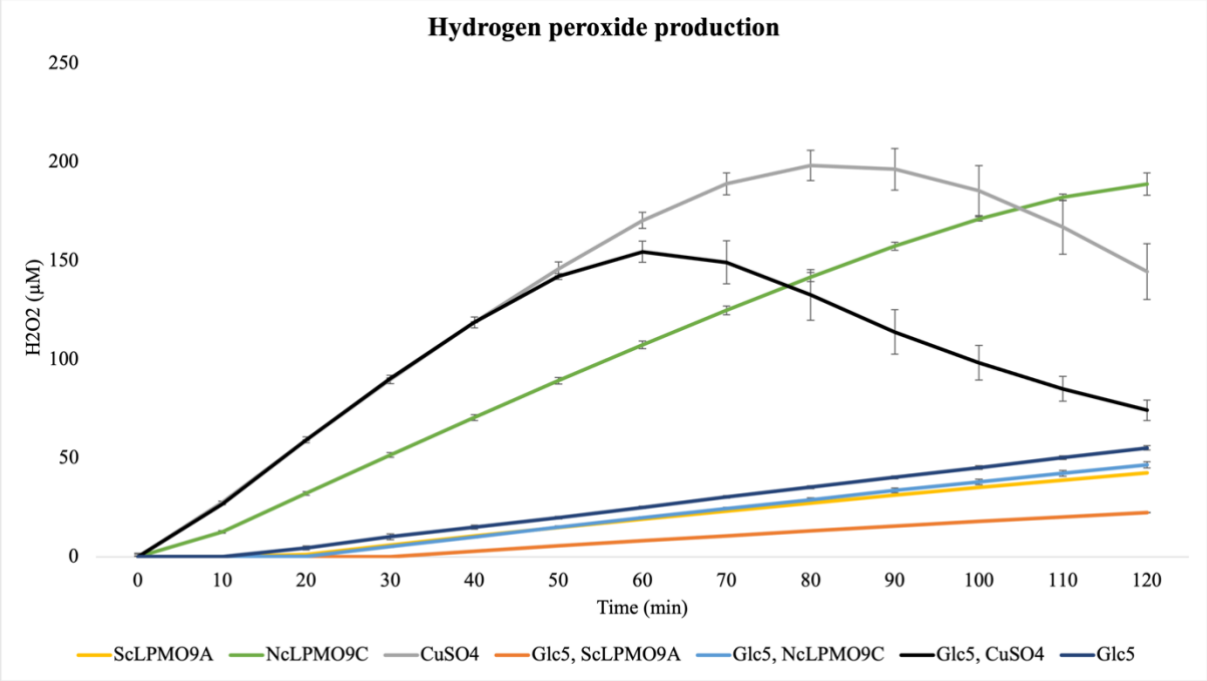

Figure 4.4.1. Amplex Red Hydrogen Peroxide assay performed in 50 mM Bis-Tris-HCl buffer pH 6.5, 100 µM Amplex Red, 5 U HRP, 1 mM AscA, 1 µM LPMO/$CuSO_4$ and 1 mM cellopentaose. The absorbances was measured using A_{563} and the concentrations were calculated using the standard curve shown in Figure S2. Some of the controls had values outside of the standard curve, which are expressed as 0 in the figure. Data are expressed as mean values for 3 independent repeats.

*Nc*LPMO9C had produced approximately 189 µM H_2O_2 after 2 hours, while *Sc*LPMO9A had almost the same rate and production as the controls (cellopentaose without LPMOs/$CuSO_4$ and enzymes with substrate) after 2 hours (Figure 4.4.1). It was also observed that H_2O_2 production was influenced by the presence of cellopentaose in samples with *Nc*LPMO9C and *Sc*LPMO9A, while the $CuSO_4$ control did not appear to be affected by cellopentaose.

4.5 H_2O_2 consumption

Breslmayr assay was used to observe how *Sc*LPMO9A and *Nc*LPMO9C consumed H_2O_2 under standard conditions and to see if the LPMOs were properly folded with copper in their active site.

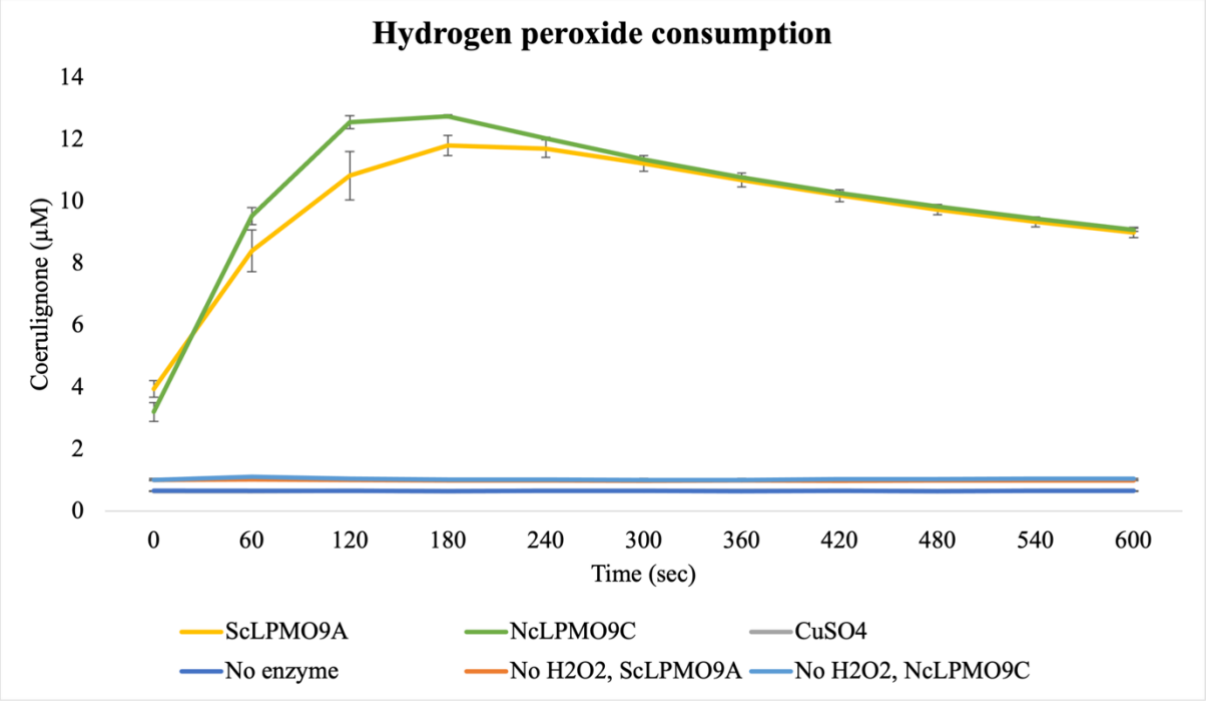

Figure 4.5.1. Breslmayr assay performed in 50 mM Bis-Tris-HCl buffer pH 6.5, 100 µM H_2O_2, 1 mM 2,6-DMP and 3 µM enzyme/$CuSO_4$. The concentration of coerulignone was measured by dividing the absorbance by the coerulignone ε_{469}=53.200 M^{-1} cm^{-1} and multiplying with 1000. Data are expressed as mean values for 3 independent repeats.

Breslmayr assay showed that both *Sc*LPMO9A and *Nc*LPMO9C were active, and that they consumed about the same amount of H_2O_2 under standard conditions (Figure 4.5.1). Free copper did not consume any H_2O_2, indicating that the consumption was dependent on LPMO.

4.6 Redox potential

The redox potential of *Sc*LPMO9A-Cu^{2+}/*Sc*LPMO9A-Cu^{+} was measured as described in Section 3.10, with a value of 186 ± 10 mV. This was 17% lower than for *Nc*LPMO9C, which has a redox potential of 224 ± 3 mV (Borisova et al., 2015). In other words, *Nc*LPMO9C gets more readily reduced than *Sc*LPMO9A, while *Sc*LPMO9A reduces other substances more readily than *Nc*LPMO9C.

4.7 Method optimalization

4.7.1 Choice of buffer

Before using HPAEC-PAD to quantify products, different buffers (sodium phosphate pH 6.0, sodium citrate pH 6.0 and sodium acetate pH 5.0) were analysed to find the best suited buffer.

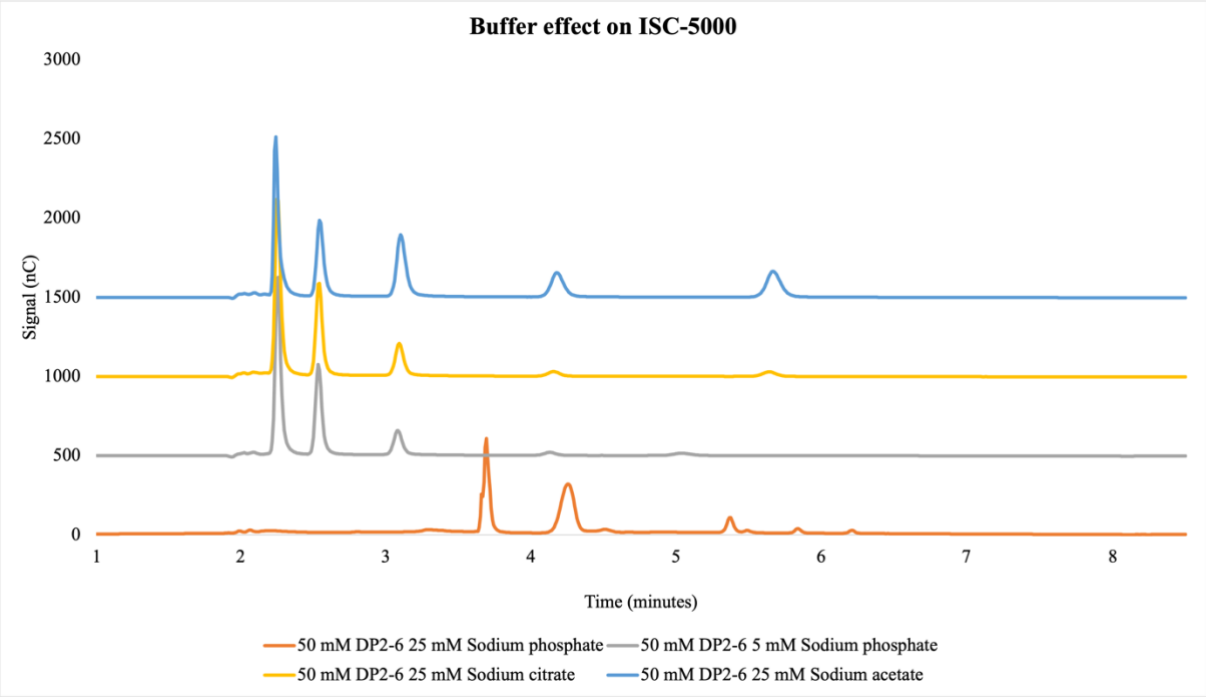

Figure 4.7.1. HPAEC-PAD chromatogram with 50 µM DP2-6 cello-oligo standards in different buffers. The standards were analysed with HPAEC-PAD using a Dionex ISC-5000 system. The chromatogram has a signal offset at 500 nC between each line. Cellobiose is shown to the left, while cellohexaose is the peaks furthers to the right in each chromatogram.

As shown in Figure 4.7.1, sodium phosphate buffer pH 6.0 was not suited in high concentrations as the chromatogram showed less sharp peaks and the peaks elated different than the other buffers. Both sodium acetate buffer pH 5.0 and sodium citrate buffer pH 6.0 gave sharp and separated peaks, however, sodium citrate is not a suitable buffer for LPMO reactions as it can act as a chelator of copper. Based on these observations, sodium acetate buffer pH 5.0 was the chosen buffer used for further experiments.

4.7.2 Choice of enzyme inactivation method

In addition to choosing buffer, both heath inactivation at 100 °C for 10 minutes and 200 mM NaOH were tested to stop the reactions to decide which method to use for further experiments.

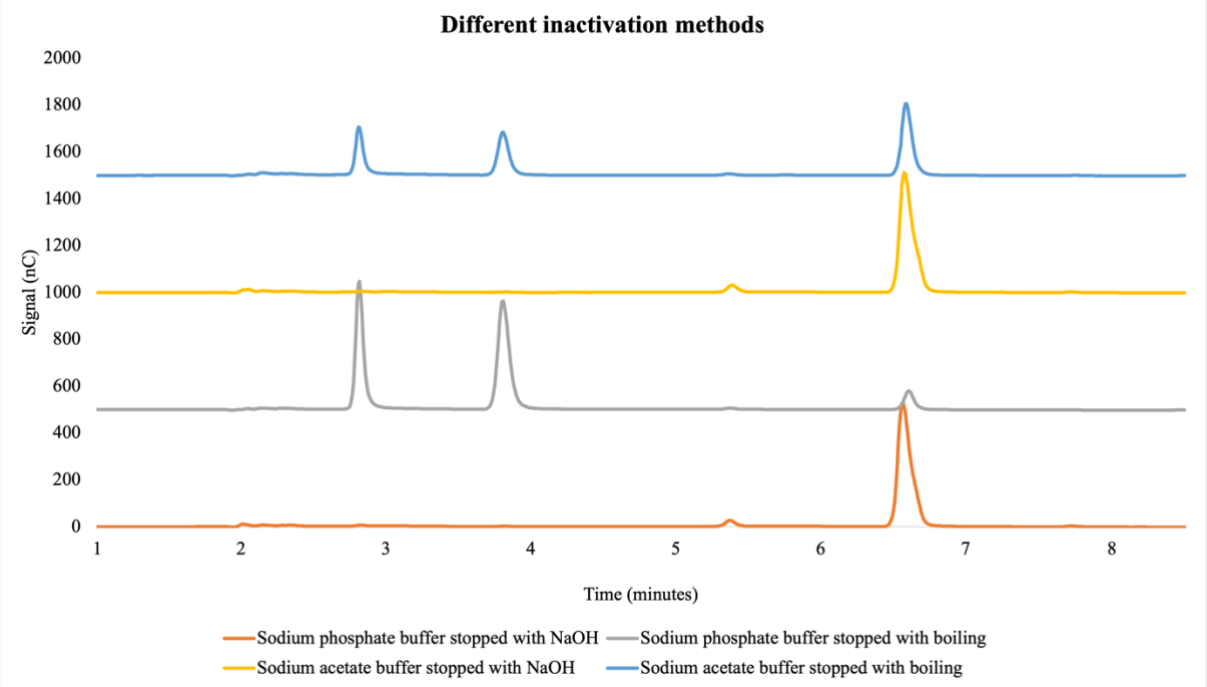

Figure 4.7.2. HPAEC-PAD chromatogram of cellopentaose exposed to NaOH or heat in different buffers. The chromatogram shows samples with cellopentaose in both 50 mM sodium phosphate buffer pH 6.0 and 50 mM sodium acetate buffer pH 5.0, stopped with 200 mM NaOH and stopped with heat inactivation at 100 °C for 10 minutes. The samples were analysed with HPAEC-PAD using a Dionex ISC-5000 system. The chromatogram has a signal offset at 500 nC between each line. The peaks between 6 and 7 minutes are cellopentaose, while the peaks at 4 minutes are cellotriose and the peaks at 3 minutes are cellobiose.

Reactions with cellopentaose stopped with heat inactivation showed that when cellopentaose was boiled at 100 °C for 10 minutes, the substrate was degraded (Figure 4.7.2). The

degradation was more significant in the reactions with sodium phosphate buffer pH 6.0, but the reaction in sodium acetate buffer pH 5.0 also showed degradation when the reactions were boiled. This degradation did not happen when the reactions were stopped with 200 mM NaOH. Therefore, 200 mM NaOH was used to stop reactions for further experiments. This decision was based only on native product quantification, as NaOH would not be suitable if C4 oxidized products were quantified.

4.8 Activity of *Sc*LPMO9A and *Nc*LPMO9C on soluble substrates

Overnight reactions with *Sc*LPMO9A and *Nc*LPMO9C on cellotetraose, cellopentaose and cellohexaose were analysed at HPAEC-PAD to observe how the enzymes degraded these substrates.

4.8.1 Overnight reaction on cellotetraose

Reactions with *Sc*LPMO9A and *Nc*LPMO9C with and without AscA were incubated with cellotetraose for 24 hours and analysed with HPAEC-PAD.

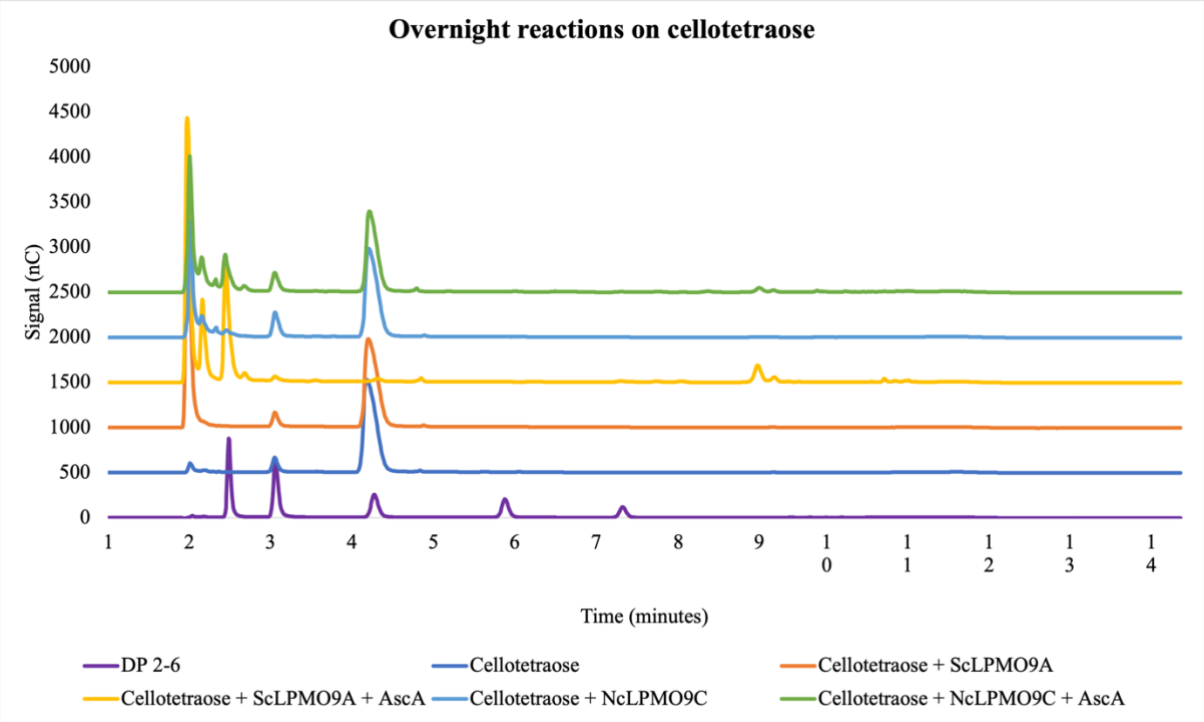

Figure 4.8.1. HPAEC-PAD chromatograms of overnight reactions with 1 mM cellotetraose in 50 mM sodium acetate buffer pH 5.0 stopped with 200 mM NaOH. The chromatogram has a signal offset of 500 nC between each line. The peak at 9 minutes in the yellow and green chromatogram are Glc4gemGlc, the peaks at 4 minutes are cellotetraose, the peaks at 3 minutes are cellotriose and the peaks between 2 and 3 minutes are cellobiose. The samples were analysed with HPAEC-PAD using a Dionex ICS-5000 system.

*Sc*LPMO9A depolymerized cellotetraose mainly to cellobiose (Figure 4.8.1). *Sc*LPMO9A also produced Glc4gemGlc. After 24 hours, the cellotetraose in the reaction with *Sc*LPMO9A and AscA was completely degraded.

*Nc*LPMO9C showed less activity on cellotetraose, but it produced some native cellobiose and Glc4gemGlc. The endoglucanases in the *Nc*LPMO9C batch produced some cellotriose, as there was formation of cellotriose in both samples with *Nc*LPMO9C, with and without AscA (Figure 4.8.1).

4.8.2 Overnight reaction on cellopentaose

The same reaction was incubated with cellopentaose.

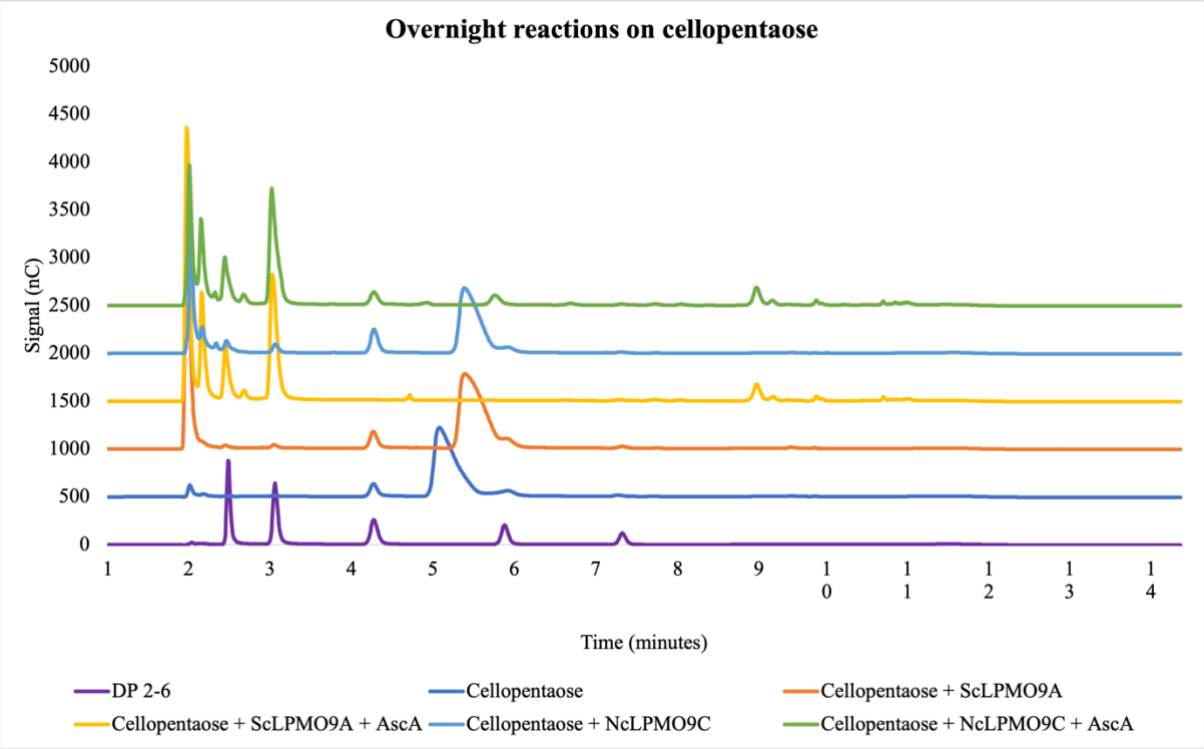

Figure 4.8.2. HPAEC-PAD chromatograms of overnight reactions with 1 mM cellopentaose in 50 mM sodium acetate buffer pH 5.0 stopped with 200 mM NaOH. The chromatogram has a signal offset of 500 nC between each line. The peaks at 9 and 10 minutes in the yellow and green chromatograms are Glc4gemGlc and Glc4gemGlc$_2$. The peaks at approximately 6 minutes are cellopentaose, the peaks at approximately 4 minutes are cellotetraose, the peaks at 3 minutes are cellotriose, lastly, the peaks between 2 and 3 minutes are cellobiose. The samples were analysed with HPAEC-PAD using a Dionex ICS-5000 system.

Both *Sc*LPMO9A and *Nc*LPMO9C depolymerized cellopentaose (Figure 4.8.2). The main product after degradation with *Sc*LPMO9A was cellotriose, but also cellobiose. After 24 hours, the cellopentaose was completely degraded with *Sc*LPMO9A in the presence of AscA. *Nc*LPMO9C broke down cellopentaose mainly to cellotriose and cellobiose. However, after 24 hours, there was still some cellopentaose left.

Both enzymes also produced Glc4gemGlc and Glc4gemGlc$_2$, as expected since native cellobiose and cellotriose were produced from the cellopentaose.

4.8.3 Overnight reaction on cellohexaose

Activity of *Sc*LPMO9A and *Nc*LPMO9C were tested on cellohexaose in the same conditions as for cellopentaose and cellotetraose.

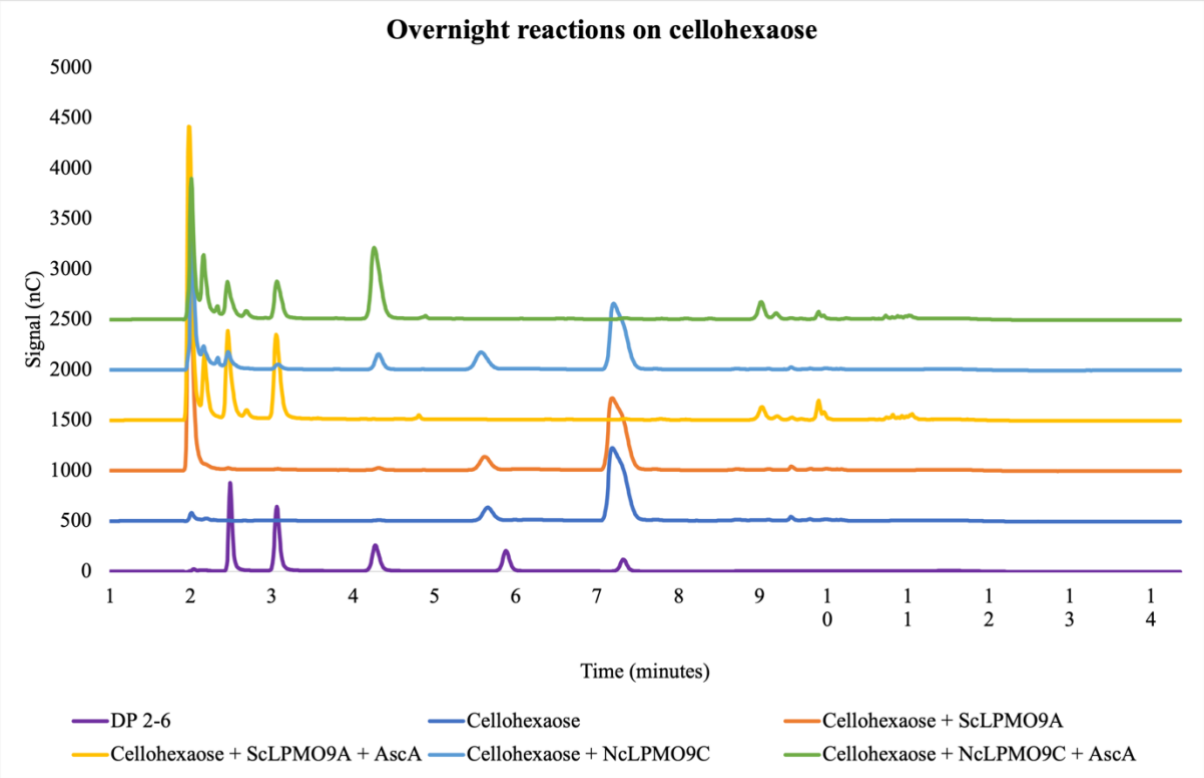

Figure 4.8.3. HPAEC-PAD chromatograms of overnight reactions with 1 mM cellohexaose in 50 mM sodium acetate buffer pH 5.0 stopped with 200 mM NaOH. The chromatogram has a signal offset of 500 nC between each line. The peaks at 9 and 10 minutes in the yellow and green chromatograms are Glc4gemGlc and Glc4gemGlc$_2$. The peaks at approximately 7 minutes are cellohexaose, the peaks at approximately 6 minutes are cellopentaose, the peaks at approximately 4 minutes are cellotetraose, the peaks at 3 minutes are cellotetraose and the peaks between 2 and 3 minutes are cellobiose. The samples were analysed with HPAEC-PAD using a Dionex ICS-5000 system.

Both enzymes depolymerized cellohexaose completely after 24 hours (Figure 4.8.3). *Sc*LPMO9A depolymerized cellohexaose to cellotriose and cellobiose, while *Nc*LPMO9C depolymerized cellohexaose mainly to cellotetraose, but also some cellotriose and cellobiose.

In addition to native products, both *Sc*LPMO9A and *Nc*LPMO9C produced Glc4gemGlc and Glc4gemGlc$_2$.

4.9 *Sc*LPMO9A and NcLPOM9C time course reactions

Following the observation that the enzymes showed activity on the soluble substrates tested, different time course experiments with cellopentaose, cellotriose and cellohexaose were

performed. This was done to get an indication of how fast *Sc*LPMO9A and *Nc*LPMO9C degrade these substrates.

4.9.1 Time course reactions on cellopentaose

A time course reaction on cellopentaose was analysed to obtain an indication of how fast *Sc*LPMO9A catalyse the degradation compared to *Nc*LPMO9C. As cellobiose and cellotriose were the main products formed from cellopentaose degradation, these products were analysed using HPAEC-PAD and quantified with Chromeleon 7.2.9.

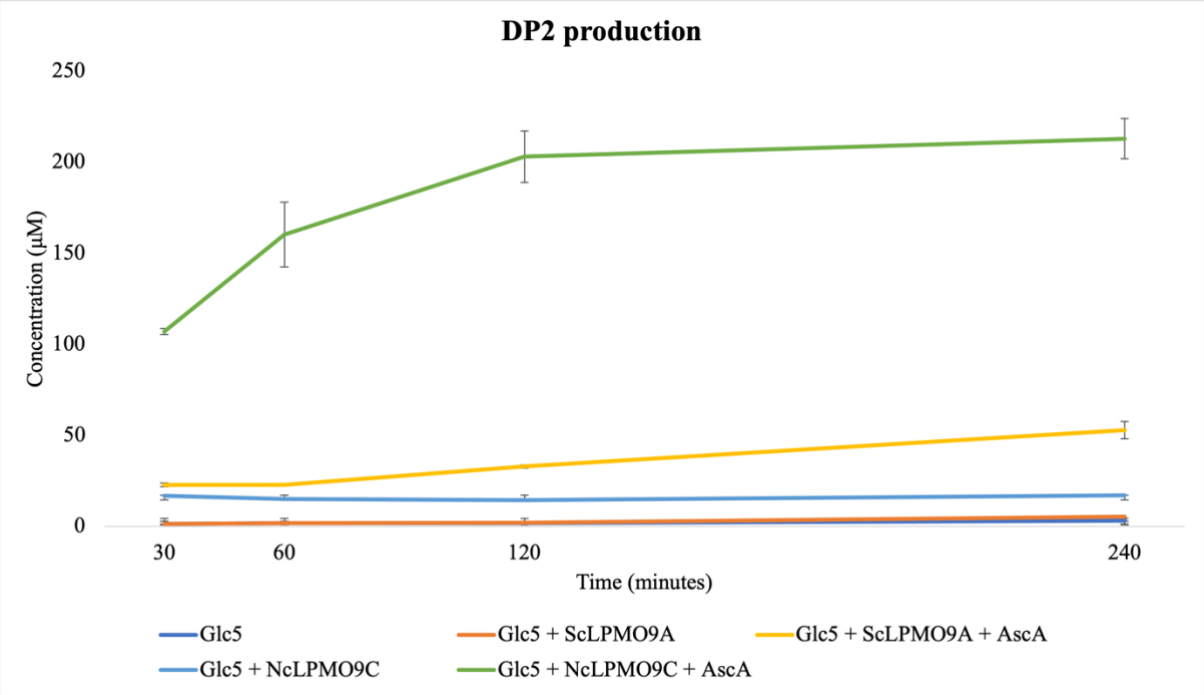

Figure 4.9.1. Cellobiose production of *Sc*LPMO9A and *Nc*LPMO9C. Reactions were performed in 50 mM sodium acetate buffer pH 5.0, 1 mM cellopentaose, 1 µM *Sc*LPMO9A/*Nc*LPMO9C and 1 mM AscA. Samples were taken after 30, 60, 120 and 240 minutes and enzymes were inactivated using 200 mM NaOH. The reactions were analysed with HPAEC-PAD using a Dionex ISC-5000 system. Data are expressed as mean values for 3 independent repeats.

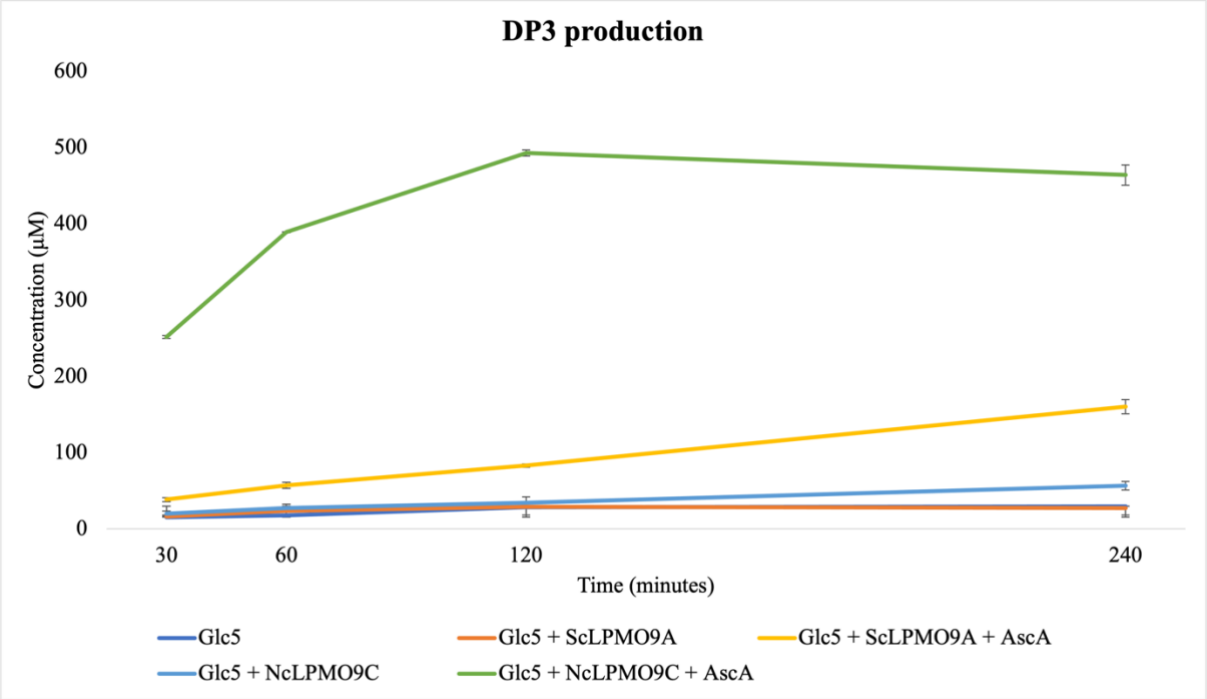

Figure 4.9.2. Cellotriose production of *Sc*LPMO9A and *Nc*LPMO9C. Reactions were performed in 50 mM sodium acetate buffer pH 5.0, 1 mM cellopentaose, 1 µM *Sc*LPMO9A/*Nc*LPMO9C and 1 mM AscA. Samples were taken after 30, 60, 120 and 240 minutes and enzymes were inactivated using 200 mM NaOH. The reactions were analysed with HPAEC-PAD using a Dionex ISC-5000 system. Data are expressed as mean values for 3 independent repeats.

*Nc*LPMO9C showed a faster reaction rate than *Sc*LPMO9A (Figure 4.9.1. and 4.9.2). For *Nc*LPMO9C, the reactions hit a limit after approximately 2 hours, while for *Sc*LPMO9A the product formation was still increasing after 4 hours. Therefore, a similar time course experiment was tested for 24 hours.

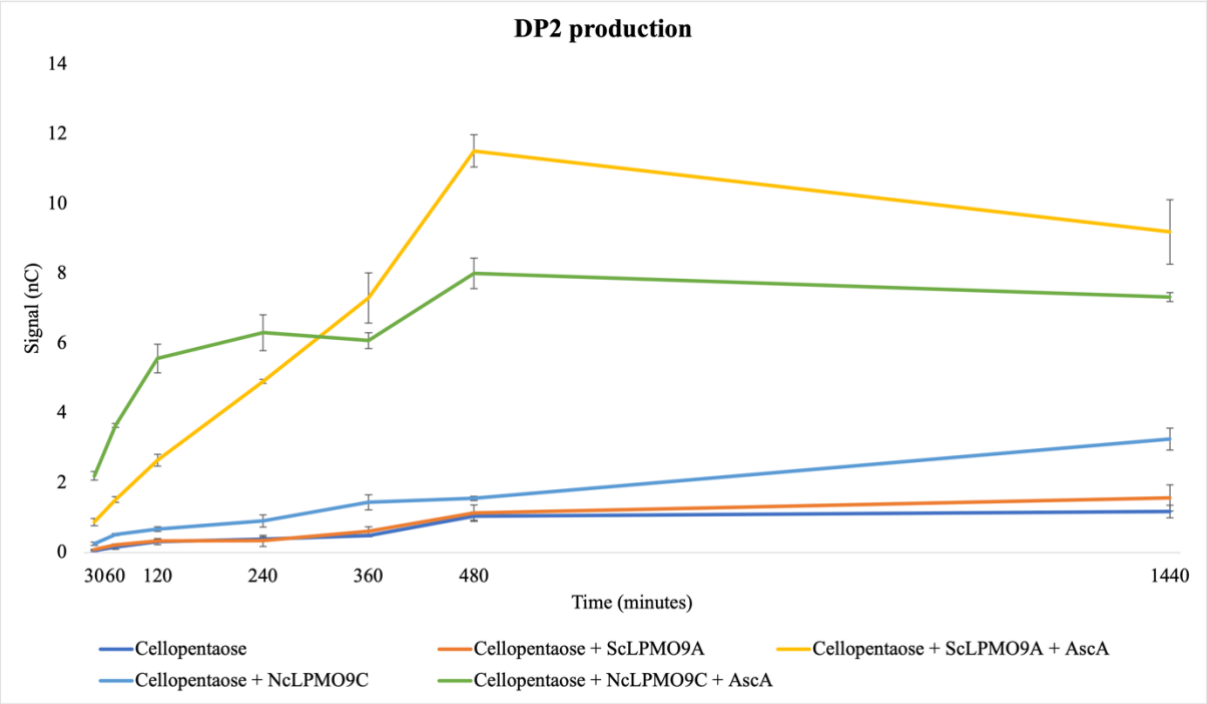

Figure 4.9.3. Cellobiose production of *Sc*LPMO9A and *Nc*LPMO9C. Reactions were performed in 50 mM sodium acetate buffer pH 5.0, 1 mM cellopentaose, 1 µM *Sc*LPMO9A/*Nc*LPMO9C and 1 mM AscA. Samples were taken after 30 minutes, 1, 2, 4, 6, 8 and 24 hours. The reactions were analysed with HPAEC-PAD using a Dionex ISC-6000 system. Data are expressed as mean values for 3 independent repeats.

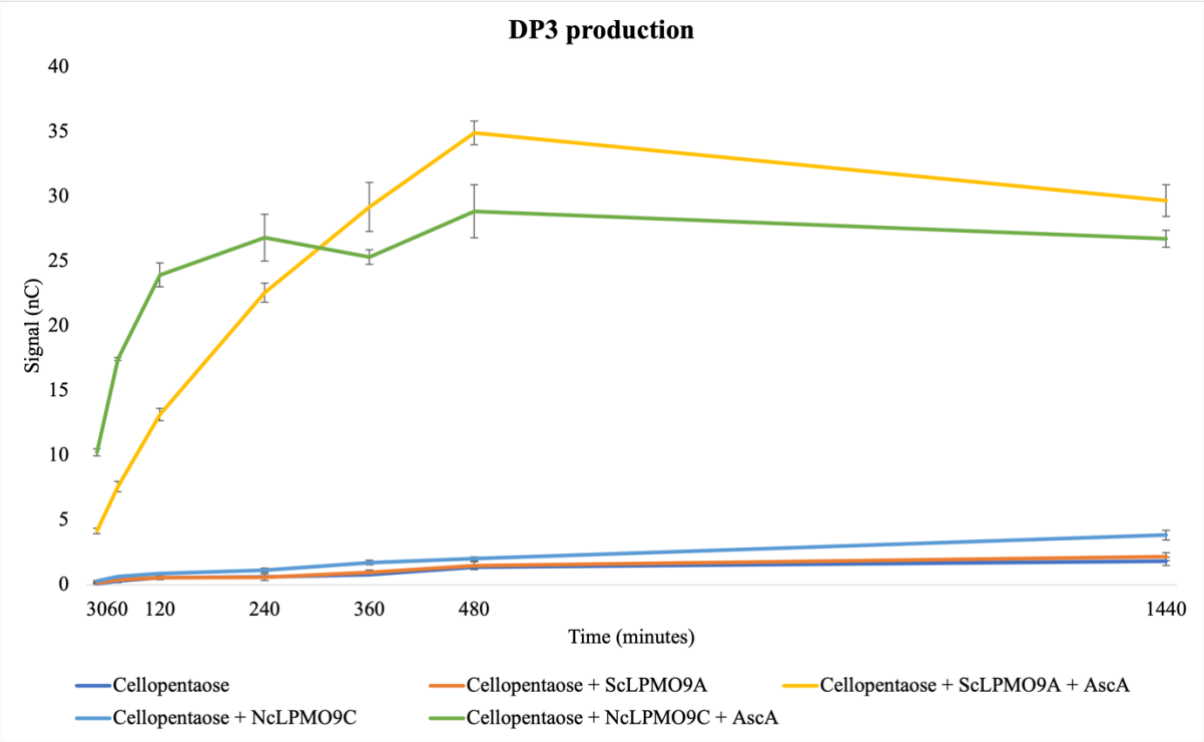

Figure 4.9.4. Cellotriose production of *Sc*LPMO9A and *Nc*LPMO9C. Reactions were performed in 50 mM sodium acetate buffer pH 5.0, 1 mM cellopentaose, 1 µM *Sc*LPMO9A/*Nc*LPMO9C and 1 mM AscA. Samples were taken after 30 minutes, 1, 2, 4, 6, 8 and 24 hours. The reactions were analysed with HPAEC-PAD using a Dionex ISC-6000 system. Data are expressed as mean values for 3 independent repeats.

*Nc*LPMO9C produced native cellobiose and cellotriose faster than *Sc*LPMO9A (Figure 4.9.3 and 4.9.4). On the other hand, *Sc*LPMO9A degraded more of the substrate, making the final production yield higher after 24 hours.

The chromatogram from the cellopentaose time course (Figure S5) revealed that with *Nc*LPMO9C, there was still some cellopentaose left after 24 hours, while *Sc*LPMO9A degraded all the substrate. The chromatogram also showed C4 oxidized products with both *Sc*LPMO9A and *Nc*LPMO9C, as expected. These results support the results from overnight reactions on cellopentaose (Figure 4.8.4)

The y-axis is presented as signal instead of concentration for Figures 4.9.3 and 4.9.4, as there were issues with product quantification as discussed in Section 5.10.1. The measured concentrations are shown in Figure S4 and S4.

4.9.2 Time course reaction on cellotetraose

A time course experiment was incubated with cellotetraose, but without *Nc*LPMO9C as Figure 4.8.1 showed that *Nc*LPMO9C was hardly active on cellotetraose.

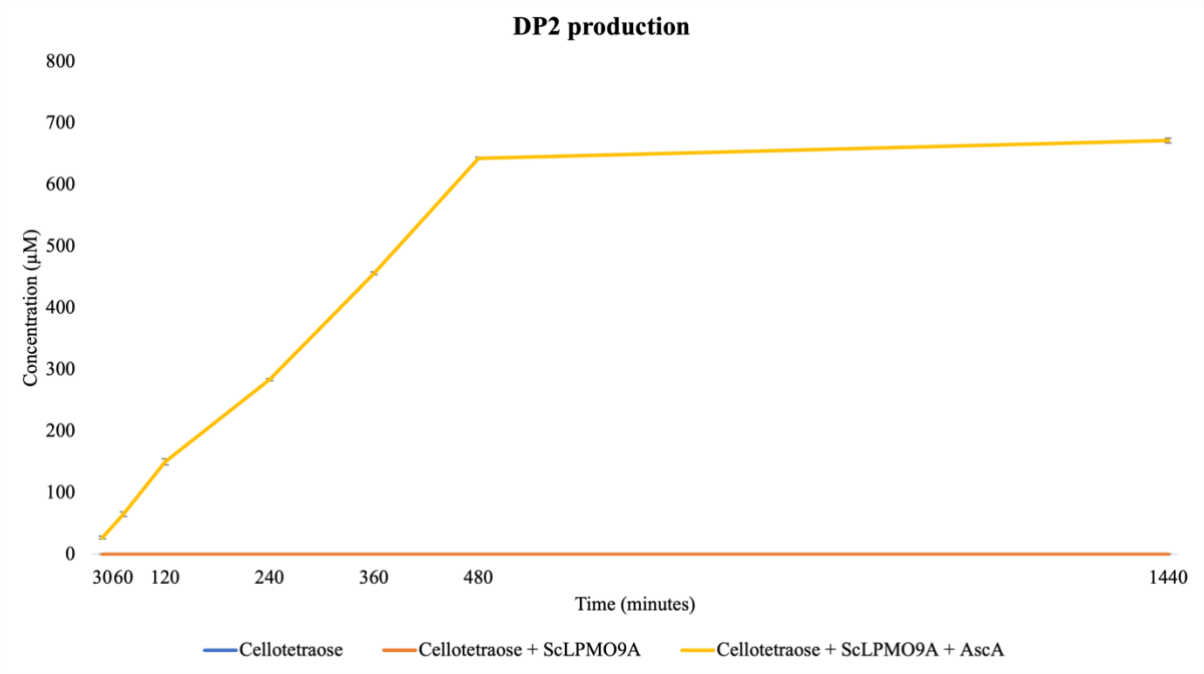

Figure 4.9.5. Cellobiose production of *Sc*LPMO9A. Reactions were performed in 50 mM sodium acetate buffer pH 5.0, 1 mM cellotetraose, 1 µM *Sc*LPMO9A and 1 mM AscA. Samples were taken after 30 minutes, 1, 2, 4, 6, 8 and 24 hours. The reactions were analysed with HPAEC-PAD using a Dionex ISC-6000 system. Data are expressed as mean values for 3 independent repeats. The controls had values outside of the standard curve and are expressed as 0.

The total production after 24 hours was 672 µM (Figure 4.9.4), even though 1 mM cellotetraose was added to the reaction. As shown in Figure S6, there was still some cellotetraose left after 24 hours. In addition to this, a glucose standard was added to the sequence, also shown in Figure S6, and it appears that some glucose was produced from cellotetraose.

The cellotriose production is not shown, as reactions with *Sc*LPMO9A and cellotetraose did not yield significant amounts of cellotriose (Figure 4.8.1 and Figure S6).

4.9.3 Time course reaction on cellohexaose

Both *Sc*LPMO9A and *Nc*LPMO9C was used a time course with cellohexaose.

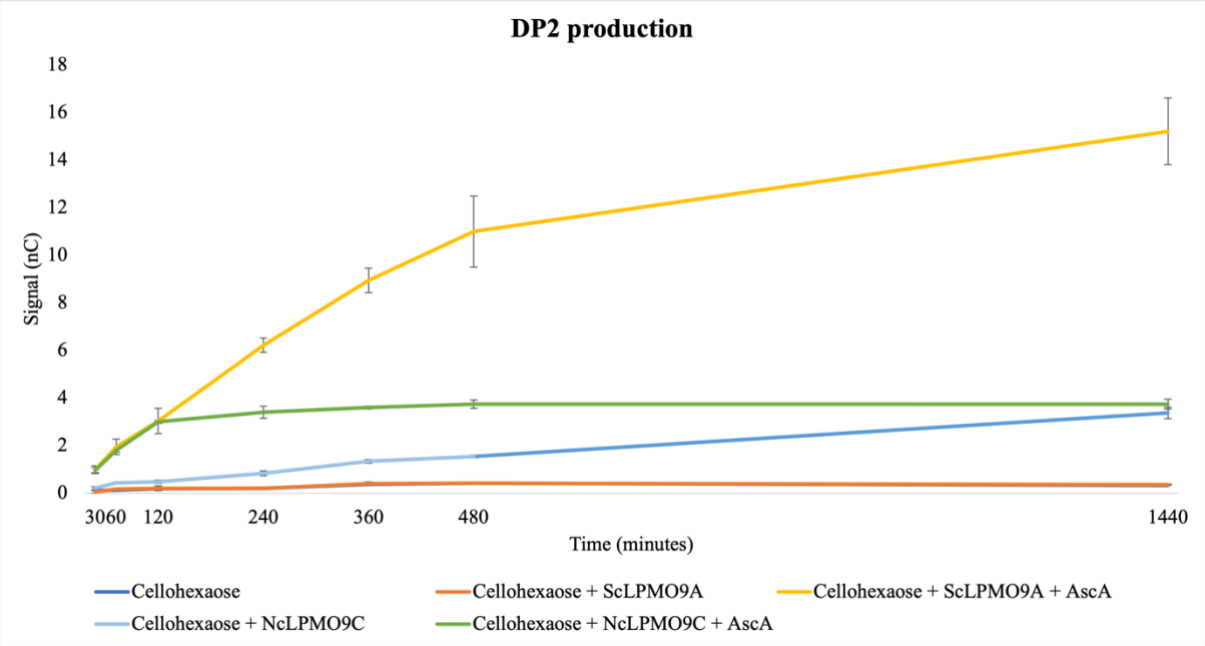

Figure 4.9.6. Cellobiose production of *Sc*LPMO9A and *Nc*LPMO9C. Reactions were performed in 50 mM sodium acetate buffer pH 5.0, 1 mM cellohexaose, 1 µM *Sc*LPMO9A/*Nc*LPMO9C and 1 mM AscA. Samples were taken after 30 minutes, 1, 2, 4, 6, 8 and 24 hours. The reactions were analysed with HPAEC-PAD using a Dionex ISC-6000 system. Data are expressed as mean values for 3 independent repeats.

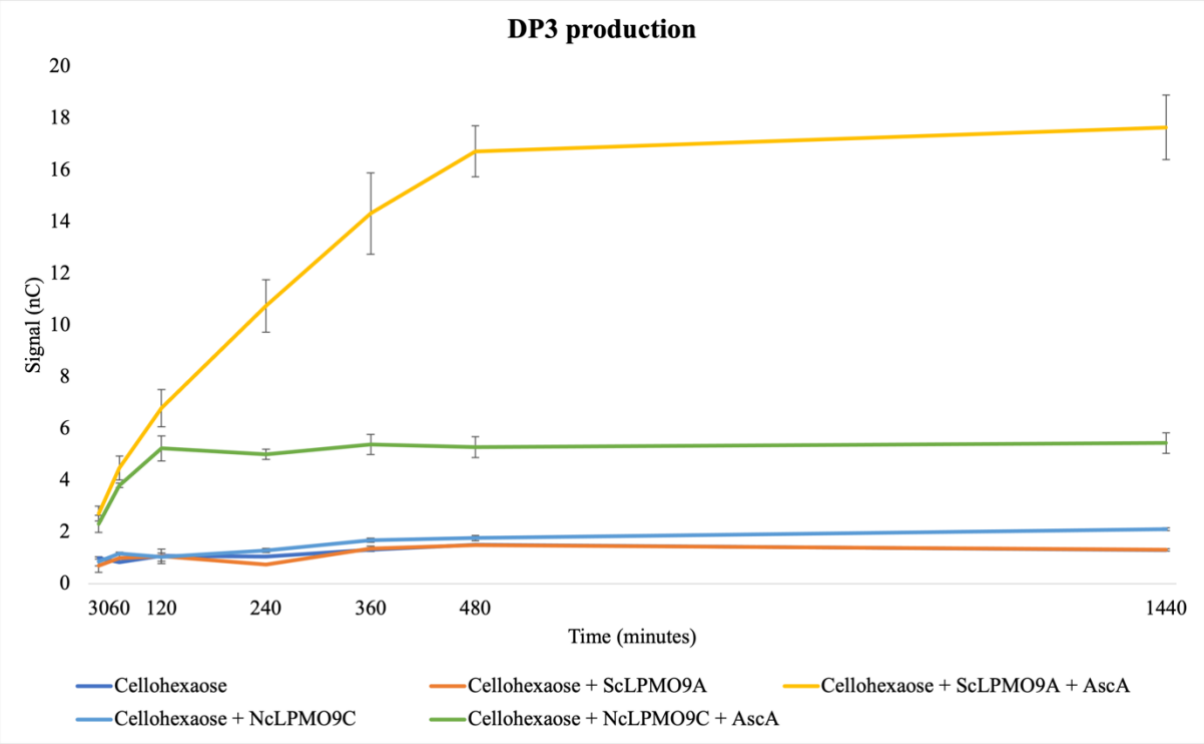

Figure 4.9.7. Cellotriose production of ScLPMO9A and NcLPMO9C. Reactions were performed 50 mM sodium acetate buffer pH 5.0, 1 mM cellohexaose, 1 µM *Sc*LPMO9A/*Nc*LPMO9C and 1 mM AscA. Samples were taken after 30 minutes, 1, 2, 4, 6, 8 and 24 hours. The reactions were analysed with HPAEC-PAD using a Dionex ISC-6000. Data are expressed as mean values for 3 independent repeats.

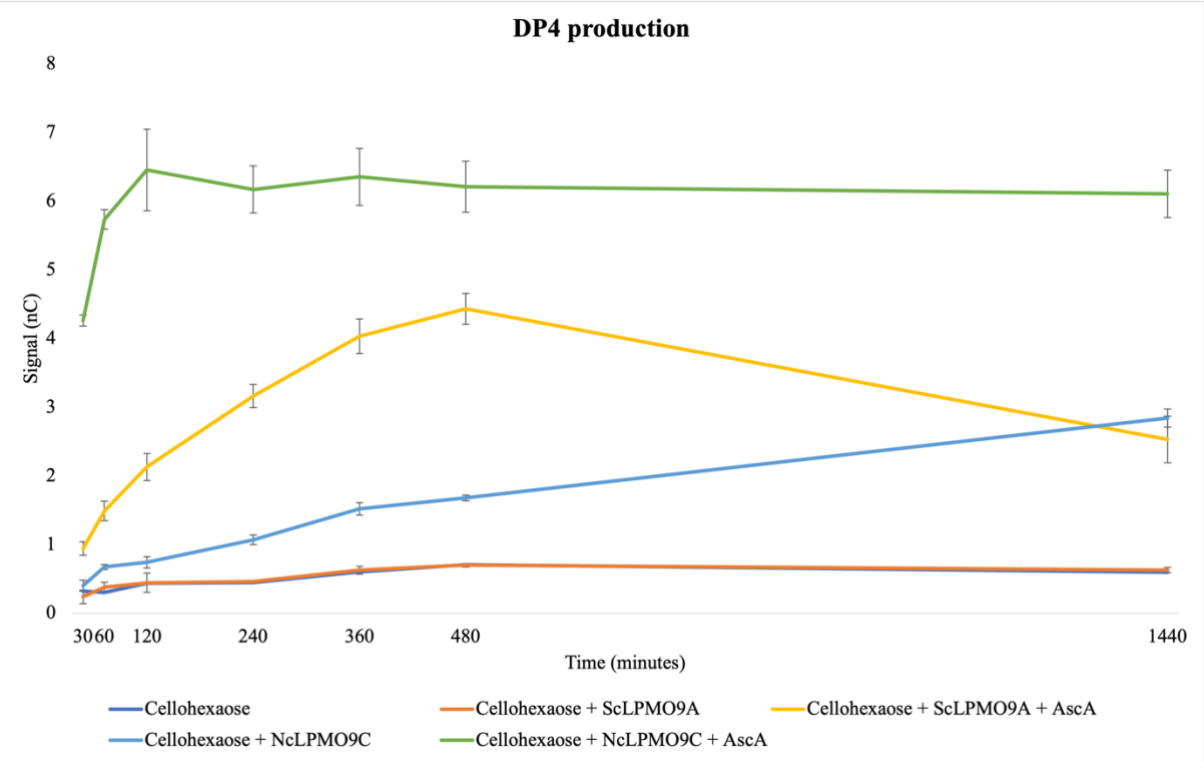

Figure 4.9.8. Cellotetraose production of ScLPMO9A and NcLPMO9C. Reaction were performed in 50 mM sodium acetate buffer pH 5.0, 1 mM cellohexaose, 1 µM *Sc*LPMO9A/*Nc*LPMO9C and 1 mM AscA. Samples were taken after 30 minutes, 1, 2, 4, 6, 8 and 24 hours. The reactions were analysed with HPAEC-PAD using a Dionex ISC-6000 system. Data are expressed as mean values for 3 independent repeats.

Both *Sc*LPMO9A and *Nc*LPMO9C were active on cellohexaose (Figures 4.9.6, 4.9.7 and 4.9.8). *Sc*LPMO9A produced cellobiose and cellotetraose while it degraded cellohexaose and cellotetraose. In contrast, *Nc*LPMO9C produced cellobiose, cellotriose and cellotetraose from cellohexaose. Both enzymes utilised all the substrate after 24 hours, as shown in Figure S7.

The y-axis was given in signal instead of concentration for the same reasons as the time course on cellopentaose.

4.10 Activity of *Sc*LPMO9A and *Nc*LPMO9C in the presence of exogenous H_2O_2

4.10.1 Time course with 1 mM AscA

To see how H_2O_2 influenced the reaction rates and product yields with *Sc*LPMO9A and *Nc*LPMO9C, a time course reaction with different concentrations of H_2O_2 and 1 mM AscA was performed and analysed.

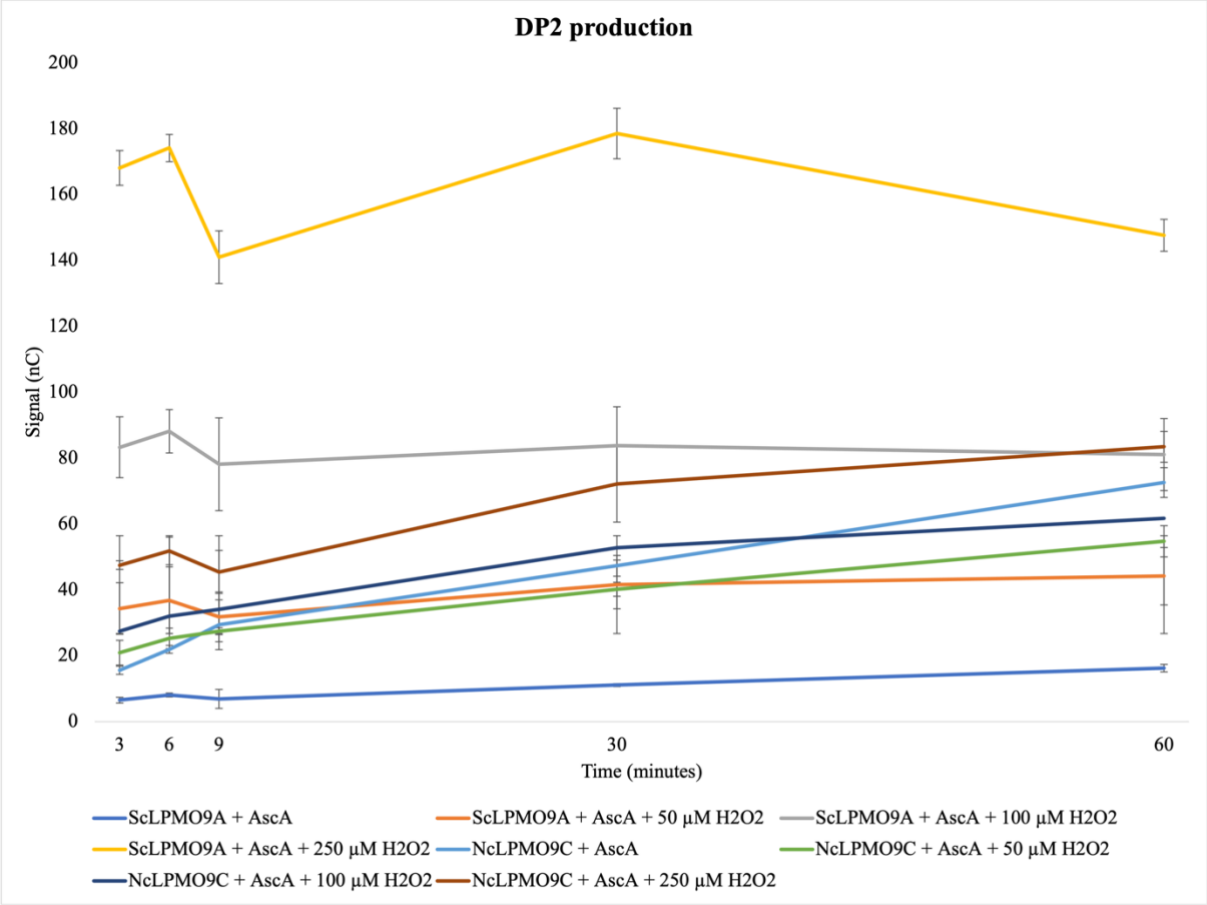

Figure 4.10.1. Cellobiose production of *Sc*LPMO9A and *Nc*LPMO9C. Reactions were performed in 50 mM sodium acetate buffer pH 5.0, 1 mM cellopentaose, 1 µM *Sc*LPMO9A/*Nc*LPMO9C, 1 mM AscA and 0, 50, 100 and 250 µM H_2O_2. Samples were taken after 3, 6, 9, 30 and 60 minutes. The reactions were analysed with HPAEC-PAD using a Dionex ISC-6000 system. Data are expressed as mean values for 3 independent repeats.

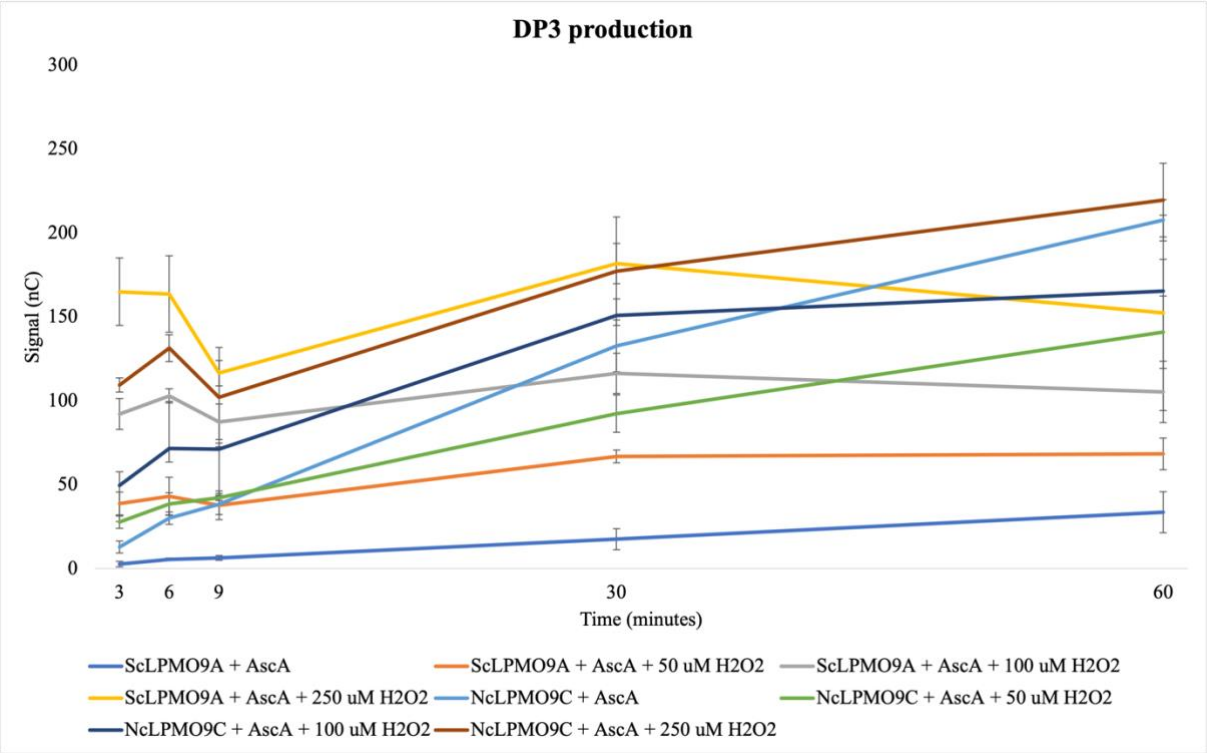

Figure 4.10.2. Cellotriose production of *Sc*LPMO9A and *Nc*LPMO9C. Reactions were performed in 50 mM sodium acetate buffer pH 5.0, 1 mM cellopentaose, 1 µM *Sc*LPMO9/*Nc*LPMO9c, 1 mM AscA and 0, 50, 100 and 250 µM H_2O_2. Samples were taken after 3, 6, 9, 30 and 60 minutes. The reactions were analysed with HPAEC-PAD using a Dionex ISC-6000 system. Data are expressed as mean values for 3 independent repeats.

Both *Sc*LPMO9A and *Nc*LPMO9C reacted faster when H_2O_2 was added to the reaction compered to when reactions were performed without added H_2O_2 (Figures 4.10.1 and 4.10.2). In the reactions without added H_2O_2, the activity continued after 1 hour for both *Sc*LPMO9A and *Nc*LPMO9C. In reactions with *Sc*LPMO9A where H_2O_2 was added, the activity had stopped before 3 minutes for all H_2O_2 concentrations tested. In contrast, in all reactions with *Nc*LPMO9C, maximum yield was observed after 1 hour.

*Nc*LPMO9C produced more product without added H_2O_2 after 1 hour than *Sc*LPMO9A did. However, when concentrations higher than 100 µM H_2O_2 was added to the reactions, *Sc*LPMO9A outcompeted the production yield after 3 minutes compared to *Nc*LPMO9C. This effect was more significant on cellobiose than cellotriose. For cellotriose, the results were more similar between *Sc*LPMO9A and *Nc*LPMO9C with added H_2O_2.

Native cellobiose and cellotriose, as well as C4 oxidized products after 1 hour are shown as a chromatogram in Figure S8.

4.10.2 Time course with 50 µM AscA

Since the reactions with *Sc*LPMO9A stopped before 3 minutes with added H_2O_2, and the first time point in this experiment was 3 minutes, the figures did not show the reaction rate. Therefore, the same experiment was performed, only with 50 µM AscA, to observe if the reaction rate decreased with lower AscA concentration.

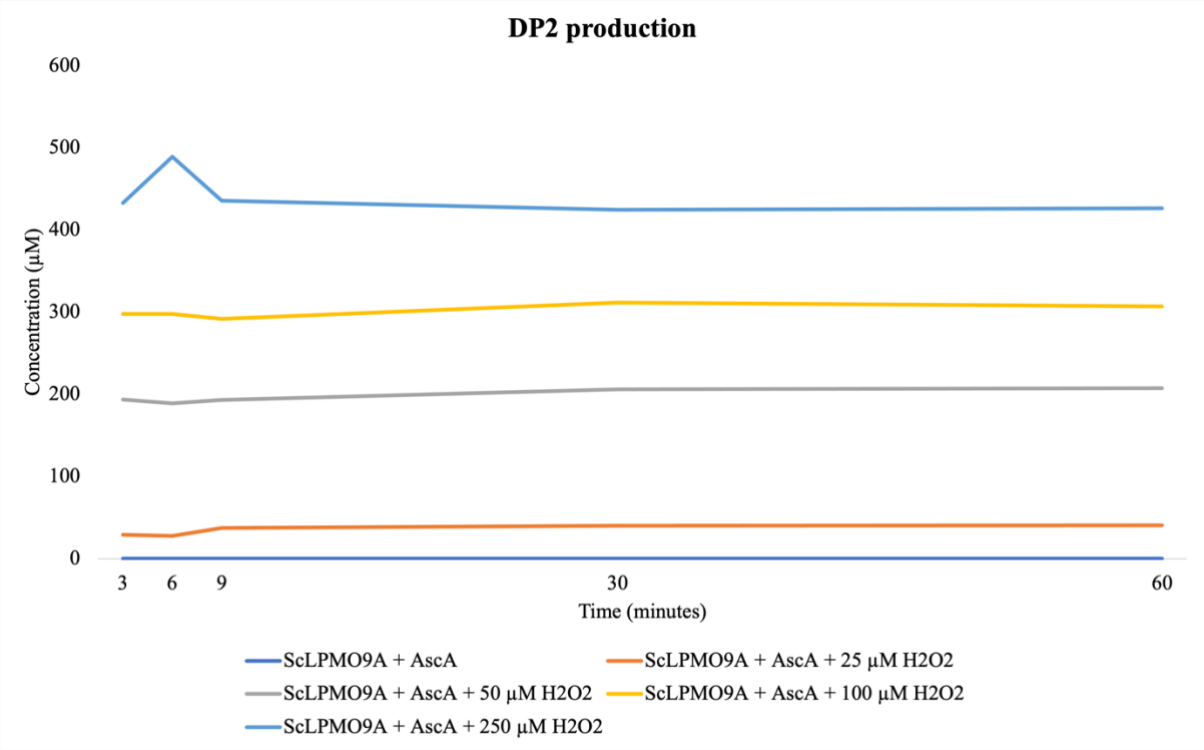

Figure 4.10.3. Cellobiose production of *Sc*LPMO9A. Reactions were performed in 50 mM sodium acetate buffer pH 5.0, 1 mM cellopentaose, 1 µM *Sc*LPMO9A, 50 µM AscA and 0, 25, 50, 100 and 250 µM H_2O_2. Samples were taken after 3, 6, 9, 30 and 60 minutes. The reactions were analysed with HPAEC-PAD using a Dionex ISC-6000 system. Data are expressed as mean values for 3 independent repeats.

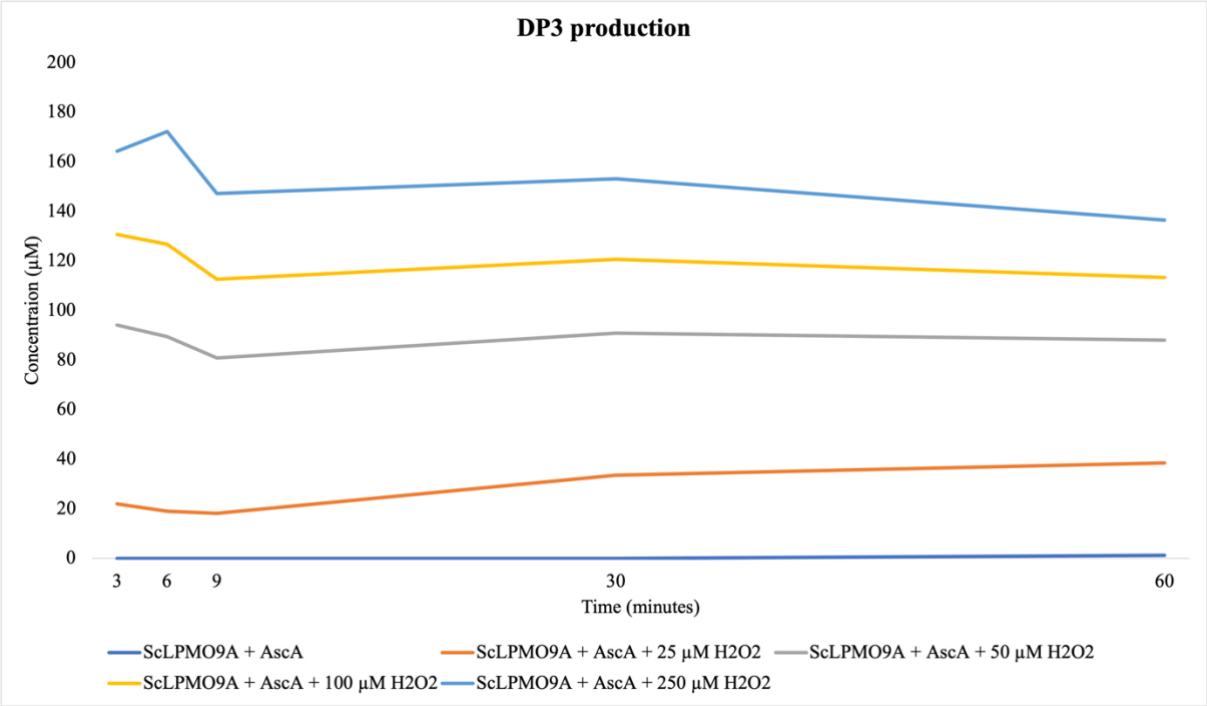

Figure 4.10.4. Cellotriose production of *Sc*LPMO9A. Reactions were performed in 50 mM sodium acetate buffer pH 5.0, 1 mM cellopentaose, 1 µM *Sc*LPMO9A, 50 µM AscA and 0, 25, 50, 100 and 250 µM H_2O_2. Samples were taken after 3, 6, 9, 30 and 60 minutes. The reactions were analysed with HPAEC-PAD using a Dionex ISC-6000 system. Data are expressed as mean values for 3 independent repeats.

The reactions still hit a limit before 3 minutes with lower concentrations of AscA. It was also added an additional concentration of H_2O_2 at 25 µM, but even with low concentrations of both reductant and H_2O_2, the reaction rate was not decreased enough to obtain an actual view of the rate.

Figure S9 show the chromatogram after 1 hour. The chromatogram shows both native cellobiose and cellotriose, as well as C4 oxidized products.

4.11 Synergy experiment

Reactions from the synergy experiment with a celluclast and BG on sulfite pulped Norway spruce was analysed on Dionex Ultimate 3000 RSCL with a long Rezex column.

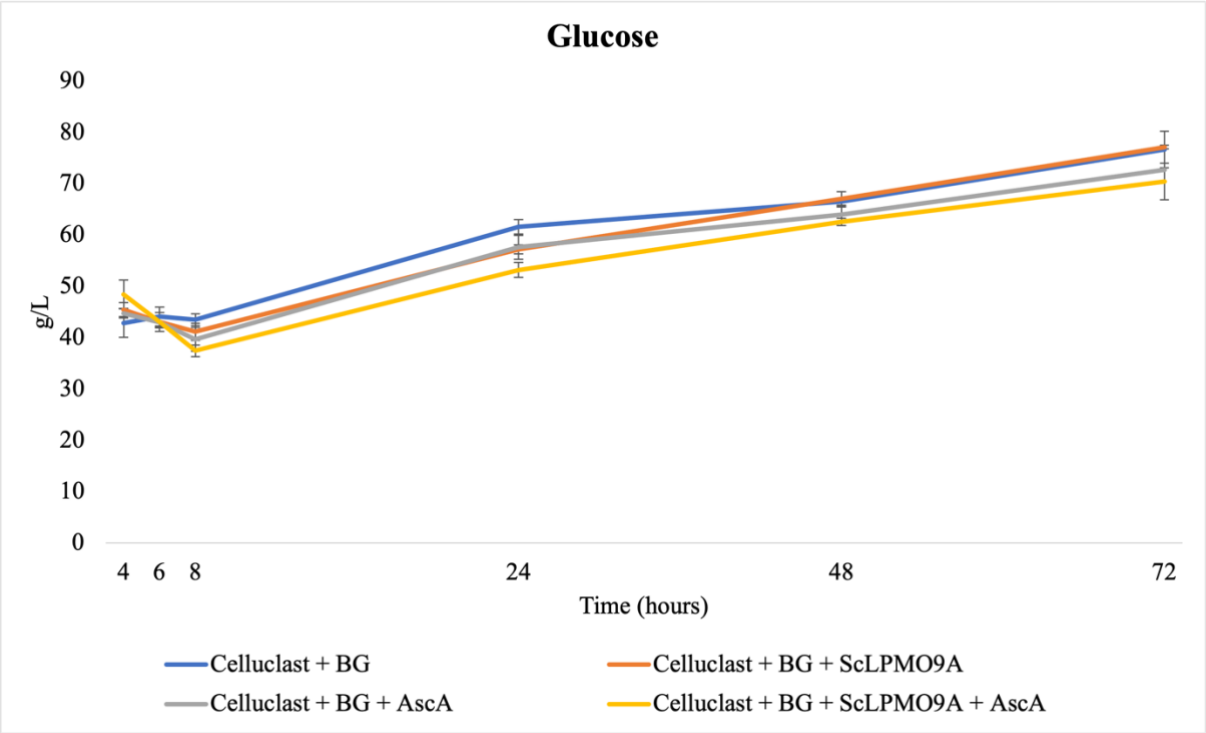

Figure 4.11.1. Glucose production after depolymerization of sulfite pulped Norway spruce by celluclast, BG and *Sc*LPMO9A. Reaction performed in sodium acetate buffer pH 5.0 (50 mM), 100 g/L VASP, 3.6 mg/g dry matter (DM) celluclast, 0.4 mg/g DM *Sc*LPMO9A, 0.4 mg/g DM β-glucosidase and 1 mM AscA. Samples were taken after 4, 6, 8, 24, 48 and 72 hours. Data are expressed as mean values for 2 independent repeats.

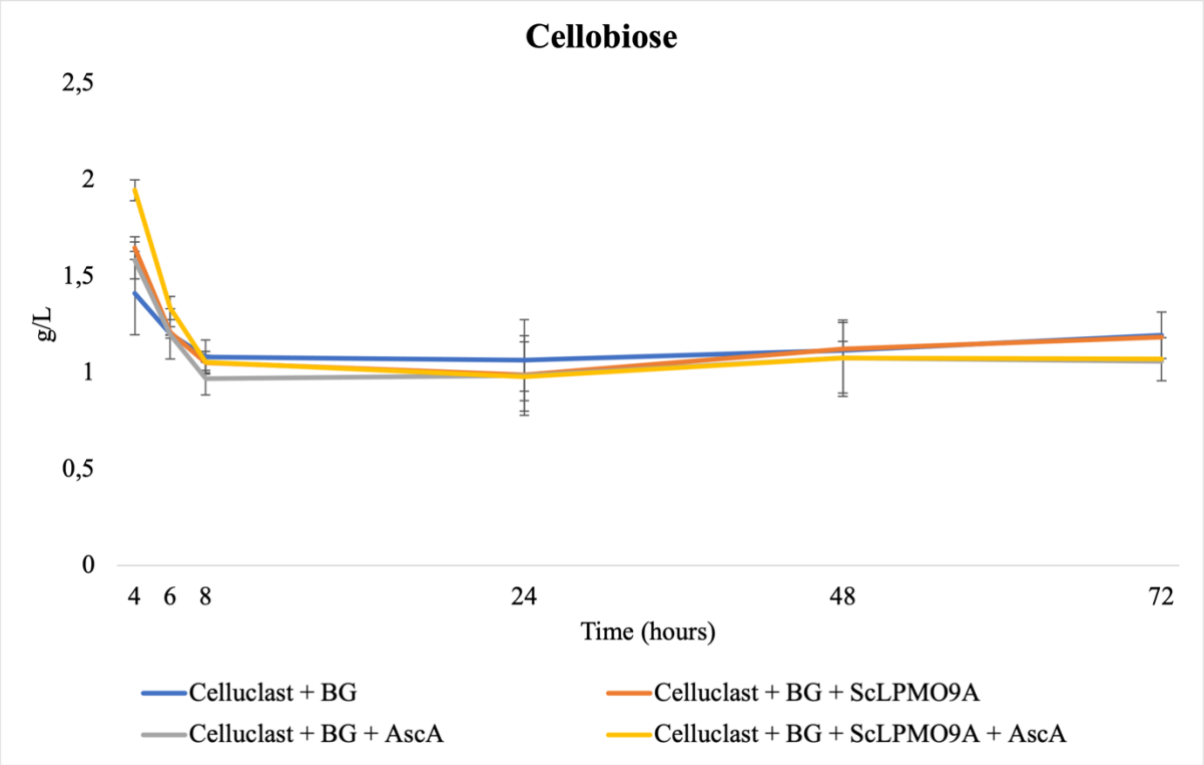

Figure 4.11.2. Cellobiose production after depolymerization of sulfite pulped Norway spruce by celluclast, BG and *Sc*LPMO9A. Reaction performed in sodium acetate buffer pH 5.0 (50 mM), 100 g/L VASP, 3.6 mg/g dry matter (DM) celluclast, 0.4 mg/g DM *Sc*LPMO9A, 0.4 mg/g DM β-glucosidase and 1 mM AscA. Samples were taken after 4, 6, 8, 24, 48 and 72 hours. Data are expressed as mean values for 2 independent repeats.

The experiments with *Sc*LPMO9A and AscA did not yield more product than the experiments without LPMO (Figure 4.12.1. and 4.12.2).

The same samples were also analysed using HPAEC-PAD to observe if there were any C4 oxidized products.

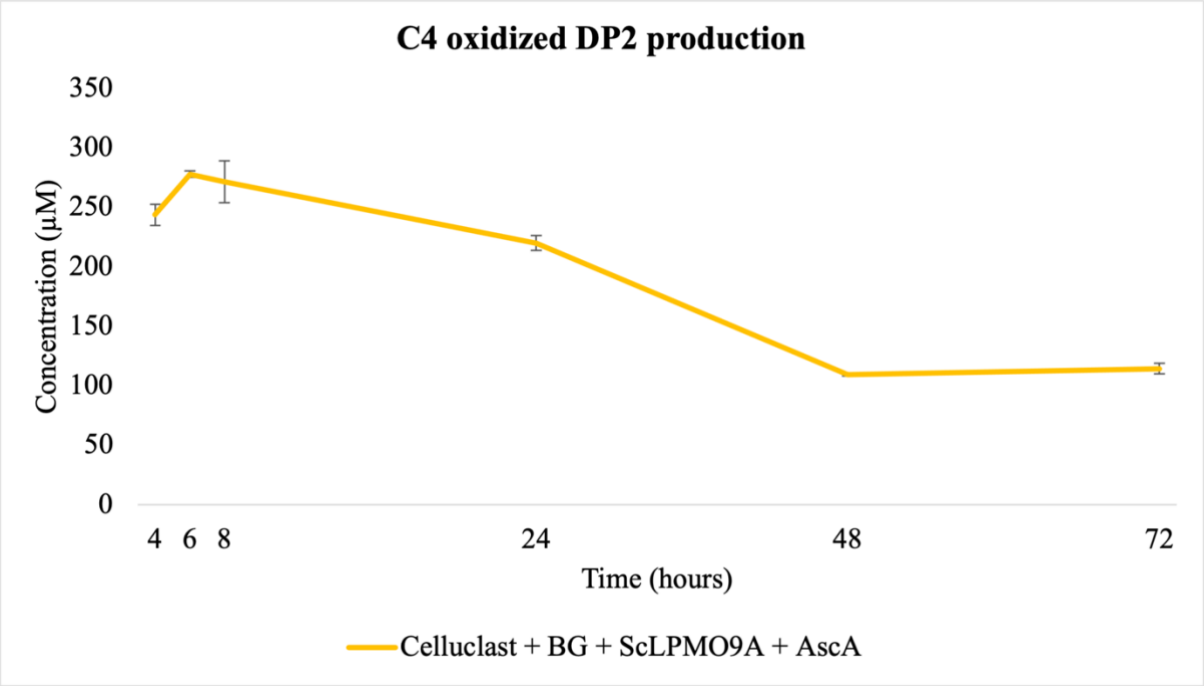

Figure 4.11.3. Glc4gemGlc production after depolymerization of sulfite pulped Norway spruce by celluclast, BG and *Sc*LPMO9A. Reaction performed in sodium acetate buffer pH 5.0 (50 mM), 100 g/L VASP, 3.6 mg/g dry matter (DM) celluclast, 0.4 mg/g DM *Sc*LPMO9A, 0.4 mg/g DM β-glucosidase and 1 mM AscA. Samples were taken after 4, 6, 8, 24, 48 and 72 hours. The reactions were analysed with HPAEC-PAD using a Dionex ISC-5000 system. Data are expressed as mean values for 2 independent repeats. Controls without *Sc*LPMO9A and AscA was not shown, as they did not show any Glc4gemGlc product formation.

There was some production of Glc4gemGlc from *Sc*LPMO9A (Figure 4.11.3). The Glc4gemGlc product was degraded after approximately 8 hours, probably because of low pH combined with a high temperature in the reactions.

5 Discussion

In this study, *Sc*LPMO9A was characterized and compared to *Nc*LPMO9C. The main objective was to obtain a better insight into how *Sc*LPMO9A works on different soluble substrates, both in the presence and absence of added H_2O_2. These analyses can give a better understanding of how *Sc*LPMO9A works and how the enzyme can be used in the industry, in addition to giving a better understanding of the biological role to *Sc*LPMO9A.

5.1 Bioinformatics and previous work

5.1.1 Multiple sequence alignment

As the MSA alignment in Figure 4.1.1 shows, the active site histidines (His1 and His81), and the tyrosine (Tyr163) coordinating the copper atom in LPMO9s is conserved in ScLPMO9A and the five other LPMO9s showed, highlighting the importance of these residues for catalysis.

The MSA also showed that the LPMO9s mostly consist of β-sheets and loops that connect the β-strands (Figure 4.1.1). These loops vary within LPMO families and make the dimensions and topologies of the substrate-binding surface vary. For example, the L2 region influences the regioselectivity and specificity to LPMO9s (Vaaje-Kolstad et al., 2017). In addition, the LS and LC regions are exclusive to LPMO9s and LPMO13s, and are most likely involved in substrate binding (Vaaje-Kolstad et al., 2017).

Figure 4.1.1 probably contain some errors, as the loops were only based on the structure of *Nc*LPMO9C. If LPMOs from different families were compared, these differences would be even bigger, but since all the LPMOs in Figure 4.1.1 are in family 9, they are predicted to have more similar positions of the loops. In addition to the loops only being based on *Nc*LPMO9C, the secondary structure is based on *Ls*LPMO9A. Therefore, the secondary structure is not 100% accurate for the five others, but it is used as an indication.

5.1.2 *Sc*LPMO9A structure model

*Ls*LPMO9A is the closest homolog to *Sc*LPMO9A with a known crystal structure (Frandsen et al., 2016). The results from the SWISS-MODEL show that the *Sc*LPMO9A catalytic domain had 61.09% sequence identity with the catalytic domain of *Ls*LPMO9A (PDB ID: 5AC1) from *Lentinus similis*, which allows for accurate homology modelling.

The secondary structure of *Sc*LPMO9A consist of β-sheets, α-helixes, and loops, also shown in the MSA (Figures 4.1.2 and 4.1.3). The structure model also show how *Sc*LPMO9A

interacts with cellohexaose as a substrate (Figure 4.1.2 and 4.1.3). In addition, Figure 4.1.4 show the histidine brace interacting with the copper.

Since it is known that the structure influences the regioselectivity and specificity, it makes sense that *Sc*LPMO9A and *Ls*LPMO9A are both C4 oxidizing LPMOs that can cleave soluble substrates. It has previously been described that *Ls*LPMO9A works on several polysaccharides including cellulose, xyloglucan, mixed-linkage glucan and glucomannan (Simmons et al., 2017). Previous work for this thesis has shown that *Sc*LPMO9A works on several cellulose and hemicellulose substrates, for example, PASC, TXG, KGM, BG and XO.

5.1.3 Previous work

HPAEC-PAD were used for substrate screening on celluloses, hemicelluloses, and hemicelluloses together with PASC.

*Sc*LPMO9A was active on several celluloses and hemicelluloses (Figure 4.1.5). The enzyme acted on insoluble substrates such as PASC, as well as soluble substrates such as xyloglucan. On the other hand, *Sc*LPMO9A was not active on Avicel, in contrast to *Nc*LPMO9C that have shown activity on Avicel (Isaksen et al., 2014).

Figures 4.1.6, 4.1.7, 4.1.8 and 4.1.9 show *Sc*LPMO9A on different hemicelluloses combined with PASC. The reason why PASC was added to the reactions was because PASC makes the hemicelluloses more linear, which makes it easier for the flat binding site of *Sc*LPMO9A to bind (Frommhagen et al., 2018). However, only based on the figures, it was not possible to state if PASC boosted the activity on the hemicelluloses as the products were not quantified. On the other hand, the figures showed that *Sc*LPMO9A and *Nc*LPMO9C have different substrate preferences and product profiles. For example, *Sc*LPMO9A was more active on BG than *Nc*LPMO9C (Figure 4.1.7), and this was most distinct in the reactions without PASC.

5.2 Purification of *Sc*LPMO9A

Chemically competent *E. coli* cells containing *Sc*LPMO9A were cultivated as described in Section 3.2.

*Sc*LPMO9A was overexpressed in the supernatant, and there was no protein with a molecular weight of the predicted 24.5 kDa in the pellet, indicating that the osmotic shock had been successful and that *Sc*LPMO9A was secreted into the periplasm (Figure 4.2.1). The observed molecular mass of *Sc*LPMO9A on the gel was ~28 kDa, which is higher than the predicted mass of 24.49 kDa. There can be several explanations to this, for example post-translational modifications, or that the protein was not fully denaturated prior to electrophoresis.

*Sc*LPMO9A protein bound to the HiTrap DEAF FF column in anion exchange chromatography (Figure 4.2.2). However, the binding was might not optimal since the injection peak was not sharp and the SDS-PAGE gel of the fractions (Figure 4.2.3) showed that *Sc*LPMO9A eluted together with other proteins. On the other hand, there was no significant amount of *Sc*LPMO9A in the flow through, confirming that the protein did bound to the column. Other conditions could be tested, like different flow rates or a steeper gradient. By adding two columns, the binding capacity could also be increased. The HiTrap DEAF FF column used could also be defected, discussed later in this section.

The chromatogram from SEC showed successful purification based on the sharp peak (Figure 4.2.4), combined with the SDS-PAGE gel (Figure 4.2.5), showing no other proteins than *Sc*LPMO9A in the fractions from the eluted peak.

Bradford protein assay was used to measure the concentration of *Sc*LPMO9A after purification and concentration. This method is based on a common standard curve using bovine serum albumin; therefore, the accuracy of the protein concentration will vary depending on the protein being analysed. Since the sample protein often differs from the standard curve protein in both size and chemistry, both under- and over-estimation of the concentration is common when using Bradford protein assay, which in turn can influence downstream experiments where knowing protein concentration is important.

The reason why Bradford assay was used to calculate concentrations was because the *Nc*LPMO9C batch purified for this thesis consisted of pigments. Samples containing pigments are more suitable for Bradford than for example, A_{280}, because the pigments can absorb light

at 280 nm, and influence the concentration. Since every method of measurement has advantages and disadvantages, the same method was used for both *Sc*LPMO9A and *Nc*LPMO9C, to obtain as few sources of error as possible.

Endoglucanase background activity screening was done following copper saturation of the purified LPMOs. The *Sc*LPMO9A batch did not contain any endoglucanase background (Figure 4.2.6), and this was evident by the fact that the controls without AscA did not show any degradation of PASC, unlike the sample with ScLPMO9A and PASC where AscA was added.

The purification yield for ScLPMO9A varied between the different rounds of purification (Table 4.2.1.). There can be several explanations as to why the yield varied from time to time. The main reason was probably that some of the samples were purified with anion exchange chromatography and SEC, while other samples were determined to be pure enough after only anion exchange chromatography. Since protein was lost in every step of purification, purification with fewer steps would likely give a higher concentration of protein. Purification round 3 and 5 had the highest concentration (Table 4.2.1.), and these were also the batches only purified with anion exchange chromatography.

The reason why some of the batches appear more purified after anion exchange chromatography than others is hard to tell. The same method was used in all purification rounds. However, different HiTrap DEAF FF columns were used. An explanation could therefore be that some of the columns were cleaner than others, or that some of the columns were defected because of other issues, for example, if some of them had been dried out previously.

In addition to some proteins being lost when an additional purification step was used, the samples of the proteins purified with only anion exchange chromatography probably had some other proteins in the sample as well, making the calculated concentration even higher. In addition to this, there were some difficulties with the harvesting in the first purification, making the yield unusually low. This was most likely because the cultivation medium was mixed with water to fill the centrifuge tube, which may have affected the osmotic shock. Therefore, the following batches were cultivated in 1 litre medium instead of 500 mL.

5.3 Purification of *Nc*LPMO9C

P. pastoris containing *Nc*LPMO9C were cultivated as described in Section 3.5.

Based on the SDS-PAGE gel after harvesting it appeared that there was some *Nc*LPMO9C left in the pellet, however, this was hard to state based on the gel picture (Figure 4.3.1). The gel also showed that the molecular weight of *Nc*LPMO9C was higher than the predicted 35.8 kDa (approximately 45 kDa). This was most likely because of glycosylations. To test this hypothesis, the amino acid sequence of *Nc*LPMO9C was analysed using the NetNGlyc and NetOGlyc tools (Gupta & Brunak, 2002). These databases predict the likelihood of N-glycosylations and O-glycosylations. According to this analysis, the full length of *Nc*LPMO9C consist of two asparagines that are predicted to be N-glycosylated and 30 potential O-glycosylation sites. As such, it is likely that the *Nc*LPMO9C used in this study had some glycosylations and it was, therefore, as expected that the molecular weight was higher than the theoretical weight.

The gel did not show a distinct bond of *Nc*LPMO9C in either pellet or supernatant (Figure 4.3.1). A protein with a molecular weight of 160 kDa had a vaster bond, even though the glycerol stock used to cultivate *Nc*LPMO9C should have *Nc*LPMO9C as the main protein. The protein with a mass of 160 kDa was not identified. However, after purification with HIC, the SDS-PAGE gel showed a clear bond with *Nc*LPMO9C (Figure 4.3.2). Therefore, the reason why the bond was not distinct after harvesting was most likely because the protein was too diluted.

The chromatogram from HIC showed that *Nc*LPMO9C bound to the Phenyl FF columns. This chromatogram was not shown in this thesis as it got saved in the wrong format. However, the binding may not be optimal because the flow through after HIC showed protein with the same mass as *Nc*LPMO9C (Figure 4.3.2). However, it is not possible to tell if this protein is *Nc*LPMO9C or another protein with a similar weight.

The chromatogram from SEC (Figure 4.3.3) showed that the injection peak was split into a shoulder and a broad peak, making it a challenge to separate *Nc*LPMO9C from the other

proteins. The shoulder and the broad peak could indicate that the *P. pastoris* had been contaminated.

Before the endoglucanase screening, the concentration of *Nc*LPMO9C was calculated with Bradford protein assay, in the same manner as for *Sc*LPMO9A, before being incubated with PASC for endoglucanase screening.

The endoglucanase screening (Figure 4.3.5) showed that both pooled fractions contained endoglucanase. Since two batches of the fractions from SEC were pooled separately, HPAEC-PAD was used to test for endoglucanase background for both batches. The sample with only PASC and AscA showed no degradation of PASC, as expected since there was no enzyme added to this reaction. In one of the controls with only *Nc*LPMO9C (2) and PASC, the chromatogram clearly showed a degradation of PASC, which indicates that there was endoglucanase activity in the sample. In the control with the other sample of *Nc*LPMO9C (1) and PASC, the chromatogram did not show as distinct product formation, but it still had some minor degradation. Since product formation was so small, the sample was used further in the laboratory experiments, but this have probably impacted some of the results, making higher product concentration than the real *Nc*LPMO9C production.

Based on the SDS-PAGE gel of the eluted fractions from SEC (Figure 4.3.4), the fractions did appear purified. This prove that an SDS-PAGE gel is not an accurate method to check for endoglycanases, and this was the reason why HPAEC-PAD was used for all purified batches in this study to screen for endoglucanase activity.

It is hard to tell why some of the purified *Nc*LPMO9C contained endoglucanases. For this thesis, *Nc*LPMO9C was purified twice, and after both attempts, the protein samples consisted of endoglucanases. Two rounds of HIC were also tested, to see if endoglucanases could be separated from *Nc*LPMO9C on the second round, without success. The reason why endoglucanases did not show at the SDS-PAGE gel (Figure 4.3.4) was probably that endoglucanases had almost similar molecular weight as *Nc*LPMO9C, hence there were difficult to observe if there were endoglucanases or not, only by looking at the gel.

5.4 H_2O_2 production by LPMOs

LPMOs produce H_2O_2 when they are not bound to a substrate, in presence of a reductant (Hangasky et al., 2018). It is also stated that when LPMOs are bound to a substrate, the production of H_2O_2 is reduced (Rieder et al., 2021).

From the Amplex Red Hydrogen Peroxide assay, *Nc*LPMO9C produced about 200 µM H_2O_2 but had a slower reaction rate than copper (Figure 4.4.1). However, the production with *Nc*LPMO9C seemed to still increase after 120 minutes, while the production with copper hit a limit after 60 minutes.

*Sc*LPMO9A showed almost the same production as the controls (cellopentaose and cellopentaose with LPMOs/$CuSO_4$), making it hard to state if the production was due to the enzyme or not (Figure 4.4.1). The copper had produced about the same amount of H_2O_2 as *Nc*LPMO9C after 2 hours, making it clear that free copper also produces H_2O_2, in accordance with Stepnov et al. (2022). The copper was not affected when a substrate was added to the reaction, unlike the reactions with LPMOs that did not produce H_2O_2 when bound to a substrate.

Why the rate and final concentration of H_2O_2 produced by *Sc*LPMO9A in the presence of AscA was significantly lower than for *Nc*LPMO9C could be an indication that the latter had a higher redox potential, since a higher redox potential will lead to faster reduction of Cu(II)→Cu(I). The redox potential of LPMO-Cu(II) was measured for this thesis, showing that *Nc*LPMO9C indeed had a higher redox potential than *Sc*LPMO9A (186 mV vs 224 mV), but whether this difference alone can explain the observations need further investigation.

Another explanation could be that high concentrations of AscA generate too much H_2O_2, which can inactivate the enzyme. However, this is unlikely, because studies in this thesis have showed that *Sc*LPMO9A can handle high concentrations of H_2O_2 (shown up to 250 µM). It is also possible to think that *Sc*LPMO9A utilises H_2O_2 in side-reactions not shown in the assay, such as oxidation of AscA by H_2O_2 (Bissaro, Kommedal, et al., 2020), hence giving a lower H_2O_2 production signal than actual H_2O_2 production.

Furthermore, *Sc*LPMO9A and *Nc*LPMO9C were produced in different hosts, as *Sc*LPMO9A was produced in *E. coli* while *Nc*LPMO9C was produced in *P. pastoris.* This could be an explanation, as different hosts could give different post-translational modifications that could affect the ability of the enzyme to produce H_2O_2. For further studies, it would be of interest to produce *Sc*LPMO9A in *P. pastoris* and see whether this would affect the observed results or not.

To see if a substrate impacted the apparent H_2O_2 production, cellopentaose was added to the reactions. Cellopentaose, which is a known substrate for both *Sc*LPMO9A and *Nc*LPMO9C, as shown in this thesis, affected the production of H_2O_2 for at the enzymes (Figure 4.4.1). This effect could reflect the inhibition of oxidase reaction, as Kittle et al. showed in 2012 (Kittl et al., 2012). On the other hand, the effect could also reflect the consumption of generated H_2O_2 in the LPMO reaction together with a substrate (Rieder et al., 2021).

The reason why the figure did show a minor increase in H_2O_2 production over time in the controls, was likely because the Amplex red used in this study was slightly oxidized, so the signal was probably not H_2O_2 production, but signals from the oxidized resorufin.

The Amplex Red Hydrogen Peroxide assay is a useful and fast assay to measure H_2O_2 production and to verify LPMO activity. However, the assay has some drawbacks, for example, that the reductant suppresses the signal of the HRP, which will vary between reductants. Since only AscA was used in this thesis, variations between reductants are not shown, but it is important to keep in mind that other results could occur using other reductants. H_2O_2 can also react with the reductant, leaving to underestimation of H_2O_2 (Stepnov et al., 2021), which could have happened here in the samples with *Sc*LPMO9A. Therefore, the assay can be useful to verify LPMO activity, but not so suitable for getting correct quantifications of H_2O_2 production.

5.5 H_2O_2 consumption

Figure 4.5.1 showed the consumption of H_2O_2 of *Sc*LPMO9A and *Nc*LPMO9C. These results can be used to show if the LPMOs have been properly folded and have incorporated copper in the active site, as if there were not, there would not be any H_2O_2 consumption. Both enzymes

consumed almost the same amount of H_2O_2, and free copper did not consume any H_2O_2, making it clear that it was the enzymes that consumed the H_2O_2 (Figure 4.5.1).

The Breslmayr assay is a fast and sensitive method to measure H_2O_2 consumption. 2,6-DMP was used as a substrate, while H_2O_2 was used as a co-substrate and the high molar absorption coefficient of coerulignone was measured spectrophotometrically. This provided not only the opportunity to measure the activity of the LPMOs, but it could also have been used to study binding constants or thermal stability (Breslmayr et al., 2018).

As Breslmayr showed in 2018, the conversion of 2,6-DMP increased between pH 4.0 – 8.0 (Breslmayr et al., 2018). In the reaction used in this thesis, the buffer used was Bis-Tris-HCl buffer pH 6.5. The preferred 2,6-DMP concentration varies with pH, and a 1 mM 2,6-DMP concentration was used, since Breslmayr et al. state that this was a preferred concentration for the used pH (Breslmayr et al., 2018).

An limitation of using the Breslmayr assay is that if the LPMO concentrations are higher than 1.25 μM, the activity is no longer proportional to the enzyme concentration (Breslmayr et al., 2018). In this thesis, 3 μM enzyme was used to calculate the H_2O_2 consumption. However, similar enzyme concentrations were used for both *Sc*LPMO9A and *Nc*LPMO9C, so the results should still be comparative, and activity could still be confirmed. However, to obtain a more accurate result, the enzyme concentration should have been 1.25 μM or lower.

The results from the Breslmayr assay confirmed that the LPMOs can utilise H_2O_2 as a co-substrate and that both the LPMOs were active.

5.6 Redox potential

Redox potential is a measurement of the strength and in which direction electrons move between substances. Since LPMO reactions are red-ox reactions, electrons will move between substances, where one will give off an electron and one will receive the electron. To reduce the copper in the LPMO active site, a reductant is added to the reaction, giving off electrons to the copper, which gets reduced. An LPMO with a high redox potential gets more readily reduced than an LPMO with a lower redox potential.

The redox potential of *Sc*LPMO9A-Cu^{2+}/*Sc*LPMO9A-Cu^{+} was determined as described in Section 3.10, with a value of 186± 10 mV. Compared to *Nc*LPMO9C, this was 17% lower, which makes sense, as the results in this thesis showed that *Sc*LPMO9A had a slower reaction rate than *Nc*LPMO9C. However, the redox potential for *Nc*LPMO9C was taken from Borisova et al., (2015) and was not measured together with *Sc*LPMO9A for this thesis. However, the method used here was similar to Borisova et al., and as such the results should be comparable. It should be noted that the results rely on correct estimation of enzyme concentration. In other words, the measurement is a good indication of the redox potential, but there are some potential pitfalls in how accurate the measurement is.

Keep in mind that a redox potential measurement only describes how fast the copper get reduces and clarify nothing about the reaction after the reduction. Therefore, the redox potential did not have to be the complete reason why for example *Sc*LPMO9A reacts slower than *Nc*LPMO9C.

5.7 Method optimalization

5.7.1 Choice of buffer

Different buffers give different product signals when analysing on HPAEC-PAD because they contain ions that interact with the column on the HPAEC-PAD. It is also important to note that different buffers have different pH, which can also affect the interaction with the column. In addition to this, different buffers can also have different impacts on the LPMO activity. Therefore, different buffers were tested to find the most suited for analysing on HPAEC-PAD.

Sodium phosphate buffer pH 6.0 was the least suited of the buffers tested (Figure 4.7.1), where a buffer strength of 25 mM stands out from the rest with stark differences in product retention times and less defined peaks. This impact was significantly lessened at 5 mM, however, to maintain buffer capacity, the buffer concentration should be higher than this, typically between 25 mM and 100 mM for LPMO reactions.

Sodium citrate buffer pH 6.0 gave good signals and separation on the HPAEC-PAD, however, since sodium citrate is a chelator, meaning that it reacts with metal ions, the buffer can react with the copper in the LPMOs which is not suitable.

Bis-Tris buffer is commonly used in LPMO reactions, but since the peaks eluted too early with this buffer, with cellobiose eluting together with the very strong injection peak, this buffer was not used. This is not shown in figure 4.7.1 but was confirmed in the earlier analysis. However, the ISC-5000 did undergo some service after testing with this buffer, making the overall retention times better, so Bis-Tris buffer pH 6.5 could likely be used in future studies if all analytes was visible in the chromatogram.

Sodium acetate buffer pH 5.0 gave both good separation and strong signals from all analytes of interest (cellobiose-cellohexaose), and worked well in LPMO reactions, as was apparent from subsequent experiments in this thesis. The only potential drawback with this buffer was the low pH. Since *Sc*LPMO9A has a theoretical pI of 4.63, a pH of 5.0 should not be a problem. *Nc*LPMO9C full length has a theoretical pI of 8.89, so the buffer should have a pH higher than 5.0. A buffer with a pH far from the theoretical pI is not optimal, because it can destabilize the protein. However, since sodium acetate pH 5.0 gave the clearest signals and since the reactions with *Nc*LPMO9C did not show different results in this buffer compared to with Bis-Tris buffer pH 6.5, which was used in the first reactions in the laboratory work, sodium acetate buffer pH 5.0 was the chosen buffer for further experiments.

5.7.2 Choice of enzyme inactivation method

In addition to choosing a suited buffer, 200 mM NaOH or heat inactivation of enzymes at 100 °C for 10 minutes was tested. Figure 4.7.2 shows that when the reactions with cellopentaose were stopped with boiling, the cellopentaose was degraded. Because of this, heat inactivation could not be used to stop reactions with cellopentaose, as this could give overestimations of cellobiose and cellotriose concentrations. This degradation was more significant with sodium phosphate buffer pH 6.0 than with sodium acetate buffer pH 5.0, indicating that the degradation or stability of cellopentaose was buffer dependent. The same degradation was not seen when the reactions were stopped with 200 mM NaOH in neither sodium phosphate buffer pH 6.0 nor sodium acetate buffer pH 5.0.

On the other hand, NaOH is a strong base, which will affect the pH in the solution. However, since the eluents in the Dionex ISC-5000 system also consist of NaOH, the sample would undergo a change in pH anyway. NaOH were only used when analysing native products, as the high pH can generate native products from C4 oxidized products (Kojima et al., 2016).

The other substrates were not tested with boiling, however, the chromatogram of the reactions stopped with 200 mM NaOH showed some cellotetraose in the substrate, while this were degraded in the reactions stopped with heat inactivation. Therefore, cellotetraose was also degraded with heat inactivation. It is not possible to tell if other substrates, like cellohexaose, would have been degraded with boiling. However, when comparing different substrates, all conditions should be the same. Therefore, all reactions were stopped with 200 mM NaOH, independent of substrate.

5.8 Activity of *Sc*LPMO9A and *Nc*LPMO9C on soluble substrates

Overnight reactions with *Sc*LPMO9A and *Nc*LPMO9C were incubated with cellotetraose, cellopentaose and cellohexaose. Since most enzymes are highly specific, different LPMOs are expected to have different substrate specificity, even though the enzymes are in the same family. This is shown by Figures 4.8.1, 4.8.2 and 4.8.3, which showed that *Sc*LPMO9A and *Nc*LPMO9C had different substrate preferences and different product-profiles on cellotetraose, cellopentaose and cellohexaose.

Since the sequences and topologies of the extended loops in the LPMOs are highly diverse, the substrate specificities also become diverse (Zhou & Zhu, 2020). Several substructures are proposed to influence the substrate binding. For example, the L2 loop (Zhou et al., 2019). In addition to this, the substrate-binding surface also consists of solvent-exposed aromatic residues that can be responsible for substrate binding. Lastly, posttranslational glycosylations can affect substrate binding. (Zhou et al., 2019).

ScLPMO9A was active on all the substrates tested (cellotetraose, cellopentaose and cellohexaose), while *Nc*LPMO9C showed very weak activity on cellotetraose (Figures 4.8.1, 4.8.2 and 4.8.3). This is shown since the cellotetraose peak with *Nc*LPMO9C + cellotetraose

+ AscA was almost as sizeable as for the reactions without AscA, together with narrow cellobiose and Glc4gemGlc$_2$ peaks compared with *Sc*LPMO9A. On the other hand, *Nc*LPMO9C showed strong activity towards cellopentaose and cellohexaose.

In addition to binding to different substrates, the ratio of products produced by *Sc*LPMO9A and *Nc*LPMO9C on cellopentaose and cellohexaose differed, indicating that there likely are differences in preferred binding modes for these substrates. A possible explanation for these observations could be that *Sc*LPMO9A and *Nc*LPMO9C have different residue compositions in the L2, L3, LS and LC loops, and perhaps also different solvent-exposed aromatic residues. *Nc*LPMO9C also carries a CBM1 domain that may affect substrate binding. And lastly, differences glycosylations could contribute to differences in binding affinities (Courtade et al., 2018)

5.8.1 Overnight reactions on cellotetraose

*Nc*LPMO9C only showed a slight degradation of the cellotetraose substrate while *Sc*LPMO9A degraded all the cellotetraose to native cellobiose (Figure 4.8.1). Glc4gemGlc was also produced from both enzymes. In addition to this, the controls with only substrate and *Sc*LPMO9A without AscA showed some cellotriose in the sample. It appears that this peak had vanished in the sample with *Sc*LPMO9A and AscA that could indicate that *Sc*LPMO9A had activity on cellotriose as well, but this can not be claimed without testing on cellotetraose alone.

5.8.2 Overnight reactions on cellopentaose

Both enzymes were active on cellopentaose (4.8.2.). As shown in the reaction with only substrate, the cellopentaose substrate contained a small amount of cellotetraose as well as cellopentaose. In the reaction with *Sc*LPMO9A, all cellopentaose and cellotetraose were degraded and native cellotriose and cellobiose were produced, as well as Glc4gemGlc and Glc4gemGlc$_2$.

*Nc*LPMO9C also produced native cellotriose and cellobiose combined with Glc4gemGlc and Glc4gemGlc$_2$, but some of the cellopentaose substrate was not degraded after 24 hours, and nor was the cellotetraose in the substrate.

5.8.3 Overnight reactions on cellohexaose

Both *Sc*LPMO9A and *Nc*LPMO9C produced native cellobiose and cellotriose from cellohexaose (Figure 4.8.3). They also produced Glc4gemGlc and Glc4gemGlc$_2$. The cellohexaose substrate also contained some cellopentaose, that both *Sc*LPMO9A and *Nc*LPMO9C degraded (Figure 4.8.3). Both *Sc*LPMO9A and *Nc*LPMO9C degraded all cellohexaose after 24 hours. In addition to this, *Nc*LPMO9C produced native cellotetraose which was not degraded further.

The figures also show a peak that eluted before cellobiose in all reactions (Figures 4.8.1, 4.8.2 and 4.8.3). Later experiments indicate that glucose could have been produced from the substrates, but this is hard to confirm as the glucose eluted in the injection peak.

5.9 Analysing degrees of polymerization with HPAEC-PAD

In this thesis, primarily native (non-oxidized) products were used for quantification of activity, even though *Sc*LPMO9A and *Nc*LPMO9C also produce C4 oxidized products. Oxidized products were not quantified in most cases, because of the reasons mentioned earlier (Section 3.11). However, it is important to note that to obtain a full understanding of how the LPMOs break down the substrates, all products should be quantified. These products could be analysed by other methods than HPAEC-PAD, for example, porous graphitized carbon (PGC) chromatography (Westereng et al., 2016).

However, C4 oxidized products were quantified after the synergy experiment on VASP. The reason why C4 oxidized products were quantified for the experiment on VASP, was because the celluclast cocktail also generates native cellooligos, which would make quantification separation of LPMO production and celluclast-generated products impossible.

An drawback of only quantifying native products is that it has been observed that HPAEC-PAD analysis can result in generation of native products from C4 oxidized products due to the high pH of the eluent (Kojima et al., 2016). For example, Westereng et al. 2016 experimented that with pure C4 oxidized tetramer, the chromatogram from HPAEC-PAD showed native trimer ass well as C4 oxidized product. To ensure that the native trimer was decomposed C4 tetramer, the fraction with the native trimer was desalted and analysed with PGC, which confirmed that the native trimer was a decomposed C4 tetramer (Westereng et al., 2016).

5.10 *Sc*LPMO9A and *Nc*LPMO9C time course reactions on soluble substrates

5.10.1 Time course reactions on cellopentaose

The production of cellobiose was stabilized after approximately 2 hours for *Nc*LPMO9C on cellopentaose, while product formation with *Sc*LPMO9A increased after 2 hours (Figure 4.9.1.). On the other hand, the reaction rate with *Sc*LPMO9A was significantly slower than with *Nc*LPMO9C. The production of cellobiose was reductant dependent, as products were not formed without reductant for *Sc*LPMO9A. However, in the control with *Nc*LPMO9C without reductant, there was some product formation, as expected since the batch with *Nc*LPMO9C consisted of some endoglucanase.

The total cellotriose production after 4 hours was more than double the production of cellobiose (Figure 4.9.2). This indicate that cellopentaose was mostly degraded to native cellotriose with both *Sc*LPMO9A and *Nc*LPMO9C. However, the same trend between ScLPMO9A and NcLPMO9C (slower reaction rate for *Sc*LPMO9A and stopped reactions after 2 hours with *Nc*LPMO9C) were the same.

Since 1 mM cellopentaose was added to the reaction, 1 mM product would be expected if the substrate was completely degraded. The product concentration of cellobiose + cellotriose with *Nc*LPMO9C after 4 hours was 675 μM (212 μM cellobiose and 463 μM cellotriose) and 213 μM with *Sc*LPMO9A (53 μM cellobiose and 160 μM cellotriose). However, after 24 hours incubation of cellopentaose, there was still some cellopentaose left in reaction with

*Nc*LPMO9C (Figure 4.8.2), therefore, it was not expected to be completely degradation of cellopentaose. *Sc*LPMO9A on the other hand, had broken down all the cellopentaose after 24 hours incubation (Figure 4.8.2), but since the product formation was still increasing after 4 hours, the final production was not shown after 4 hours incubation (Figure 4.9.1 and 4.9.2).

The slower apparent reaction rate of *Sc*LPMO9A versus *Nc*LPMO9C could have several explanations. *Sc*LPMO9A had a lower redox potential than *Nc*LPMO9C, which could shift the equilibrium of oxidation of the reductant by the active site copper. In addition to this, temperature, enzyme concentration, substrate concentration, and reductant concentration could affect reaction rate. The temperature optimum of *Sc*LPMO9A was not tested, neither for stability nor in reactions with substrate. The enzyme concentration could have been underestimated, as Bradford protein assay is not an optimal estimation of enzyme concentration, and this could affect the reaction rate. Lastly, it is possible that another concentration of reductant would be more optimal for *Sc*LPMO9A, and this could have been tested in a similar time course experiment.

However, as observed by Brander et al. (2021), different LPMOs have different redox properties and catalytic properties. For example, *Ta*LPMO9A is reoxidized 10 times faster with oxygen than *Hj*LPMO9A, even though both LPMOs are from the same family (Brander et al., 2021). Therefore, the differences like reaction rate and substrate preferences between *Sc*LPMO9A and *Nc*LPMO9C is not so unusual.

A biological explanation of why *Sc*LPMO9A reacts as slow with oxygen could be that in nature, LPMOs degrading soluble substrates are freer compared to LPMOs that works on insoluble substrates which are more bound to the substrate. Therefore, it would be hazardous to get readily reduced by oxygen, because this could lead to more off-pathway reactions which again could lead to oxidative damage. *Nc*LPMO9C has activity on soluble substrates, however, *Nc*LPMO9C is also active on more crystalline substrates that *Sc*LPMO9A are not active on. Therefore, *Nc*LPMO9C could likely not require as slow reaction rate with oxygen than *Sc*LPMO9A in nature.

Because of the observed slow reaction rate of *Sc*LPMO9A, similar reactions were set, but extended to 24 hours (Figures 4.9.3 and 4.9.4) Here it was observed that, although reactions with *Sc*LPMO9A were significantly slower than with *Nc*LPMO9C, they were also more

stable, resulting in higher final product concentrations. While reactions with *Nc*LPMO9C appeared to stop after 2 hours, reactions with *Sc*LPMO9A were linear until 8 hours.

Interestingly, *Nc*LPMO9C had a faster reaction rate than *Sc*LPMO9C, but stopped before all the substrate was degraded. Since reactions were performed using 1 mM reductant, reductant-depletion was not likely the cause, but rather enzyme inactivation, due to excessive oxidative damage to the enzyme (Petrović et al., 2018). An explanation to why *Sc*LPMO9A broke down more of the substrate was probably that *Sc*LPMO9A was more stable than *Nc*LPMO9C. It is logical that *Sc*LPMO9A have more stability than *Nc*LPMO9C, as *Sc*LPMO9A catalysed the reactions slower, making it more stable over time.

5.10.2 Time course reaction on cellotetraose

*Sc*LPMO9A degraded 672 µM of 1 mM cellotetraose to cellobiose (Figure 4.9.5). The remaining substrate are probably cellotetraose since reactions with *Sc*LPMO9A and AscA had some cellotetraose left after incubation with cellotetraose for 24 hours (Figure S6). Like reactions with cellopentaose, activity with *Sc*LPMO9A stopped after 8 hours.

A glucose standard was added to the sequence, showing that *Sc*LPMO9A may produce glucose from cellotetraose, also shown in Figure S6. Since the peak eluted close to the injection peak and since the DP2-6 standard also showed an elution at the same place, it can not be stated without ambiguity that this is glucose.

5.10.3 Time course reaction on cellohexaose

*Nc*LPMO9C and *Sc*LPMO9A had the same reaction rate from 30 minutes to 2 hours on cellohexaose (4.9.6.). After 2 hours, the reaction with *Nc*LPMO9C stopped, while *Sc*LPMO9A continued to produce cellobiose. For *Sc*LPMO9A, the production was linear up to 8 hours, but still increased from 8 to 24 hours. The control with *Nc*LPMO9C without AscA had almost the same product formation as the sample with AscA. This suggests that *Nc*LPMO9C depolymerize the substrate in the beginning, but after *Nc*LPMO9C got inactivated, endoglucanases continued to degrade the substrate.

The trend for cellotriose formation was like the trend for cellobiose formation, with a small increase in signal compared to cellobiose (Figure 4.9.7). Since the figure was shown in signal instead of concentrations, and different products give different signal intensities, a higher signal of cellotriose does not necessarily mean higher product concentration of cellobiose.

The control with *Nc*LPMO9C without reductant did not show the same product formation, indicating that endoglucanases produced more cellobiose than cellotriose.

Since both *Sc*LPMO9A and *Nc*LPMO9C produced cellotetraose from cellohexaose, cellotetraose production was also monitored (Figure 4.9.8). For *Sc*LPMO9A, the production was linear up to 8 hours, and after 8 hours, the cellotetraose was degraded. *Nc*LPMO9C had produced more cellotetraose after 30 minutes than *Sc*LPMO9A had produced after 8 hours. Since *Sc*LPMO9A are active on cellotetraose, the quantification of production was not accurate, as the cellotetraose was degraded. There was also cellotetraose production in the *Nc*LPMO9C control without reductant. This is obviously not optimal and makes the real LPMO product formation less accurate.

5.10.4 Quantification issues

The reason why the signal was not converted to concentration in some of the figures was because the calculated concentrations were unlikely high. The highest product concentrations were calculated to be more than 1000 µM, which was more than the substrate added (Figures S4 and S5). The problem happened when the reactions were analysed on ISC-6000 instead of ISC-5000.

The most likely explanation would either be that the dilutions was wrong or that the standard concentrations were wrong. The substrate concentration could also have been underestimated. However, when the problem was observed, new standards and substrate were made, and dilutions were double checked, but the problem still occurred.

*Nc*LPMO9C produced approximately 200 µM cellobiose and 500 µM cellotriose after 4 hours on cellopentaose, analysed using ICS-5000 (Figures 4.9.1 and 4.9.2), making the ratio 1:2.5.

Analysing on ICS-6000, *Nc*LPMO9C produces approximately 200 μM cellobiose and 1200 μM cellotriose after 4 hours, making the ratio 1:6 (Figure S4 and S5). Based on this, it seems the products are not affected the same way by the analytical problem, and that cellobiose gave the same signal on ISC-5000 and ISC-6000. On the other hand, this was not the case on cellohexaose, where both cellobiose and cellotriose gave much higher concentrations on ISC-6000 than on ISC-5000.

Since the same problem occurred in several analysis done on ISC-6000, some of the standards and samples analysed using ISC-6000 were also analysed using the ISC-5000 system. This ensured that nothing was wrong with the samples or the standard, as the quantifications from that ICS-5000 gave more likely concentrations. On the other hand, this showed that it was clearly something wrong with the quantification on the ISC-6000.

An explanation could be that the standards were diluted in water while the samples consisted of NaOH and buffer. Since ICS-6000 required higher dilutions of samples than ICS-5000, differences between standards and samples were higher at the ICS-6000 system. Standards diluted in buffer were analysed using both ISC-5000 and ISC-6000 and gave the same signal intensities as buffers diluted in water. If NaOH was the culprit, this is peculiar as the samples analysed using ISC-6000 had a lower concentration of NaOH in the samples, as they are diluted more. On the other hand, the ISC-5000 eluents consist of NaOH, and this could be an explanation of why ISC-5000 was not affected.

The signals from ICS-6000 should represent the correct product formation and trend, even though concentrations were not calculated. The downfall with using signal instead of concentrations is that the signal can not be compared between different products, as cellobiose and cellotriose have different intensities. Therefore, this is not optimal and should be investigated further.

5.11 Activity of *Sc*LPMO9A and *Nc*LPMO9C in the presence of exogenous H_2O_2

5.11.1 Time course with 1 mM AscA

Both *Sc*LPMO9A and *Nc*LPMO9C produced native cellobiose and cellotriose faster when H_2O_2 was added to the reactions (Figures 4.10.1 and 4.10.2). These results were as expected, since LPMOs can use H_2O_2 as a co-substrate and since Bissaro et al. (2017) showed in 2017 that reoxidation of LPMO-Cu(I) is 2-fold faster with H_2O_2 than with O_2.

It is also suggested that, in the reactions with no added H_2O_2, that the only H_2O_2 available to the enzyme is what is being produced either *in situ* by the LPMO or via auto-oxidation of the reductant (Bissaro, Streit, et al., 2020). Even though the LPMOs likely do not produce H_2O_2 when bound to a substrate, Stepnov et al. (2021) revealed that small amounts of free copper in the enzyme batches generate significant amount of H_2O_2.

In addition, Brander et al. show in their article from 2021 that *Ls*LPMO9A, which is the closest homolog to *Sc*LPMO9A, is dependent on H_2O_2 to catalyse reactions. Which makes sense as results from the Amplex Red Hydrogen Peroxide assay indicated that *Sc*LPMO9A produced H_2O_2 slower than *Nc*LPMO9C which again would give a slower reaction rate without added H_2O_2.

In addition to reacting faster with H_2O_2, the reactions also stopped fasted. It appears that *Sc*LPMO9A reactions stopped before 3 minutes with all concentrations of H_2O_2 tested. The reason for why the reactions stopped can be that all H_2O_2 or AscA was used or that the enzymes got inactivated. *Nc*LPMO9C, on the other hand, had a slight increase in product formation between 3 minutes and 1 hour, but most of the product was formed before 3 minutes. This increase in product formation could also be because of endoglucanases. However, based on these observations, *Sc*LPMO9A seems less stable than *Nc*LPMO9C when H_2O_2 was added.

When adding H_2O_2 to the reactions with 1 mM AscA, *Sc*LPMO9A had a higher product yield of cellobiose than *Nc*LPMO9C with 100 and 250 µM added H_2O_2.

*Nc*LPMO9C had approximately 3.5 times more product formation of cellobiose after 1 hour than *Sc*LPMO9A, when it was not added H_2O_2 (Figure 4.10.1). This was expected, since *Sc*LPMO9A had shown a slower reaction rate than *Nc*LPMO9C on cellopentaose without

H_2O_2. When it was added 50 µM H_2O_2 to the reactions, *Nc*LPMO9C had only approximately 1.25 more product than *Sc*LPMO9A. Furthermore, when 100 and 250 µM H_2O_2 was added to the reaction, the final product yield of cellobiose was higher with *Sc*LPMO9A than with *Nc*LPMO9C, and the differences was most distinct when 250 µM was added.

On the other hand, it seemed that *Nc*LPMO9C had the highest final production (after 1 hour) of cellotriose in all reactions (Figure 4.10.2). However, *Sc*LPMO9A had produced more cellotriose than NcLPMO9C before 3 minutes with 50, 100 and 250 µM H_2O_2, and since the increase in product after 3 minutes are not known to be significant or if the products are from endoglucanases, it could not be claimed that the final cellotriose product from *Nc*LPMO9C were higher than *Sc*LPMO9A.

The chromatogram from the added H_2O_2 experiment is shown in Figure S8. In the chromatogram, C4 oxidized products was shown in addition to native cellobiose and cellotriose.

5.11.2 Time course with 50 µM AscA

Since it was impossible to say anything about the reaction rate of *Sc*LPMO9A with added H_2O_2 and 1 mM AscA, as the reactions stopped before 3 minutes, the similar reaction was performed, but with only 50 µM AscA. The goal was to decrease the reductant concentration enough to get a slower reaction rate, to see whether any true rates could be observed. However, the reaction rate was still not possible to determine, as the reactions stopped before 3 minutes here as well. In addition to decreasing the reductant concentration, a lower H_2O_2 concentration (25 µM) was also included, but the reactions still stopped before 3 minutes.

Despite this, the results did show significant differences in product yield with different H_2O_2 concentrations.

When adding H_2O_2 to a reaction, the product concentration is not expected to be higher than the amount of H_2O_2 plus the amount of reductant. Here, the concentration was higher. The most likely explanation of this is that the wrong concentration of H_2O_2 was added to the reactions. This could either be a mistake done when diluting H_2O_2 or when adding the H_2O_2 to

the samples. The same samples were analysed using both ISC-5000 and ISC-6000, giving the same concentrations, so the high concentration was probably not an analytical problem as seen earlier.

As the LPMOs reactions stopped before 3 minutes with both concentrations of AscA, a dosing experiment with H_2O_2 could have been done, by adding small injections of H_2O_2 over the incubation time. This would probably not only slow the reaction rate, but also lead to higher production yield, as the enzymes would have been more stable over time and would probably be able to handle higher concentrations of H_2O_2.

5.12 Synergy experiment

The reaction with *Sc*LPMO9A together with celluclast and BG did not give a higher concentration of glucose and cellobiose than in the reaction with only celluclast and BG (Figure 4.11.1 and 4.11.2). As sulphite pulped spruce has an expected crystalline form almost as high as Avicel (Aldaeus et al., 2015), and since substrate screening showed that *Sc*LPMO9A was not active on Avicel (Figure 4.1.5), this gives an indication that *Sc*LPMO9A is not a suitable candidate for degradation of crystalline substrates.

Even though there was not shown a boost in activity when *Sc*LPMO9A was added to the cocktail, HPAEC-PAD using a Dionex ISC-5000 system reveals that there was C4 oxidized products in the reaction, confirming that *Sc*LPMO9A had degraded some of the substrate. Since *Sc*LPMO9A was active on the substrate, the degradation with *Sc*LPMO9A could probably have been boosted by using different concentrations of reductant or by adding H_2O_2. As previously shown in this thesis, *Sc*LPMO9A had a faster reaction rate when H_2O_2 was added to reactions, so it would be logical that H_2O_2 could boost the reaction rate in the synergy experiment as well.

However, since *Sc*LPMO9A was more active on less crystalline substrates, more amorphous substrates should have been tested to find a more suitable substrate for *Sc*LPMO9A.

6. Conclusion

Based on the results shown in this thesis, it is not possible to conclude if *Sc*LPMO9A is a suitable candidate for cellulase cocktails or not. To obtain a better understanding of this, *Sc*LPMO9A should have been tested on different substrates in the synergy experiment and with different conditions, such as with H_2O_2 and different concentrations of reductant.

On the other hand, the results do show that *Sc*LPMO9A is active on several substrates as cellulose, soluble cello-oligosaccharides, and various hemicelluloses. Results also indicate that *Sc*LPMO9A has less activity on insoluble substrates than *Nc*LPMO9C. Other differences shown between *Sc*LPMO9A and *Nc*LPMO9C are for example that on cellopentaose, *Sc*LPMO9A is more stable than *Nc*LPMO9C, as it gets inactivated slower and gives a higher product yield under conditions without exogeneous added H_2O_2. In addition to this, *Sc*LPMO9A also degrades cellotetraose more efficient than *Nc*LPMO9C without exogeneous added H_2O_2.

Experiments on cellopentaose with both high (1 mM) and low (50 μM) AscA concentrations show that by adding H_2O_2 to the reaction, the reaction occur faster than reactions without added H_2O_2. The experiments show that H_2O_2 has a vast effect on the reaction rate of both *Sc*LPMO9A and *Nc*LPMO9C. On the other hand, the *Sc*LPMO9A reactions stops with added H_2O_2 before the substrate is completely degraded, giving a lower product yield. *Sc*LPMO9A seems to be more sensitive to H_2O_2 than *Nc*LPMO9C as the reactions with *Sc*LPMO9A stops before 3 minutes with all concentrations of added H_2O_2. A solution could have been to add H_2O_2 in small doses instead of adding the full concentration at the beginning of the experiment. This was not tested, but it would make sense that the final product yield would probably have been higher by adding H_2O_2 dosed.

The question of why wood rot fungi have LPMOs that works on soluble substrates stays unanswered. Therefore, more research on *Sc*LPMO9A or other LPMOs working on soluble substrates can give insights into how fungi and wood-degradation work in nature.
An interesting experiment for future work would be to do a stop flow or fluorometric experiment to observe how fast or slow *Sc*LPMO9A deoxidises. As several experiments have shown in this thesis, *Sc*LPMO9A reacts slowly without adding H_2O_2 to the reactions,

therefore it is expected that the enzyme also reoxidized slowly. This could give more insight into the biological role of *Sc*LPMO9A and why it reacts as it does.

7. References

Aldaeus, F., Larsson, K., Srndovic, J. S., Kubat, M., Karlström, K., Peciulyte, A., Olsson, L., & Larsson, P. T. (2015). The supramolecular structure of cellulose-rich wood pulps can be a determinative factor for enzymatic hydrolysability. *Cellulose (London)*, *22*(6), 3991-4002. https://doi.org/10.1007/s10570-015-0766-0

Almagro Armenteros, J. J., Tsirigos, K. D., Sønderby, C. K., Petersen, T. N., Winther, O., Brunak, S., von Heijne, G., & Nielsen, H. (2019). SignalP 5.0 improves signal peptide predictions using deep neural networks. *Nat Biotechnol*, *37*(4), 420-423. https://doi.org/10.1038/s41587-019-0036-z

Armougom, F., Moretti, S. b., Poirot, O., Audic, S. p., Dumas, P., Schaeli, B., Keduas, V., & Notredame, C. (2006). Expresso: automatic incorporation of structural information in multiple sequence alignments using 3D-Coffee. *Nucl. Acids Res*, *34*(suppl-2), W604-W608. https://doi.org/10.1093/nar/gkl092

Barikani, M., Oliaei, E., Seddiqi, H., & Honarkar, H. (2014). Preparation and application of chitin and its derivatives: a review. *Iranian polymer journal*, *23*(4), 307-326. https://doi.org/10.1007/s13726-014-0225-z

Benko, Z., & Zhao, R. Y. (2011). Zeocin for selection of bleMX6 resistance in fission yeast. *Biotechniques*, *51*(1), 57-60. https://doi.org/10.2144/000113706

Bissaro, B., Kommedal, E., Røhr, Å. K., & Eijsink, V. G. H. (2020). Controlled depolymerization of cellulose by light-driven lytic polysaccharide oxygenases. *Nat Commun*, *11*(1), 890-812. https://doi.org/10.1038/s41467-020-14744-9

Bissaro, B., Streit, B., Isaksen, I., Eijsink, V. G. H., Beckham, G. T., DuBois, J. L., & Røhr, Å. K. (2020). Molecular mechanism of the chitinolytic peroxygenase reaction. *Proc Natl Acad Sci U S A*, *117*(3), 1504-1513. https://doi.org/10.1073/pnas.1904889117 (PNAS Plus)

Borisova, A. S., Isaksen, T., Dimarogona, M., Kognole, A. A., Mathiesen, G., Várnai, A., Røhr, Å. K., Payne, C. M., Sørlie, M., Sandgren, M., & Eijsink, V. G. H. (2015). Structural and Functional Characterization of a Lytic Polysaccharide Monooxygenase with Broad Substrate Specificity. *J Biol Chem*, *290*(38), 22955-22969. https://doi.org/10.1074/jbc.M115.660183

Brander, S., Tokin, R., Ipsen, J. Ø., Jensen, P. E., Hernández-Rollán, C., Nørholm, M. H. H., Lo Leggio, L., Dupree, P., & Johansen, K. S. (2021). Scission of Glucosidic Bonds by a Lentinus similis Lytic Polysaccharide Monooxygenases Is Strictly Dependent on H2O2 while the Oxidation of Saccharide Products Depends on O2. *ACS Catal*, *11*(22), 13848-13859. https://doi.org/10.1021/acscatal.1c04248

Breslmayr, E., Hanžek, M., Hanrahan, A., Leitner, C., Kittl, R., Šantek, B., Oostenbrink, C., & Ludwig, R. (2018). A fast and sensitive activity assay for lytic polysaccharide monooxygenase. *Biotechnol Biofuels*, *11*(1), 79-79. https://doi.org/10.1186/s13068-018-1063-6

Brodin, M., Vallejos, M., Opedal, M. T., Area, M. C., & Chinga-Carrasco, G. (2017). Lignocellulosics as sustainable resources for production of bioplastics – A review. *Journal of cleaner production*, *162*, 646-664. https://doi.org/10.1016/j.jclepro.2017.05.209

Cantarel, B. L., Coutinho, P. M., Rancurel, C., Bernard, T., Lombard, V., & Henrissat, B. (2009). The Carbohydrate-Active EnZymes database (CAZy): an expert resource for Glycogenomics. *Nucleic Acids Res*, *37*(suppl-1), D233-D238. https://doi.org/10.1093/nar/gkn663

Chandra, R. P., Chu, Q., Hu, J., Zhong, N., Lin, M., Lee, J.-S., & Saddler, J. (2016). The influence of lignin on steam pretreatment and mechanical pulping of poplar to achieve high sugar recovery and ease of enzymatic hydrolysis. *Bioresour Technol*, *199*, 135-141. https://doi.org/10.1016/j.biortech.2015.09.019

Chen, K., Zhang, X., Long, L., & Ding, S. (2021). Comparison of C4-oxidizing and C1/C4-oxidizing AA9 LPMOs in substrate adsorption, H2O2-driven activity and synergy with cellulase on celluloses of different crystallinity. *Carbohydrate polymers*, *269*, 118305-118305. https://doi.org/10.1016/j.carbpol.2021.118305

Chylenski, P., Bissaro, B., Sørlie, M., Røhr, Å. K., Várnai, A., Horn, S. J., & Eijsink, V. G. H. (2019). Lytic Polysaccharide Monooxygenases in Enzymatic Processing of Lignocellulosic Biomass. *ACS Catal*, *9*(6), 4970-4991. https://doi.org/10.1021/acscatal.9b00246

Cleaves, H. J. (2011). Isoelectric Point. In M. Gargaud, R. Amils, J. C. Quintanilla, H. J. Cleaves, W. M. Irvine, D. L. Pinti, & M. Viso (Eds.), *Encyclopedia of Astrobiology* (pp. 858-858). Springer Berlin Heidelberg. https://doi.org/10.1007/978-3-642-11274-4_819

Cocinero, E. J., & Çarçabal, P. (2015). Carbohydrates. *Top Curr Chem*, *364*, 299-333. https://doi.org/10.1007/128_2014_596 (Topics in Current Chemistry)

Corradini, C., Cavazza, A., & Bignardi, C. (2012). High-Performance Anion-Exchange Chromatography Coupled with Pulsed Electrochemical Detection as a Powerful Tool to Evaluate Carbohydrates of Food Interest: Principles and Applications. *International Journal of Carbohydrate Chemistry*, *2012*, 487564. https://doi.org/10.1155/2012/487564

Courtade, G., Forsberg, Z., Heggset, E. B., Eijsink, V. G. H., & Aachmann, F. L. (2018). The carbohydrate-binding module and linker of a modular lytic polysaccharide monooxygenase promote localized cellulose oxidation. *J Biol Chem*, *293*(34), 13006-13015. https://doi.org/10.1074/jbc.RA118.004269

Courtade, G., Le, S. B., Sætrom, G. I., Brautaset, T., & Aachmann, F. L. (2017). A novel expression system for lytic polysaccharide monooxygenases. *Carbohydr Res*, *448*, 212-219. https://doi.org/10.1016/j.carres.2017.02.003

Darriba, D., Taboada, G. L., Doallo, R., & Posada, D. ProtTest-HPC: Fast Selection of Best-Fit Models of Protein Evolution. In (pp. 177-184). Berlin, Heidelberg: Springer Berlin Heidelberg. https://doi.org/10.1007/978-3-642-21878-1_22

Dimarogona, M., & Sandgren, M. (2016). Backbone and side-chain H-1, C-13, and (15) N chemical shift assignments for the apo-form of the lytic polysaccharide monooxygenase NcLPMO9C. *Biomolecular NMR Assignments*, *10*, 277. https://doi.org/10.1007/s12104-016-9683-x

Drula, E., Garron, M.-L., Dogan, S., Lombard, V., Henrissat, B., & Terrapon, N. (2022). The carbohydrate-active enzyme database: functions and literature. *Nucleic Acids Res*, *50*(D1), D571-D577. https://doi.org/10.1093/nar/gkab1045

Ernst, O., & Zor, T. (2010). Linearization of the bradford protein assay. *J Vis Exp*(38). https://doi.org/10.3791/1918

Forsberg, Z., Sørlie, M., Petrović, D., Courtade, G., Aachmann, F. L., Vaaje-Kolstad, G., Bissaro, B., Røhr, Å. K., & Eijsink, V. G. H. (2019). Polysaccharide degradation by lytic polysaccharide monooxygenases. *Curr Opin Struct Biol*, *59*, 54-64. https://doi.org/10.1016/j.sbi.2019.02.015

Forsberg, Z. K. (2014). Discovery and characterization of cellulose-active lytic polysaccharide monooxygenases. In: Norwegian University of Life Sciences, Ås.

Frandsen, K. E. H., Haon, M., Grisel, S., Henrissat, B., Lo Leggio, L., & Berrin, J.-G. (2021). Identification of the molecular determinants driving the substrate specificity of fungal lytic polysaccharide monooxygenases (LPMOs). *J Biol Chem*, *296*, 100086-100086. https://doi.org/10.1074/jbc.RA120.015545

Frandsen, K. E. H., Simmons, T. J., Dupree, P., Poulsen, J.-C. N., Hemsworth, G. R., Ciano, L., Johnston, E. M., Tovborg, M., Johansen, K. S., von Freiesleben, P., Marmuse, L., Fort, S., Cottaz, S., Driguez, H., Henrissat, B., Lenfant, N., Tuna, F., Baldansuren, A., Davies, G. J., . . . Walton, P. H. (2016). The molecular basis of polysaccharide cleavage by lytic polysaccharide monooxygenases. https://doi.org/10.1038/nchembio.2029

Frommhagen, M., Westphal, A. H., Berkel, v. W. J. H., & Kabel, M. A. (2018). Distinct substrate specificities and electron-donating systems of fungal lytic polysaccharide monooxygenases. *Front Microbiol*, *9*, 1080-1080. https://doi.org/10.3389/fmicb.2018.01080

Gasser, B., Prielhofer, R., Marx, H., Maurer, M., Nocon, J., Steiger, M., Puxbaum, V., Sauer, M., & Mattanovich, D. (2013). Pichia pastoris: protein production host and model organism for biomedical research. *Future Microbiol*, *8*(2), 191-208. https://doi.org/10.2217/fmb.12.133

Gasteiger, E., Gattiker, A., Hoogland, C., Ivanyi, I., Appel, R. D., & Bairoch, A. (2003). ExPASy: the proteomics server for in-depth protein knowledge and analysis. *Nucl. Acids Res*, *31*(13), 3784-3788. https://doi.org/10.1093/nar/gkg563

Gupta, R., & Brunak, S. (2002). Prediction of glycosylation across the human proteome and the correlation to protein function. *Pac Symp Biocomput*, 310-322.

Hamre, A. G., Frøberg, E. E., Eijsink, V. G. H., & Sørlie, M. (2017). Thermodynamics of tunnel formation upon substrate binding in a processive glycoside hydrolase. *Arch Biochem Biophys*, *620*, 35-42. https://doi.org/10.1016/j.abb.2017.03.011

Hangasky, J. A., Iavarone, A. T., & Marletta, M. A. (2018). Reactivity of O_2 versus H_2O_2 with polysaccharide monooxygenases. *Proceedings of the National Academy of Sciences - PNAS*, *115*(19), 4915-4920. https://doi.org/10.1073/pnas.1801153115

Hemsworth, G. R., Henrissat, B., Davies, G. J., & Walton, P. H. (2014). Discovery and characterization of a new family of lytic polysaccharide monooxygenases. https://doi.org/10.1038/nchembio.1417

Horn, S. J., Vaaje-Kolstad, G., Westereng, B., & Eijsink, V. G. (2012). Novel enzymes for the degradation of cellulose. *Biotechnol Biofuels*, *5*(1), 45-45. https://doi.org/10.1186/1754-6834-5-45

IPCC. (2021). Climate Change 2021: The Physical Science Basis [Report]. *IPCC*. https://www.ipcc.ch/report/ar6/wg1/downloads/report/IPCC_AR6_WGI_Full_Report.pdf

Isaksen, T., Westereng, B., Aachmann, F. L., Agger, J. W., Kracher, D., Kittl, R., Ludwig, R., Haltrich, D., Eijsink, V. G. H., & Horn, S. J. (2014). A C4-oxidizing Lytic Polysaccharide Monooxygenase Cleaving Both Cellulose and Cello-oligosaccharides. *J Biol Chem*, *289*(5), 2632-2642. https://doi.org/10.1074/jbc.M113.530196

Karkehabadi, S., Hansson, H., Kim, S., Piens, K., Mitchinson, C., & Sandgren, M. (2008). The First Structure of a Glycoside Hydrolase Family 61 Member, Cel61B from Hypocrea jecorina, at 1.6 Å Resolution. *J Mol Biol*, *383*(1), 144-154. https://doi.org/10.1016/j.jmb.2008.08.016

Kielkopf, C. L., Bauer, W., & Urbatsch, I. L. (2021). Sodium Dodecyl Sulfate-Polyacrylamide Gel Electrophoresis of Proteins. *Cold Spring Harb Protoc*, *2021*(12). https://doi.org/10.1101/pdb.prot102228

Kittl, R., Kracher, D., Burgstaller, D., Haltrich, D., & Ludwig, R. (2012). Production of four Neurospora crassa lytic polysaccharide monooxygenases in Pichia pastoris monitored by a fluorimetric assay. *Biotechnol Biofuels*, *5*(1), 79-79. https://doi.org/10.1186/1754-6834-5-79

Kojima, Y., Varnai, A., Ishida, T., Sunagawa, N., Petrovic, D., Igarashi, K., Jellison, J., Goodell, B., Alfredsen, G., Westereng, B., Eijsink, V., & Yoshida, M. (2016). Characterization of an LPMO from brown-rot fungus Gloeophyllum trabeum with broad xyloglucan specificity and its action on cellulose-xyloglucan complexes. https://doi.org/https://doi.org/10.1128/AEM.01768-16

Kostanski, L. K., Keller, D. M., & Hamielec, A. E. (2004). Size-exclusion chromatography—a review of calibration methodologies. *J Biochem Biophys Methods*, *58*(2), 159-186. https://doi.org/10.1016/j.jbbm.2003.10.001

Kües, U., Schmutz, J., Ohm, R. A., Lilly, W. W., vanKuyk, P. A., Lucas, S., Raudaskoski, M., Kothe, E., Record, E., Stajich, J. E., Horton, J. S., Lindquist, E., Henrissat, B., Coutinho, P. M., Knabe, N., Gathman, A. C., Aerts, A., Lugones, L. G., Schwarze, F. W. M. R., . . . Fowler, T. J. (2010). Genome sequence of the model mushroom Schizophyllum commune. *Nat Biotechnol*, *28*(9), 957-963. https://doi.org/10.1038/nbt.1643

Larsson, A. (2014). AliView: a fast and lightweight alignment viewer and editor for large data sets. https://doi.org/10.1093/bioinformatics/btu531

Letunic, I., & Bork, P. (2021). Interactive Tree Of Life (iTOL) v5: an online tool for phylogenetic tree display and annotation. *Nucleic Acids Res*, *49*(W1), W293-W296. https://doi.org/10.1093/nar/gkab301

Lombard, V., Golaconda Ramulu, H., Drula, E., Coutinho, P. M., & Henrissat, B. (2014). The carbohydrate-active enzymes database (CAZy) in 2013. *Nucleic Acids Res*, *42*(Database issue), D490-D495. https://doi.org/10.1093/nar/gkt1178

Lund, H. (2007). Renewable energy strategies for sustainable development. *Energy (Oxford)*, *32*(6), 912-919. https://doi.org/10.1016/j.energy.2006.10.017

Madeira, F., Pearce, M., Tivey, A. R. N., Basutkar, P., Lee, J., Edbali, O., Madhusoodanan, N., Kolesnikov, A., & Lopez, R. (2022). Search and sequence analysis tools services from EMBL-EBI in 2022. *Nucleic Acids Res*. https://doi.org/10.1093/nar/gkac240

Mankar, A. R., Pandey, A., Modak, A., & Pant, K. K. (2021). Pretreatment of lignocellulosic biomass: A review on recent advances. *Bioresour Technol*, *334*, 125235-125235. https://doi.org/10.1016/j.biortech.2021.125235

Mechelke, M., Herlet, J., Benz, J. P., Schwarz, W. H., Zverlov, V. V., Liebl, W., & Kornberger, P. (2017). HPAEC-PAD for oligosaccharide analysis—novel insights into analyte sensitivity and response stability. *Anal Bioanal Chem*, *409*(30), 7169-7181. https://doi.org/10.1007/s00216-017-0678-y

Mistry, J., Chuguransky, S., Williams, L., Qureshi, M., Salazar, Gustavo A., Sonnhammer, E. L. L., Tosatto, S. C. E., Paladin, L., Raj, S., Richardson, L. J., Finn, R. D., & Bateman, A. (2021). Pfam: The protein families database in 2021. *Nucleic Acids Res*, *49*(D1), D412-D419. https://doi.org/10.1093/nar/gkaa913

Mohammed, N. B., Ahmed, M. A. H., Roop, S. B., Mohamed, M. M. A., Hassan, A. I. R., Kulvinder, S. S., Nabih, A. B., & Elrashdy, M. R. (2015). Review : Production of Biopharmaceuticals in E. coli: Current Scenario and Future Perspectives. *Journal of Microbiology and Biotechnology*, *25*(7), 953.

Oregon-State, U. III. Carbohydrates, Structures and Types. *Oregeon State University* https://open.oregonstate.education/animalnutrition/chapter/chapter-3/

Petrović, D. M., Bissaro, B., Chylenski, P., Skaugen, M., Sørlie, M., Jensen, M. S., Aachmann, F. L., Courtade, G., Várnai, A., & Eijsink, V. G. H. (2018). Methylation of the N-terminal histidine protects a lytic polysaccharide monooxygenase from auto-oxidative inactivation. *Protein Sci*, *27*(9), 1636-1650. https://doi.org/10.1002/pro.3451

Petrović, D. M., Várnai, A., Dimarogona, M., Mathiesen, G., Sandgren, M., Westereng, B., & Eijsink, V. G. H. (2019). Comparison of three seemingly similar lytic polysaccharide monooxygenases from Neurospora crassa suggests different roles in plant biomass degradation. *J Biol Chem*, *294*(41), 15068-15081. https://doi.org/10.1074/jbc.RA119.008196

Quinlan, R. J., Sweeney, M. D., Lo Leggio, L., Otten, H., Poulsen, J.-C. N., Johansen, K. S., Krogh, K. B. R. M., Jørgensen, C. I., Tovborg, M., Anthonsen, A., Tryfona, T., Walter, C. P., Dupree, P., Xu, F., Davies, G. J., & Walton, P. H. (2011). Insights into the oxidative degradation of cellulose by a copper metalloenzyme that exploits biomass components. *Proc Natl Acad Sci U S A*, *108*(37), 15079-15084. https://doi.org/10.1073/pnas.1105776108

Rafailidis, P. I., Ioannidou, E. N., & Falagas, M. E. (2007). Ampicillin/Sulbactam: Current Status in Severe Bacterial Infections. *Drugs*, *67*(13), 1829-1849. https://doi.org/10.2165/00003495-200767130-00003

Rieder, L., Stepnov, A. A., Sørlie, M., & Eijsink, V. G. H. (2021). Fast and Specific Peroxygenase Reactions Catalyzed by Fungal Mono-Copper Enzymes. *Biochemistry*, *60*(47), 3633-3643. https://doi.org/10.1021/acs.biochem.1c00407

Rodrigues, K. B., Macêdo, J. K. A., Teixeira, T., Barros, J. S., Araújo, A. C. B., Santos, F. P., Quirino, B. F., Brasil, B. S. A. F., Salum, T. F. C., Abdelnur, P. V., & Fávaro, L. C. L. (2017). Recombinant expression of Thermobifida fusca E7 LPMO in Pichia pastoris and Escherichia coli and their functional characterization. *Carbohydr Res*, *448*, 175-181. https://doi.org/10.1016/j.carres.2017.04.008

Sabbadin, F., Urresti, S., Henrissat, B., Avrova, A. O., Welsh, L. R. J., Lindley, P. J., Csukai, M., Squires, J. N., Walton, P. H., Davies, G. J., Bruce, N. C., Whisson, S. C., & McQueen-Mason, S. J. (2021). Secreted pectin monooxygenases drive plant infection by pathogenic oomycetes. *Science (American Association for the Advancement of Science)*, *373*(6556), 774-779. https://doi.org/10.1126/science.abj1342

Sanchez, C. (2009). Lignocellulosic residues: Biodegradation and bioconversion by fungi. *Biotechnol Adv*, *27*(2), 185-194. https://doi.org/10.1016/j.biotechadv.2008.11.001

Scheller, H. V., & Ulvskov, P. (2010). Hemicelluloses. *Annu Rev Plant Biol*, *61*(1), 263-289. https://doi.org/10.1146/annurev-arplant-042809-112315

Si-Quiang Ye, Y. Z., Qian-Wang Zheng, Ying-Li Liu, Roi-Rong Li, Jun-Fang Lin, Li-Qiong Guo. (2020). TMT-MS/MS proteomic analysis of the carbohydrate-active enzymes in the fruiting body of Pleurotus tuoliensis during storage [TMT-MS/MS proteomic analysis of the carbohydrate-active enzymes in the fruiting body of Pleurotus tuoliensis during storage]

[Research Article]. *Journal of Science of Food and Agriculture*, *101*(5), 1879-1891. https://doi.org/https://doi.org/10.1002/jsfa.10803

Simmons, T. J., Frandsen, K. E. H., Ciano, L., Tryfona, T., Lenfant, N., Poulsen, J. C., Wilson, L. F. L., Tandrup, T., Tovborg, M., Schnorr, K., Johansen, K. S., Henrissat, B., Walton, P. H., Lo Leggio, L., & Dupree, P. (2017). Structural and electronic determinants of lytic polysaccharide monooxygenase reactivity on polysaccharide substrates. *Nat Commun*, *8*(1), 1064-1064. https://doi.org/10.1038/s41467-017-01247-3

Stalbrand, H., Mansfield, S. D., Saddler, J. N., Kilburn, D. G., Warren, R. A. J., & Gilkes, N. R. (1998). Analysis of Molecular Size Distributions of Cellulose Molecules during Hydrolysis of Cellulose by Recombinant Cellulomonas fimiβ-1,4-Glucanases. *Appl Environ Microbiol*, *64*(7), 2374-2379. https://doi.org/10.1128/AEM.64.7.2374-2379.1998

Stepnov, A. A., Forsberg, Z., Sørlie, M., Nguyen, G.-S., Wentzel, A., Røhr, Å. K., & Eijsink, V. G. H. (2021). Unraveling the roles of the reductant and free copper ions in LPMO kinetics. *Biotechnol Biofuels*, *14*(1), 28-28. https://doi.org/10.1186/s13068-021-01879-0

Tokin, R., Ipsen, J. Ø., Westh, P., & Johansen, K. S. (2020). The synergy between LPMOs and cellulases in enzymatic saccharification of cellulose is both enzyme- and substrate-dependent. *Biotechnol Lett*, *42*(10), 1975-1984. https://doi.org/10.1007/s10529-020-02922-0

Tovar-Herrera, O. E., Martha-Paz, A. M., Pérez-Llano, Y., Aranda, E., Tacoronte-Morales, J. E., Pedroso-Cabrera, M. T., Arévalo-Niño, K., Folch-Mallol, J. L., & Batista-García, R. A. (2018). Schizophyllum commune: An unexploited source for lignocellulose degrading enzymes. *Microbiologyopen*, *7*(3), e00637-n/a. https://doi.org/10.1002/mbo3.637

Tuveng, T. R., Jensen, M. S., Fredriksen, L., Vaaje-Kolstad, G., Eijsink, V. G. H., & Forsberg, Z. (2020). A thermostable bacterial lytic polysaccharide monooxygenase with high operational stability in a wide temperature range. *Biotechnology for biofuels*, *13*(1), 194-194. https://doi.org/10.1186/s13068-020-01834-5

Van Dyk, J. S., & Pletschke, B. I. (2012). A review of lignocellulose bioconversion using enzymatic hydrolysis and synergistic cooperation between enzymes—Factors affecting enzymes, conversion and synergy. *Biotechnol Adv*, *30*(6), 1458-1480. https://doi.org/10.1016/j.biotechadv.2012.03.002

Villares, A., Moreau, C., Bennati-Granier, C., Garajova, S., Foucat, L., Falourd, X., Saake, B., Berrin, J.-G., & Cathala, B. (2017). Lytic polysaccharide monooxygenases disrupt the cellulose fibers structure. *Sci Rep*, *7*(1), 40262-40262. https://doi.org/10.1038/srep40262

Vivien, F. D., Nieddu, M., Befort, N., Debref, R., & Giampietro, M. (2019). The Hijacking of the Bioeconomy. *Ecological economics*, *159*, 189-197. https://doi.org/10.1016/j.ecolecon.2019.01.027

Vaaje-Kolstad, G., Forsberg, Z., Loose, J. S. M., Bissaro, B., & Eijsink, V. G. H. (2017). Structural diversity of lytic polysaccharide monooxygenases. *Curr Opin Struct Biol*, *44*, 67-76. https://doi.org/10.1016/j.sbi.2016.12.012

Vaaje-Kolstad, G., Horn, S. J., van Aalten, D. M. F., Synstad, B., & Eijsink, V. G. H. (2005). The Non-catalytic Chitin-binding Protein CBP21 from Serratia marcescens Is Essential for Chitin Degradation. *J Biol Chem*, *280*(31), 28492-28497. https://doi.org/10.1074/jbc.M504468200

Waterhouse, A., Bertoni, M., Bienert, S., Studer, G., Tauriello, G., Gumienny, R., Heer, F. T., de Beer, T. A P., Rempfer, C., Bordoli, L., Lepore, R., & Schwede, T. (2018). SWISS-MODEL: homology modelling of protein structures and complexes. *Nucleic Acids Res*, *46*(W1), W296-W303. https://doi.org/10.1093/nar/gky427

Westereng, B., Arntzen, M. Ø., Aachmann, F. L., Várnai, A., Eijsink, V. G. H., & Agger, J. W. (2016). Simultaneous analysis of C1 and C4 oxidized oligosaccharides, the products of lytic polysaccharide monooxygenases acting on cellulose. *Journal of Chromatography A*, *1445*, 46-54. https://doi.org/10.1016/j.chroma.2016.03.064

Westereng, B., Loose, J. S. M., Vaaje-Kolstad, G., Aachmann, F. L., Sørlie, M., & Eijsink, V. (2018). Analytical Tools for Characterizing Cellulose-Active Lytic Polysaccharide Monooxygenases (LPMOs).

Wood, T. M. (1988). Preparation of crystalline, amorphous, and dyed cellulase substrates. In *Methods in Enzymology* (Vol. 160, pp. 19-25). Academic Press. https://doi.org/https://doi.org/10.1016/0076-6879(88)60103-0

Zhou, X., Qi, X., Huang, H., & Zhu, H. (2019). Sequence and Structural Analysis of AA9 and AA10 LPMOs: An Insight into the Basis of Substrate Specificity and Regioselectivity. *Int J Mol Sci*, *20*(18), 4594. https://doi.org/10.3390/ijms20184594

Zhou, X., & Zhu, H. (2020). Current understanding of substrate specificity and regioselectivity of LPMOs. *Bioresources and bioprocessing*, *7*(1), 1-19. https://doi.org/10.1186/s40643-020-0300-6

Zoghlami, A., & Paës, G. (2019). Lignocellulosic Biomass: Understanding Recalcitrance and Predicting Hydrolysis. *Front Chem*, *7*, 874-874. https://doi.org/10.3389/fchem.2019.00874

Østby, H., Hansen, L. D., Horn, S. J., Eijsink, V. G. H., & Várnai, A. (2020). Enzymatic processing of lignocellulosic biomass: principles, recent advances and perspectives. *J Ind Microbiol Biotechnol*, *47*(9-10), 623-657. https://doi.org/10.1007/s10295-020-02301-8

Supplementary

Appendix 1

Figure S1 shows a Phylogenetic tree with 46 LPMO9.

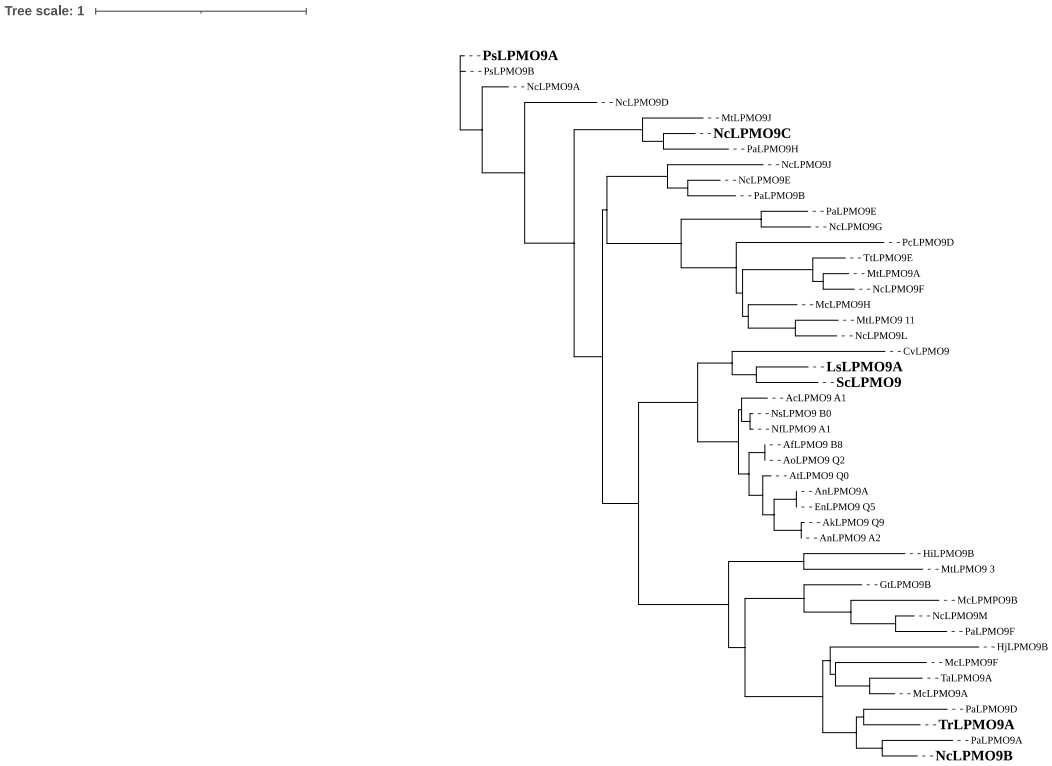

Figure S1. Phylogenetic tree of LPMO9s. The LPMO9s outlined are the ones used to predict a multiple sequence alignment. LPMO9s sequences were downloaded from CAZy, and signal peptide and CBMs were removed before the phylogenetic tree was annotated using Itol. As the phylogenetic tree shows, *Sc*LPMO9A clusters with *Ls*LPMO9A, as expected based on the knowledge that *Ls*LPMO9A is the closest homolog.

Appendix 2

The standard curve used to calculate H_2O_2 production in Amplex Red Hydrogen Peroxide assay is shown in Figure S2.

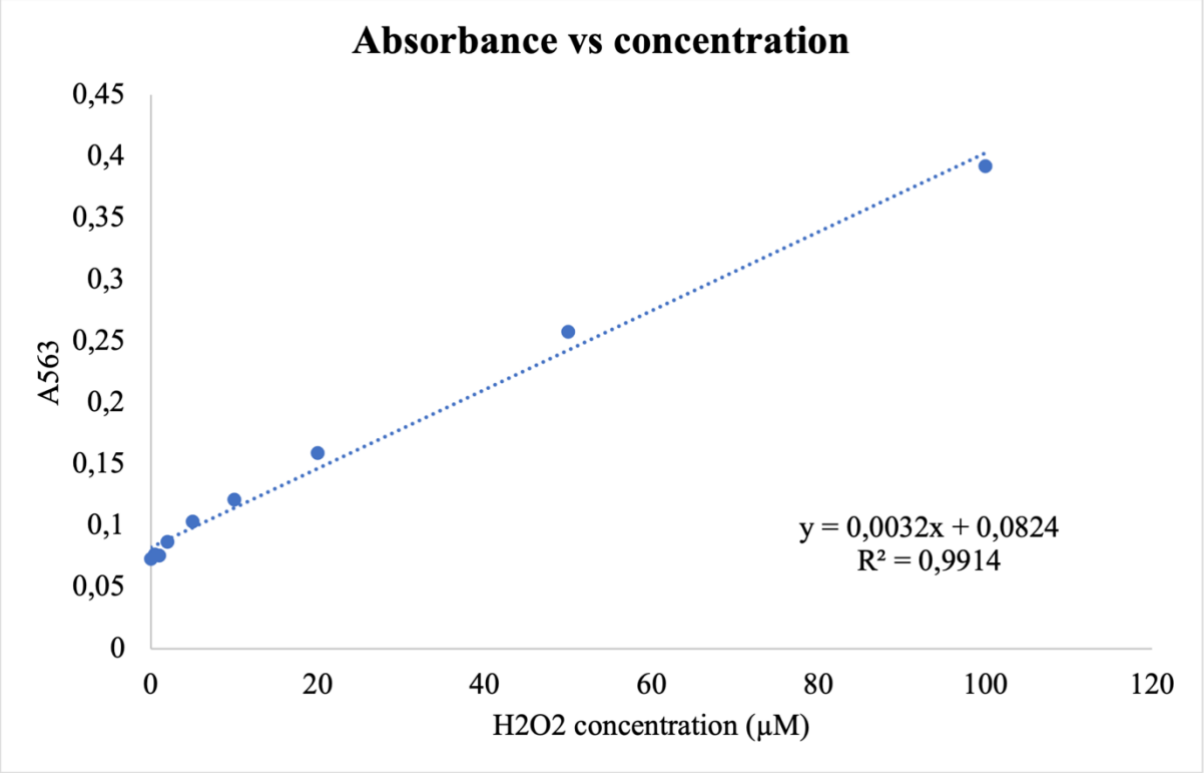

Figure S2. Standard curve for Amplex Red Hydrogen Peroxide assay. The values are the average values of 3 runs.

Appendix 3

Chromatogram from time course experiments on cellopentaose, together with measured cellobiose and cellotriose concentrations are shown in Figure S3, S4 and S5. The measured product concentrations are higher than substrate concentration added, and are discussed in Section 5.10.4

Figures S6 and S7 show chromatogram from time course experiments on cellotetraose and cellohexaose respectively.

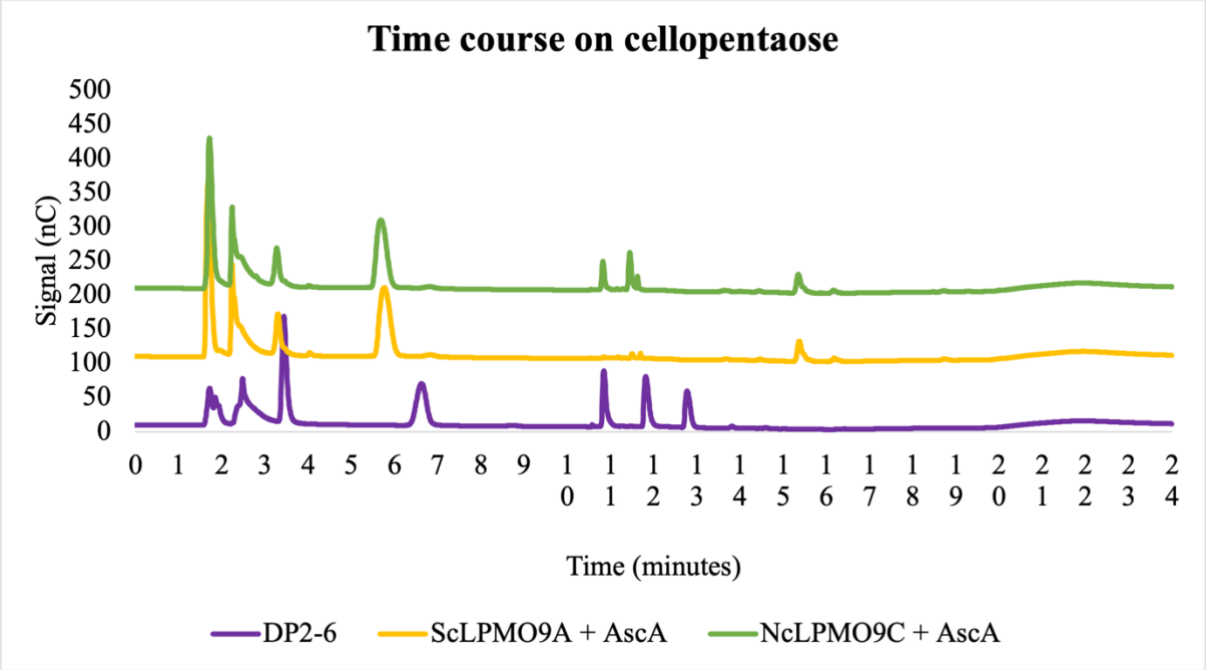

Figure S3. Chromatogram after 24 hours time course on cellopentaose. The time course was performed in 50 mM sodium acetate buffer pH 5.0, 1 mM cellopentaose, 1 µM *Sc*LPMO9A/*Nc*LPMO9C and 1 mM AscA. The chromatogram has a signal offset of 100 nC. The peaks between 15 and 16 minutes show Glc4gemGlc, while the peaks at 12 minutes are cellopentaose, the peaks at 11 minutes are cellotetraose, the peaks at approximately 7 minutes are cellotriose and the peaks between 3 and 4 minutes are cellobiose. The products have a slight shift to the left as standards are prepared in MilliQ water while reactions are performed in sodium acetate buffer pH 5.0 buffer. The reactions were analysed using HPAEC-PAD using a Dionex ISC-6000 system. Data are expressed as mean values for 3 independent repeats.

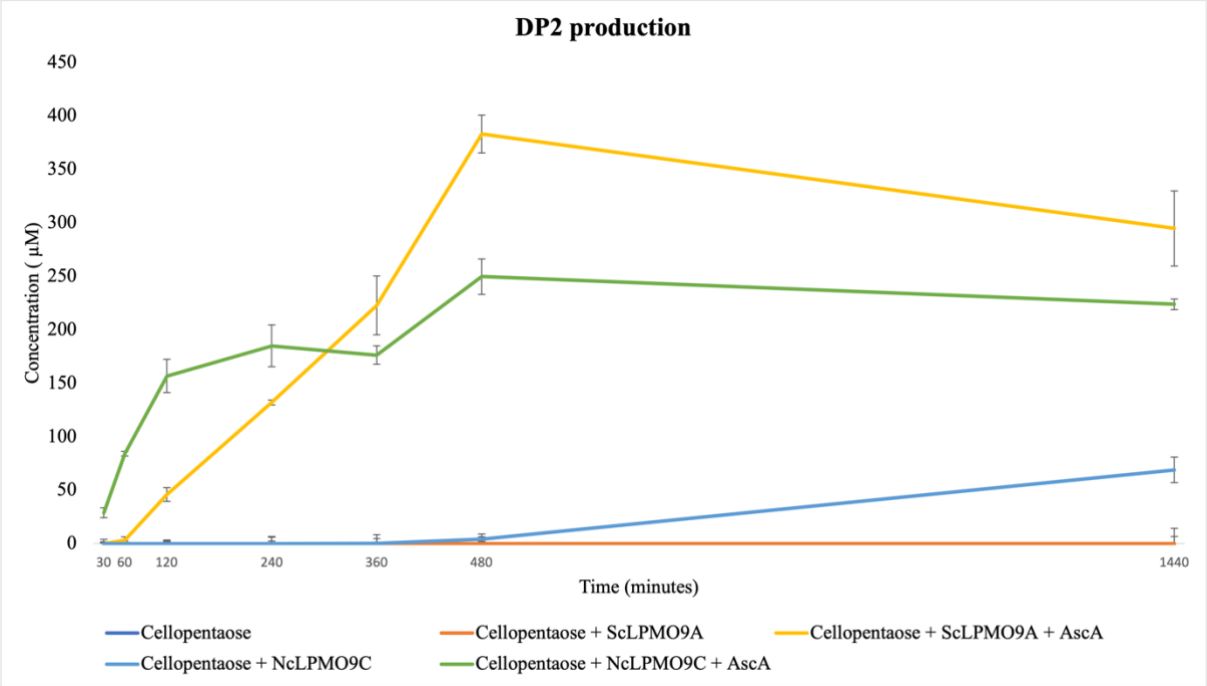

Figure S4. Cellobiose production after time course reaction performed in MilliQ water, 50 mM sodium acetate buffer pH 5.0, 1 mM cellopentaose, 1 µM *Sc*LPMO9A/*Nc*LPMO9C and 1 mM AscA. The reactions were analysed using HPAEC-PAD using a Dionex ISC-6000 system. Some of the controls had values outside the standard curve and are expressed as 0. Data are expressed as mean values for 3 independent repeats.

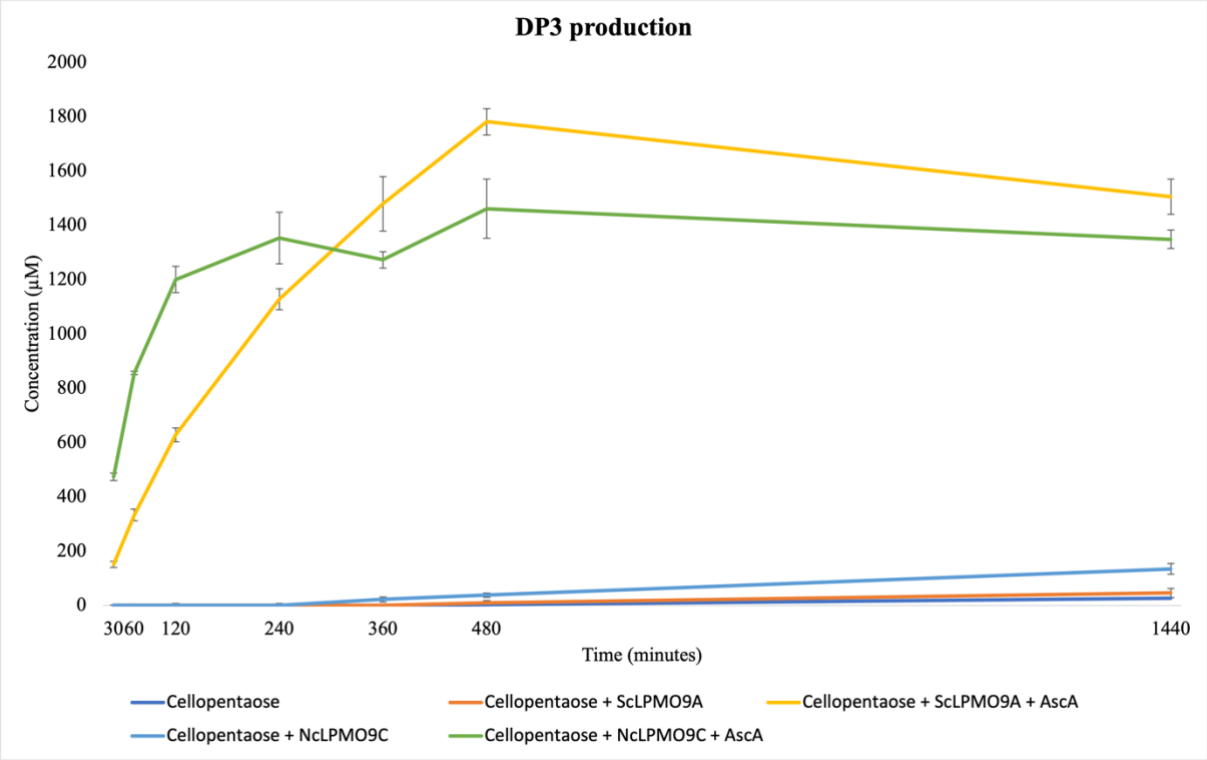

Figure S5. Cellotriose production after time course reaction performed in MilliQ water, 50 mM sodium acetate buffer pH 5.0, 1 mM cellopentaose, 1 µM *Sc*LPMO9A/*Nc*LPMO9C and 1 mM AscA. The reactions were analysed using HPAEC-PAD using a Dionex ISC-6000 system. Some of the controls had values outside the standard curve and are expressed as 0. Data are expressed as mean values for 3 independent repeats.

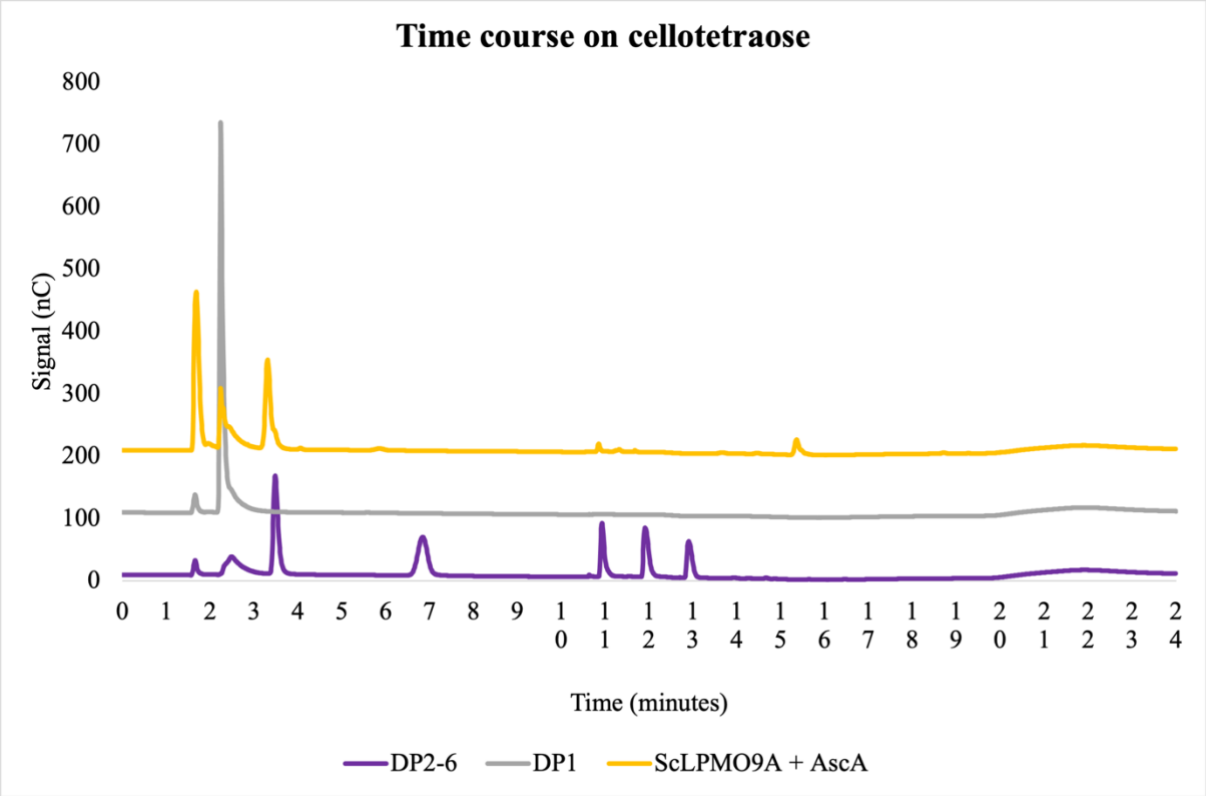

Figure S6 Chromatogram after 24 hours time course on cellotetraose. The time course was performed in 50 mM sodium acetate buffer pH 5.0, 1 mM cellotetraose, 1 µM *Sc*LPMO9A and 1 mM AscA. The reactions were analysed HPAEC-PAD using a Dionex ISC-6000 system. Data are expressed as mean values for 3 independent repeats. The chromatogram has a signal offset of 100 nC. The peak at approximately 15 minutes is Glc4gemGlc, the peak at 11 minutes is cellotetraose and the peak at 3 minutes are cellobiose.

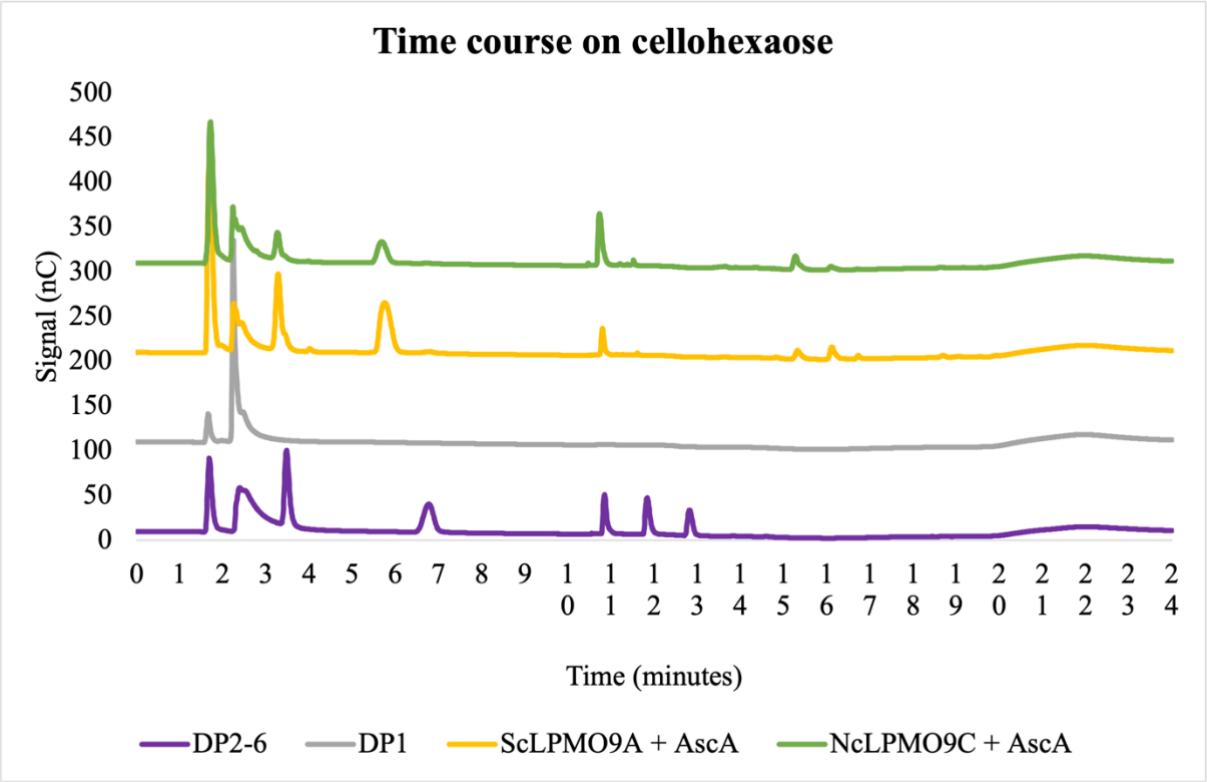

Figure S7 Chromatogram after 24 hours time course on cellohexaose. The time course was performed in 50 mM sodium acetate buffer pH 5.0, 1 mM cellohexaose, 1 µM *Sc*LPMO9A/*Nc*LPMO9C and 1 mM AscA. The reactions were analysed using HPAEC-PAD using a Dionex ISC-6000 system. Data are expressed as mean values for 3 independent repeats.
The chromatogram has a signal offset at 100 nC. The peaks at 15 minutes are Glc4gemGlc, while the peaks at 16 minutes are $Glc4gemGlc_2$. Cellohexaose is shown at the purple chromatogram at 13 minutes. The peaks at 11 minutes are cellotetraose, the peaks at 7 minutes are cellotriose and the peaks between 3 and 4 minutes are cellobiose.

Appendix 4

Chromatograms from time course experiments with added H_2O_2 are shown in Figures S8 and S9, with 1 mM AscA in Figure S8 and 50 mM AscA in Figure S9.

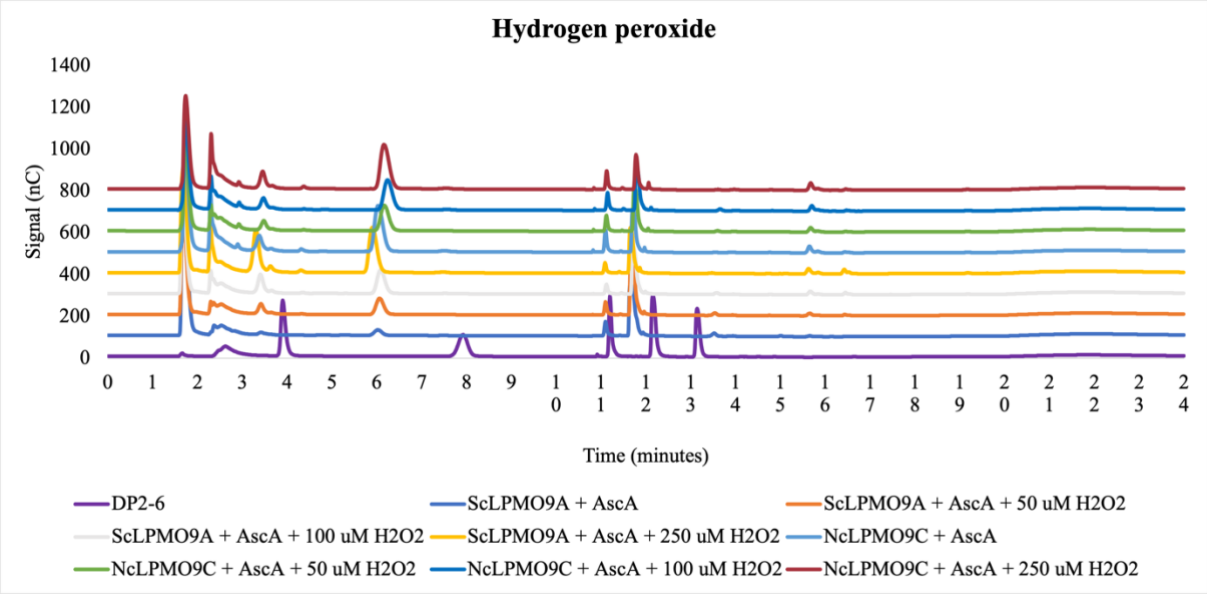

Figure S8. Chromatogram after 1 hour time course on cellopentaose with added H_2O_2. The time course was performed in 50 mM sodium acetate buffer pH 5.0, 1 mM cellopentaose, 1 µM *Sc*LPMO9A/*Nc*LPMO9C and 1 mM AscA. The reactions were analysed using HPAEC-PAD using a Dionex ISC-6000 system. Data are expressed as mean values for 3 independent repeats. The chromatogram has a signal offset at 100 nC. The peaks at approximately 16 minutes are Glc4gemGlc, while the peaks between 16 and 17 minutes are $Glc4gemGlc_2$. The purple line show cellohexaose at 13 minutes, cellopentaose at 12 minutes, cellotetraose at 11 minutes, cellotriose at 8 minutes and cellobiose at 4 minutes. The cellotetraose has a shift to the left in the samples.

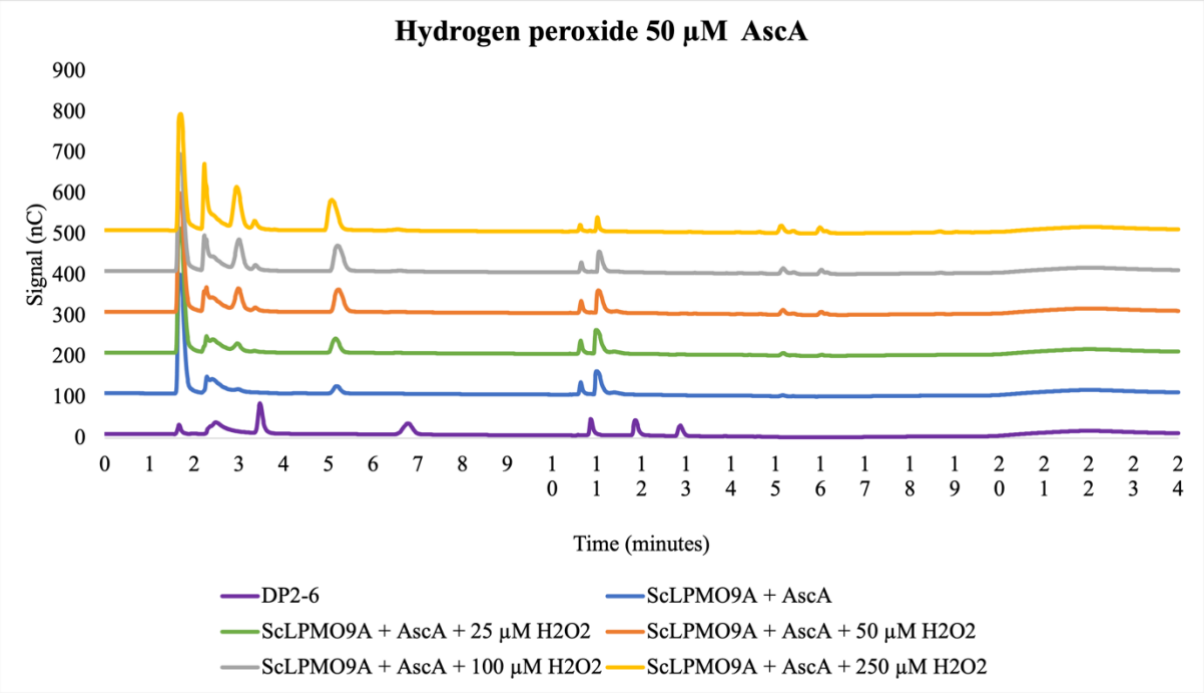

Figure S9. Chromatogram after 1 hour time course on cellopentaose with added H_2O_2. The time course was performed in 50 mM sodium acetate buffer pH 5.0, 1 mM cellopentaose, 1 µM *Sc*LPMO9A/*Nc*LPMO9C and 50 µM AscA. The reactions were analysed using HPAEC-PAD using a Dionex ISC-6000 system. Data are expressed as mean values for 3 independent repeats. The chromatogram has a signal offset at 100 nC. The peaks at approximately 16 minutes are Glc4gemGlc, while the peaks between 16 and 17 minutes are $Glc4gemGlc_2$. The purple line show cellohexaose at 13 minutes, cellopentaose at 12 minutes, cellotetraose at 11 minutes, cellotriose at 8 minutes and cellobiose at 4 minutes. The cellotetraose has a shift to the left in the samples.

Norges miljø- og biovitenskapelige universitet
Noregs miljø- og biovitskapelege universitet
Norwegian University of Life Sciences

Postboks 5003
NO-1432 Ås
Norway